Study of the Formation of Metal Nitrides by Use of NH_3

1999

Takashi Nakagawa

Doctoral Thesis

Study of the Formation of Metal Nitrides by Use of NH_3

(NH_3を用いた金属窒化物生成に関する研究)

1999

Takashi NAKAGAWA

Contents

Chapter 1

General Introduction

1.1 Introductory remarks

Transmutation reactors to change minor actinides (MA) contained in the spent fuels into shorter half-life elements are proposed [1]. One choice may be the utilization of nitrides as the transmutation reactor fuels, because the nitrides have many excellent properties as nuclear fuels compared to other ceramic or metal fuels e.g. high fuel densities, high thermal conductivities, high melting temperatures and large negative enthalpy of formations [2]. In the case that these nitrides are used as fuel materials in nuclear power reactors, their fission products may be present in solution in the fuel matrix, form metal or another nitride phases, or be released in gas phases according to ambient nitrogen potential. The fission products contain a relatively large amount of rare earth group and Eu, Sm and Gd isotopes are neutron absorption materials (burnable poison or control material). To examine the chemical behavior of rare earth elements in nitride fuel matrix, it is necessary to prepare pure rare earth nitrides and investigate their thermodynamic properties. Rare earth nitrides in themselves are interesting as magnetic materials, electric conductors and refractory materials. However, only a small amount of work on the preparation of rare earth nitride has been reported in the literature. One of the purpose of this thesis is to develop experimental methods for formation of several rare earth (La~Tb) nitrides by use of ammonia. When N_2 is used instead of NH_3, higher reaction temperature and longer reaction period will be required. In addition, by use of NH_3 the oxides, more stable substance than metals, can be used as the starting materials. Actinide nitrides are usually prepared by carbothermic reduction of oxides under nitrogen atmosphere [3-11]. However, it is difficult to prepare americium nitride by carbothermic reduction as vapor pressure of americium is very high at temperatures where carbothermic reduction may occur (for example 3×10^2 Pa at 1570 K) [12]. Thus, it is desirable to develop the method of americium nitride

formation at lower temperatures. Some of rare earth elements are often employed as dummy of actinide elements in some preliminary experiments due to chemical similarity of rare earth to actinide elements. Thus, the nitriding method developed in the present work may be adopted for americium nitride formation.

There are several reports on nitride formation by reaction of transition metal oxides with ammonia [13-17]. However, these reports have neither clarified the reaction process nor analyzed the gas phase in nitriding reaction. No report is found for actinide nitride formation by reaction of oxides with ammonia. In this work, the condition at which uranium nitride is prepared by reaction of oxides with ammonia is researched. Although a great deal of effort has been made on the formation of metal nitrides using ammonia up to today by many investigators, what seems to be lacking, however, is the analysis of gas phase in nitride formation. Thus, another aim of this thesis is to deal with reactant gases thermodynamically.

1.2 Outline of the thesis

This thesis consists of six chapters, including this one. In chapter 2, the experimental results of the reactions of rare earth metals with NH_3 or N_2 and H_2 mixture are described. The rare earth nitrides were synthesized by the reaction of the rare earth metals with NH_3 at lower temperatures where rare earth metals never reacted with N_2. The work was undertaken mainly in order to examine the role of nitriding ability of NH_3. The rare earth hydrides were once formed before the nitride formation during the reactions of the rare earth metals with a mixture of N_2 and H_2. The role of H_2 in the formation of rare earth nitrides by the reactions of metals with a mixture of N_2 and H_2 is discussed.

Chapter 3 is concerned with the formation of rare earth carbides and nitrides. CeC_2, PrC_2, NdC_2, GdC_2 and TbC_2 were obtained by carbothermic reduction of oxides with amorphous carbon. However, SmC_2 and EuC_2 were not formed under the same conditions where the other carbides were synthesized. Graphite was formed in the heat-treatment of mixtures of, Sm_2O_3 and Eu_2O_3, and amorphous carbon, even at a low temperature such as 1450°C. Rare earth nitride formation by the reactions of rare earth dicarbides with flowing NH_3 is discussed in this chapter. The reaction of dicarbide

with flowing ammonia consists of two steps, i.e. the nitriding reaction and removal of precipitated carbon. Rare earth dicarbides are nitrided by either NH_3 or N_2. The precipitated carbon, which is amorphous carbon, reacts with NH_3 at 900°C but does not react with H_2 at this temperature. This can be explained by the idea that flowing NH_3 possesses high hydrogen activity. Rare earth mixed nitrides, $Ce_xPr_{1-x}N$ and $Ce_xTb_{1-x}N$, were prepared by reaction of rare earth dicarbides, $Ce_xPr_{1-x}C_2$ and $Ce_xTb_{1-x}C_2$ with NH_3.

XAFS study of *K*-edges of rare earth elements in oxides, carbides and nitrides are described in chapter 4. This is the first report of *K*-edge XAFS study for rare earth carbides and nitrides. It has been claimed elsewhere that chemical shifts could not be observed in such high energies like rare earth *K* absorption edge energies because of the much broadened transition peak forced by short lifetimes of excited core levels [11]. It is, however, found that there are significant and clear chemical shifts in edge energy depending on chemical states. The interatomic distances between Ce and the nearest light elements (O, C and N) calculated from Ce *K*-edge EXAFS spectra of oxide, carbide and nitride agree with those from XRD.

In chapter 5, direct nitride formation by reactions of transition metal oxides with flowing NH_3 is discussed. A modified Ellingham diagram, which employs partial pressure of water and dissociation degree of ammonia in addition to temperature and free energy of formation, is suggested under the idea that metal oxides are once reduced by ammonia followed by nitrided in the reaction of oxides with ammonia. The condition where uranium oxides can be reduced by ammonia is also suggested.

The conclusions drawn from the present study are summarized in chapter 6.

References

[1] T. Wakabayashi, S. Ohki and T. Ikegami, "Feasibility Studies of an Optimized Fast Reactor Core for MA and FP transmutation", Global' 95, Proc. of Int. Conf. on Evaluation of Emerging Nuclear Fuel Recycle System, Vol. 1, pp. 800, 1995

[2] V. C. Truscello and H. S. Davis, *IEEE Spectrum*, **21**(1984)58.

[3] T. Muromura and H. Tagawa, *J. Nucl. Mater.* **71**(1977)65.

[4] T. Muromura and H. Tagawa, *J. Nucl. Mater.* **80**(1979)330.

[5] R. B. Matthews, K. M. Chidester, C. W. Hoth, R. E. Mason and R. L. Petty, *J. Nucl. Mater.* **151**(1988)334.

[6] R. D. Shoup, *J. Am. Ceram. Soc.* **60**(1977)332

[7] G. Pautasso, K. Richter and C. Sari, *J. Nucl. Mater.* **158**(1988)12

[8] Y. Arai, S. Fukushima, K. Shiozawa and M. Handa, *J. Nucl. Mater.* **168**(1989)280.

[9] Y. Arai, C. Sari and J. C. Spirlet, *J. Nucl. Mater.* **185**(1991)159.

[10] P. Bardelle and D. Warin, *J. Nucl. Mater.* **188**(1992)36

[11] T. Ogawa, T. Ohmichi, A. Maeda, Y. Arai and Y. Suzuki, *J. Alloys Comp.* **224**(1995)55.

[12] M. Takano, A. Itoh, M. Akabori, T. Ogawa, S. Kikkawa, H. Okamoto, S. Matsumoto and K. Somobe, *1999 Annual Meeting of Atomic Energy Society of Japan*, Vol. III, pp. 546.

[13] V. G. Brauer, J. Weidlein and J. Strähle, *Z. Anorg. Allg. Chem.* **348**(1966)298.

[14] C. H. Shin, G. Bugli and G. Djega-Mariadassou, *J. Solid State Chem.* **95**(1991)145.

[15] K. Kamiya, T. Yoko and M. Bessho, *J. Mater. Sci.* **22**(1987)937.

[16] C. H. Jaggers, J. N. Mlchaels and A. M. Stacy, *Chem. Mater.* **2**(1990)150.

[17] L. Volpe and M. Boudart, *J. Solid State Chem.* **59**(1985)332.

[18] J. C. Fuggle and J. E. Inglesfield, " Unoccupied electronic states : fundamentals for XANES, EELS, IPS and BIS," J. C. Fuggle and J. E. Inglesfield, ed., Springer-Verlag, Berlin (1992), pp. 1--21.

Chapter 2

Nitridation of rare earth metals

2.1 Introduction

Uranium mononitride and plutonium mononitride are considered to be promising nuclear fuel materials for liquid metal fast breeder reactors (LMFBRs) or space power reactors, as these nitrides are admitted to have many desirable properties compared to the other nuclear fuel materials, that is, high fuel densities, high thermal conductivities, high melting points and large negative enthalpy of formation [1]. Especially, as for LMFBRs, nitride fuel possesses some beneficial abilities with regard to lower fission product (FP) gas release, less interactive chemical response with Na, and shorter time for doubling fuel. When these nitrides are used as fuel materials for nuclear power reactors, FPs may be present in the form of solid solutions in the fuel matrix, metals, gases, or another nitrides depending on their nitrogen potential. Properties of FP nitrides and their behavior in power reactors, therefore, have to be examined. Because FP involves relatively large abundance of rare earth group, chemical behavior of rare earth in nitride fuel becomes very important. However, even on the preparations of rare earth nitrides, little work has been reported in the literature. The purpose of this work is to develop a feasible method of rare earth nitride preparation.

Since Matignon discovered rare earth nitrides [2], several authors have published the studies on the rare earth nitrogen systems. Existence of mononitrides for all rare earth elements, which have NaCl-type structure, was verified except for promethium [3]. Kobzenko and Ivanchenko examined the cerium-nitrogen system between 0 and 50 atomic percent N (0 and 9.1 weight percent N) [4]. Phase diagrams of binary systems of the other rare earth metals and nitrogen have not been reported yet.

It is known that rare earth mononitride can be prepared by the reaction of rare earth metal or rare earth hydride with nitrogen or ammonia at temperatures around the

melting points of the rare earth metals, or higher. Kieffer *et al.* obtained rare earth mononitrides by the reactions of lanthanum, cerium, praseodymium and neodymium with nitrogen at 1 bar at 1000-1100°C [5]. Holleck *et al.* prepared mononitride of cerium at temperatures higher than 1100°C, and that of neodymium at temperatures higher than 1550°C, respectively, in 1 bar nitrogen atmosphere [6], while Gambino and Cuomo obtained rare earth nitrides in consolidated form by reactive arc melting in nitrogen atmosphere at 2000°C [7]. About preparation of rare earth mononitride at relatively low temperature, only Samsonov and Lyutaya reported the formation of cerium mononitride by the reaction of metallic cerium and current of ammonia at temperatures higher than 200°C [8]. Rare earth nitrides, except for cerium, were prepared above the melting point of each rare earth metal. It is known that ammonia has higher nitriding ability than nitrogen [9]. Unstable ammonia phase particularly possesses extremely high nitrogen activity. This may suggest that at lower temperatures such as below the melting points of rare earth metals, rare earth nitrides can be formed by use of ammonia. No report of the rare earth nitride formation by the reaction of rare earth metal with a mixture of N_2 and H_2 has been yet published. A large number of reports have been published on rare earth hydrides since Matignon noted that hydrogen was taken up by lanthanum, cerium praseodymium and neodymium to form solid products [2]. An isomorphous series of non-stoichiometric hydrides of composition MH_2 to MH_3 are formed for La, Ce, Pr and Nd [10]. MH_2 hydrides have a fluorite-type structure. The additional hydrogen in the $MH_{>2}$ compositions is statistically distributed in the octahedral interstices of a fluorite-type structure [11].

2.2 Experimental

Rare earth metals treated in this work were lanthanum, cerium, praseodymium and neodymium. These rectangular-shaped metal specimens (4 × 4 × 15mm) were supplied from Nihon Yttrium Co. Ltd. Nominal impurity of the lanthanum metal specimen was in ppm as Ce (<100), Pr (<100), Nd (<100), Fe (340), Ca (40) and Mg(<10). That of cerium was La (<100), Nd (<100), Fe (70), Ca (20) and Mg (60). That of praseodymium metal was La (<100), Ce (<100), Nd (<100), Fe (20), Ca (40)

and Mg(70). That of neodymium metal was La (<100), Ce (<100), Pr (<100), Sm (<100), Fe (120), Ca (15) and Mg (180). Commercial ammonia whose impurity was 99.998% was used.

The experimental apparatus used in this work, shown schematically in Fig. 2.1, consisted of a gas-supply system, a cylindrical resistance furnace, a vacuum system and a gas analysis system. The apparatus could be evacuated to 10^{-6} Pa. A quartz reaction tube was fitted in the cylindrical resistance furnace. This furnace can be divided into the upper and the lower halves connected by a hinge, in such a way that it can be opened for quenching and visual observation for operation in replacing a quartz-made specimen boat into the center of the reaction tube. The temperature of the furnace was controlled by an on-off type thermoregulator controlled by a chromel alumel thermocouple whose ends were mounted on the center of the outer surface of the reaction tube. Temperature of the specimen was measured by this thermocouple. Ammonia gas provided from the commercial gas cylinder was fed into the reaction tube through a gas flow meter and a stainless steel capillary without purification. A capacitance manometer (MKS VARATRON type 122A, MKS Japan) was used to measure the total pressure within the range from 10^{-2} kPa to 10^{2} kPa. The gas analysis system consisted of a gas sampler with two sampling cocks, a gas chromatograph (type GC-8APT, Shimadzu & Co., ltd., Kyoto, Japan) and a digital integrator (type C-R6A, Shimadzu & Co., ltd., Kyoto, Japan). The gas chromatograph contained four stainless steel columns, 2000 mm in length and 3 mm in inner diameter, a column-thermostat, a four-direction value, a thermal conductivity detector (TCD) and a TCD-thermostat. The four columns were packed with stationary phases which could separate a gaseous mixture into individual gases. The columns were kept at 70°C and the TCD at 110°C. The current value of the TCD was 120 mA. Helium gas with nominal purity 99.999% was passed as a carrier gas at a flow rate of 40 ml/min. An X-ray diffraction powder pattern for the reaction product was obtained with a diffractometer (Rigaku Denki, Geiger flex rad-rA) using crystal-monochromatized CuKα radiation at room temperature.

In this work, two types of experiments were performed, the ammonia flow type and the static type. The procedure of flowing method experiments is as follows. About 1.5 g of a rectangular-shaped metal specimen cleaned up with acetone was leached in

10N-HNO_3 for a few seconds and was washed with distilled water. This treatment was repeated a few times to get rid of the oxide layer on the surface. The bright metal specimen thus prepared was weighed accurately. Thus prepared metal was put on the quartz boat, and it was placed onto the center of the reaction tube. The system was evacuated to 10^{-5} Pa at room temperature. Then the temperature of reaction tube was raised up to 110°C and kept for more than 9 hours. After outgassing of prepared metal at 300°C for another 3 hours, the temperature of the system was set to the desired temperature. Then ammonia gas was introduced into the reaction tube and kept on flowing at the rate of 200 ml/min. After 20 hours the reaction tube was quenched to room temperature and the system was evacuated. The solid sample pulverized in an agate mortar, and was identified by X-ray powder diffraction analysis. The experimental procedure of the static ammonia method was similar to that of the ammonia flowing method. But in the static ammonia method the composition of gases in the reaction tube was analyzed by use of the gas chromatograph regularly till the total pressure unvaried. For comparative experiments these rare earth metals were also exposed to the nitrogen atmosphere. Reactions of lanthanum, cerium, praseodymium and neodymium with a mixture of N_2 and H_2 were also performed. As for lanthanum metal, the reaction temperature was 500°C and reaction time was 17 hours. Cerium metal was reacted with the gaseous mixture at 300°C for 40 hours. The neodymium metal was reacted for 6 hours at 700°C. The experiments of praseodymium metal were carried out at the temperatures of 350°C, 450°C, 550°C and 600°C for 49 hours, 11 hours, 10 hours and 8 hours, respectively.

2.3 Results and Discussion

2.3.1 Reactions of rare earth metals with NH_3 gas

The conditions and results of all experiments in this work are summarized in Table 2.1. Lanthanum, praseodymium and neodymium were exposed to the nitrogen stream for 20 hours at 700°C of which flow rate was 200ml/min. But these specimens did not react with nitrogen and remained as metals. On the other hand, when these metals were placed in the ammonia stream at the same temperature and period, all of them

formed their nitrides. This indicates that ammonia is superior to nitrogen as nitriding agent.

For the measurement of the composition of the inner gas during the reaction, the static gas experiments were performed. Cerium reacted with static ammonia to form its nitride even at 200°C, lanthanum at 500°C and praseodymium at 600°C. These temperatures are much lower than the previously reported temperatures which were almost the melting points of the respective metals or higher. Although neodymium did not reacted with static ammonia at 700°C, it reacted with the ammonia stream to form its nitride at this temperature. Figure 2.2 shows the variation of the inner gaseous composition during the reaction of cerium with static ammonia at 250°C. In the early stage the partial pressure of ammonia decreased and the partial pressure of hydrogen increased, but the amount of nitrogen gas was below a detective level of a gas-chromatogragh all through this experiment. There are three conceivable reactions in this run, that is, nitride formation reaction, hydride formation reaction and ammonia decomposition which are represented by

$$Ce + NH_3 \rightarrow CeN + \frac{3}{2}H_2, \tag{2.1}$$

$$Ce + NH_3 \rightarrow CeH_3 + \frac{1}{2}N_2, \tag{2.2}$$

$$NH_3 \rightarrow \frac{1}{2}N_2 + \frac{3}{2}H_2. \tag{2.3}$$

No detection of nitrogen denies that hydriding and decomposition arose. In other words, this indicates that only nitriding reaction occurred. The X-ray diffraction pattern of the solid product shows the existence of only CeN phase. Cerium did not reacted with nitrogen at 250°C. Thus also the static ammonia is superior to nitrogen as a nitriding agent.

Figure 2.3 indicates the result of the reaction of La with ammonia at 500°C. Though the partial pressure of hydrogen was increasing from the start, nitrogen gas hardly generated during the first 2 hours. The specimen of La was almost nitrided in this period. After that the partial pressure of nitrogen increased. Nitrogen gas was generated not by hydriding formation reaction but by ammonia decomposition, because hydrogen partial pressure is always a value 1.5 times as much the decrease in ammonia

partial pressure. Figure 2.4 shows variations of nitrogen activity and hydrogen activity estimated by $a_N = \left[\left(1/K_p\right)\cdot\left(P_{NH_3}/P_{H_2}^{3/2}\right)\right]$ and $a_H = \left[\left(1/K_p\right)\cdot\left(P_{NH_3}/P_{N_2}^{1/2}\right)\right]^{1/3}$, which were derived by Katsura [9], for the reaction of La with NH_3 at 500°C. Nitrogen activity at the start was very high and according to nitride formation it became drastically smaller owing to decrease of ammonia and generation of hydrogen in the first 2 hours. Meanwhile, hydrogen activity was lower compared to nitrogen activity and did not vary so much during the reaction. This is why rare earth metals form their nitrides by use of ammonia although they tend to form hydride easily. Praseodymium was also nitrided in the similar method at 600°C.

In experiment of the reaction between Nd and static ammonia at 700°C, only decomposition of ammonia proceeded as shown in Fig. 2.5 and nitride did not formed, although Nd was nitrided when it was also exposed to flowing ammonia at the same temperature. This can be explained by the fact that in the static ammonia method nitrogen activity decreases because of ammonia dissociation but in the flowing ammonia method very high nitrogen activity of gas phase can be maintained. Flowing ammonia possesses the highest nitriding ability among flowing ammonia, static ammonia and nitrogen at the same temperature. It is expected in the flowing ammonia gas phase that La, Ce and Pr can be nitrided at lower temperatures than the temperature where each metal could be converted to nitride by use of static ammonia.

2.3.2 Reactions of rare earth metals with N_2 and H_2 mixture gas

Most of reported rare earth nitride formations by the reactions of rare earth metals and nitrogen occurred at the experimental temperatures above melting point of the rare earth metal. Nitrides could not be formed even though lanthanum, praseodymium and neodymium metal specimens were left alone in flowing nitrogen atmosphere at 700°C and cerium metal specimen was left in nitrogen gas whose pressure was 80 kPa at 300°C. The conditions and the results of all experiments in this work are summarized in Table 2.2. It is evident from the x-ray diffraction patterns of the solid products that all rare earth metal specimens reacted with the gaseous mixture of nitrogen and hydrogen formed their mononitrides. Figure 2.6 shows the variation of partial pressures of nitrogen and hydrogen during the reaction of neodymium with the gaseous

mixture at 700°C. The decrease in the partial pressure of hydrogen is seen at the early stage in the reaction. This hydrogen pressure decrease means that neodymium metal absorbed hydrogen rapidly to form neodymium hydride because all the rare earth metals are known as good hydrogen occlusion materials. However, partial pressure of hydrogen soon reaches the minimum point and turns to increase. On the other hand, the partial pressure of nitrogen decreases continuously till it reaches a point where the reaction is in equilibrium. The variation of the gas composition indicates that the formed neodymium hydride is converted into its nitride as it absorbs nitrogen and desorbing hydrogen. The variation of partial pressures of nitrogen and hydrogen during the reaction of praseodymium metal with the mixture gas at 600°C shown in Fig. 2.7 is very analogous to those in Fig. 2.6. The results of all experiments of the other rare earth metals with the gaseous mixture exhibit the similar changes in the composition of the reactant gases. Thus, the following consecutive reactions occur in the reactions between rare earth metals and the gaseous mixture of nitrogen and hydrogen;

$$\text{Rare earth metal (RE)} + H_2 + \frac{1}{2}N_2 \rightarrow REH_2 + \frac{1}{2}N_2 \rightarrow REN + H_2. \qquad (2.4)$$

The following is conceivable from these experimental results. Hydrogen atom which has small atomic radius can diffuse into metal lattice after hydrogen molecules adsorb on the metal surface and dissociate into hydrogen atoms. Diffused hydrogen atoms cut metal bonds one after another and form hydride. Then, nitrogen is adsorbed on the newly bare hydride surface and ousts hydrogen atoms to form nitride. All part of the metal specimen is replaced by nitride through such a process like this. Hydrogen in gaseous mixture behaves as if it were a catalyst in course of nitride formations.

The existence ratio of metal, hydride and nitride in solid phase can be calculated from the variations of the nitrogen and hydrogen partial pressures during the reaction. Figure 2.8 shows the change of the existence ratio of praseodymium metal, hydride and nitride in solid phase during the reaction of praseodymium and the gaseous mixture at 600°C. The open circles, diamonds and squares mean the existence ratio of the metal, hydride and nitride, respectively. The curves were drawn in terms with the values of the reaction velocity coefficients which can be gained from this graph in the method

mentioned below. Assuming that praseodymium metal forms its hydride in first-order reaction and hydride is converted into nitride in first-order reaction, and that the respective reaction velocity coefficients of the hydride formation and the nitride formation are denoted by k_1 and k_2, the production velocities of praseodymium metal, hydride and nitride are written as follows, respectively:

$$\frac{dC_M}{dt} = -k_1 C_M \,, \tag{2.5}$$

$$\frac{dC_H}{dt} = k_1 C_M - k_2 C_H \,, \tag{2.6}$$

$$\frac{dC_N}{dt} = k_2 C_H \,, \tag{2.7}$$

where C_M, C_H and C_N are the existence ratio of metal, hydride and nitride, respectively. Integration of eqn. 2.5 is

$$C_M = C_M^\circ e^{-k_1 t} \,, \tag{2.8}$$

where C_M^0 is the initial existence ratio of metal and equal to 1. Substituting eqn. 2.8 into eqn. 2.6 and integrating eqn. 2.6 yields,

$$C_H = \frac{C_M^\circ k_1}{k_2 - k_1}(e^{-k_1 t} - e^{-k_2 t}) \,, \tag{2.9}$$

because when $t = 0$, $C_H^\circ = 0$. The initial value of the existence ratio of nitride, C_N° is also 0, thus $C_M + C_H + C_N = C_M^\circ$. And C_N is written as:

$$C_N = C_M^\circ + \frac{C_M^\circ}{k_1 - k_2}(k_2 e^{-k_1 t} - k_1 e^{-k_2 t}) \,. \tag{2.10}$$

The values of k_1 and k_2 are determined so as to fit into the measurement curves in Fig.2.8. They correspond to the reaction velocity coefficient in the experiment at 600°C. The values of k_1 and k_2 in the experiments at 550°C, 450°C and 350°C can be obtained in the similar way. The slope of Arrhenius plots of logarithm of the reaction velocity coefficients against the reciprocal of the reaction temperatures is the activation energy of the reaction. This plot for the reaction of praseodymium with the gaseous mixture is shown in Fig. 2.9. The respective activation energies of the hydride formation and the nitride conversion are 10.5kJ/mol and 50.9kJ/mol.

2.4 Conclusions

Rare earth mononitride can be obtained at much lower temperatures by the reaction of rare earth with ammonia than by the reaction with nitrogen gas. This means that ammonia works more effectively as nitriding agent compared to nitrogen. Nitrogen activity a_N, is evaluated in terms of the equilibrium constant of ammonia formation, K_p, and partial pressures of only NH_3 and H_2; e.g. $a_N=(1/K_p)[P(NH_3)/P(H_2)^{3/2}]$. At a given temperature, the higher nitrogen activity is obtained when ammonia partial pressure is higher and hydrogen partial pressure is lower. This condition can be realized by either suppressing ammonia dissociation, that is, keeping the temperature low, or supplying ammonia and removing hydrogen, namely, using ammonia stream. But nitrides are not fabricated at low temperatures due to high activation energies. Therefore, in order to obtain high nitrogen activity, it is reasonable to adopt flowing ammonia methods, so that nitrides can be formed more easily. In this work by use of a static ammonia method some rare earth nitrides were created at such low temperatures; CeN was at 200°C, LaN at 500°C and PrN at 600°C. Neodymium was not nitrided at 700°C by static ammonia but nitrided at this temperature by flowing ammonia. For the other rare earth elements, the nitrides may be formed at a lower temperature than the respective temperatures at which their nitrides were obtained in static ammonia method.

Nitrides of lanthanum, cerium, praseodymium and neodymium can be also obtained by use of the gaseous mixture of nitrogen and hydrogen at much lower temperatures than by use of only nitrogen gas. Lanthanum nitride is formed at 500°C, cerium nitride at 300°C, praseodymium nitride at 350°C and neodymium nitride at 700°C. During the reactions of rare earth metals with the gaseous mixture of nitrogen and hydrogen, hydrogen seems to behave itself like, as it were, a gaseous catalyst. The rare earth hydrides are once produced as intermediates, before the rare earth nitrides are formed. For example, as for praseodymium, the activation energy of the hydride formation is 10.5kJ/mol and that of the conversion of the hydride into the nitride is 50.9kJ/mol. That value of the nitride formation by use of only nitrogen may be higher compared to these values. When other rare earth is reacted with a mixture of N_2 and H_2, a similar consideration may be possible.

These nitriding methods above mentioned may be applicable to americium nitride formation.

References

[1] V. C. Truscello and H. S. Davis, *IEEE Spectrum*, **21**(1984)58.

[2] C. Matignon, *Compt. Tend.* **131**(1900)837.

[3] G. Busch, E. Kaldis, "Les Éléments des Terres-Rares," Paris-Grenoble(1970), 1, N 180, p.359.

[4] G. F. Kobzenko and V. G. Ivanchenko, *Dopovidi Akad. Nauk Ukr. RSR* , **1970A**(1970)1126.

[5] R.Kieffer, P.Ettmayer and SwPajakoff, *Monatsh. Chem.* **103**1972)1285.

[6] H. Holleck, E. Smailos and F. Thümmler, *J. Nucl. Mater.* **28**(1968)105.

[7] R. J. Gambino and J. J. Cuomo, *J. Elec. Soci.* **113** No.4(1966)401.

[8] G. V. Samsonov and M. D. Lyutaya, *Zhur. Prik. Khimii.* **Vol. 35** No. 11 (1962)2359.

[9] M. Katsura, *J. Alloys Comp.* **182**(1992)91.

[10] C. E. Holley, Jr., R. N. R. Mulford and F. H. Ellinger, *J. Phys. Chem.* **59**(1955)1226.

[11] A. Pebler and W. E. Wallace, *J. Phys. Chem.* **66**(1962)148.

Table 2.1 The conditions and the results of experiments.

run	Metal	Gas phase[kPa]	Method	Temperature[˚C]	Period[hrs]	Products(Lattice Parameter[nm])
2.1	La	N_2(200ml/min)	Flowing	700	20	Metal(-)
2.2	Pr	N_2(200ml/min)	Flowing	700	20	Metal(-)
2.3	Nd	N_2(200ml/min)	Flowing	700	20	Metal(-)
2.4	La	NH_3(200ml/min)	Flowing	700	20	LaN[(0.5312)
2.5	Pr	NH_3(200ml/min)	Flowing	700	20	PrN[(0.5172)
2.6	Nd	NH_3(200ml/min)	Flowing	700	20	NdN(0.5135)
2.7	Ce	NH_3[40]	Static	200	50	CeN(0.5052)
2.8	Ce	NH_3[40]	Static	250	14	CeN(0.5027)
2.9	Ce	N_2[48]	Static	250	66	Metal(-)
2.10	La	NH_3[53]	Static	500	17	LaN(0.5305)
2.11	Pr	NH_3[53]	Static	600	57	PrN(0.5174)
2.12	Nd	NH_3[53]	Static	700	17	Metal(-)

Table 2.2 The experimental conditions and results of reactions of rare earth metals with N_2/H_2 mixture.

Run	Metal	Gas phase	Temp.(°C)	Time(h)	Product(LP#)
2.13	La	N_2, H_2*	500	6	LaN(0.5305)
2.14	Ce	N_2, H_2**	300	40	CeN(0.5023)
2.15	Pr	N_2, H_2*	600	8	PrN(0.5155)
2.16	Pr	N_2, H_2*	550	10	PrN(0.5169)
2.18	Pr	N_2, H_2*	350	49	PrN(0.5176)
2.19	Nd	N_2, H_2*	700	8	NdN(0.5137)

Lattice Parameter [nm]

* N_2(20kPa), H_2(60kPa)

** N_2(17kPa), H_2(47kPa)

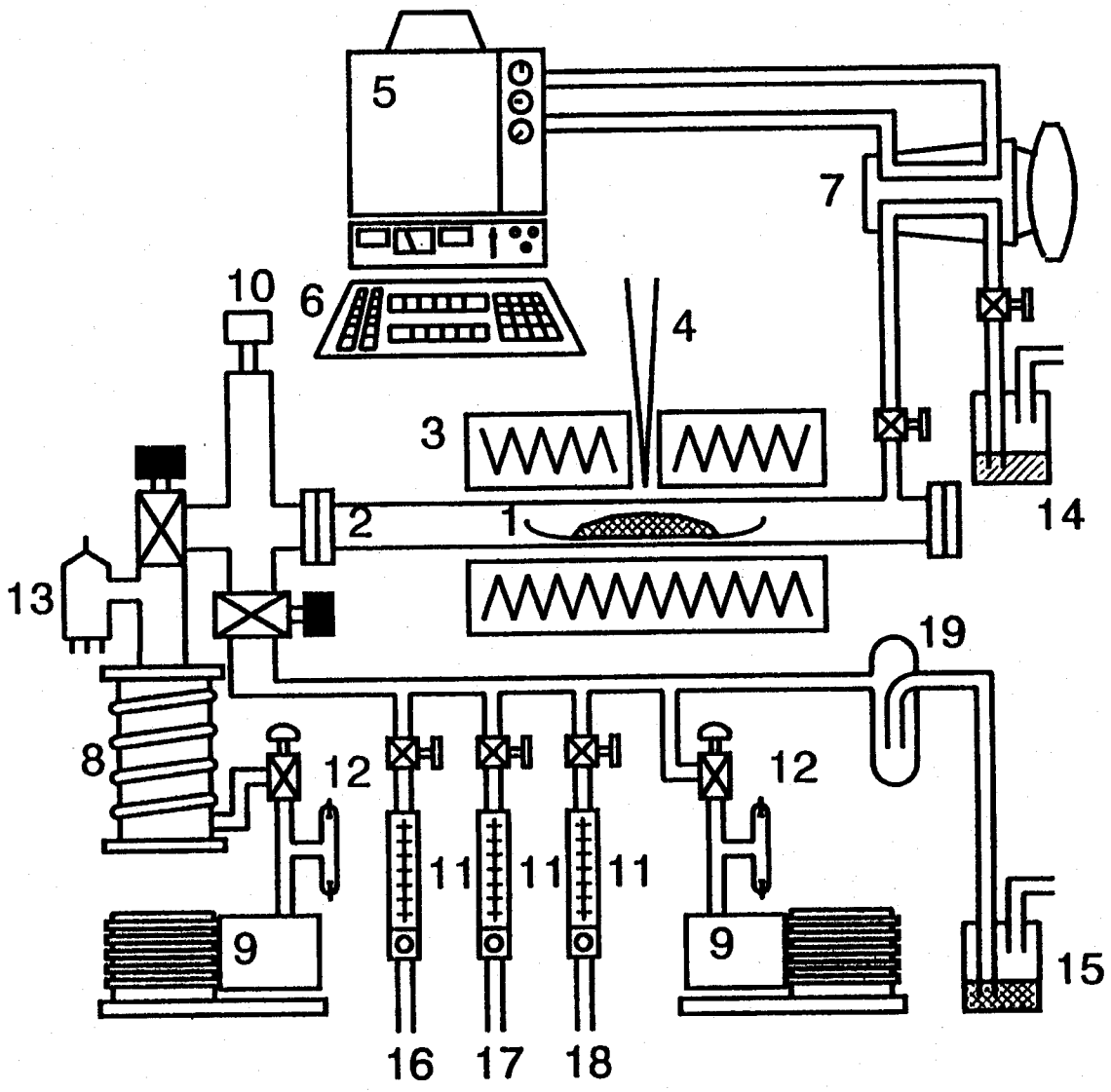

1. Quartz boat containing sample
2. Reaction tube
3. Electric furnace
4. Thermocouple
5. Gaschromatograph
6. Digital integrator
7. Gas sampling system
8. Oil diffusion pump
9. Rotary pump
10. Capacitance manometer
11. Flow meter
12. Geissler tube
13. Ionization vacuum gauge
14. Oil bubbler
15. Hg bubbler
16. NH_3 gas inlet
17. N_2 gas inlet
18. H_2 gas inlet
19. Hg trap

Fig. 2.1 Experimental apparatus

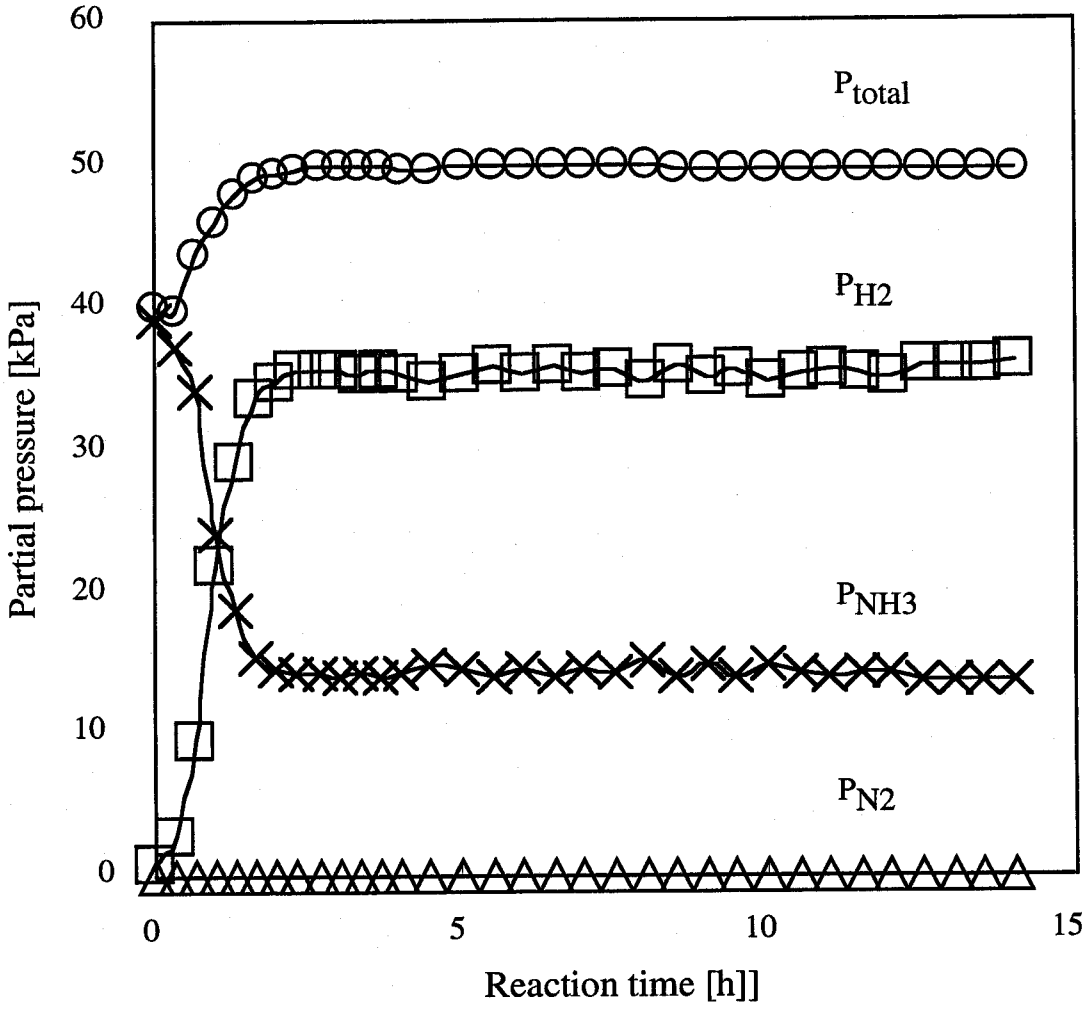

Fig. 2.2 Time variation of the total pressure and partial pressures of NH_3, N_2 and H_2 during the reaction of cerium with static NH_3 gas at 250°C

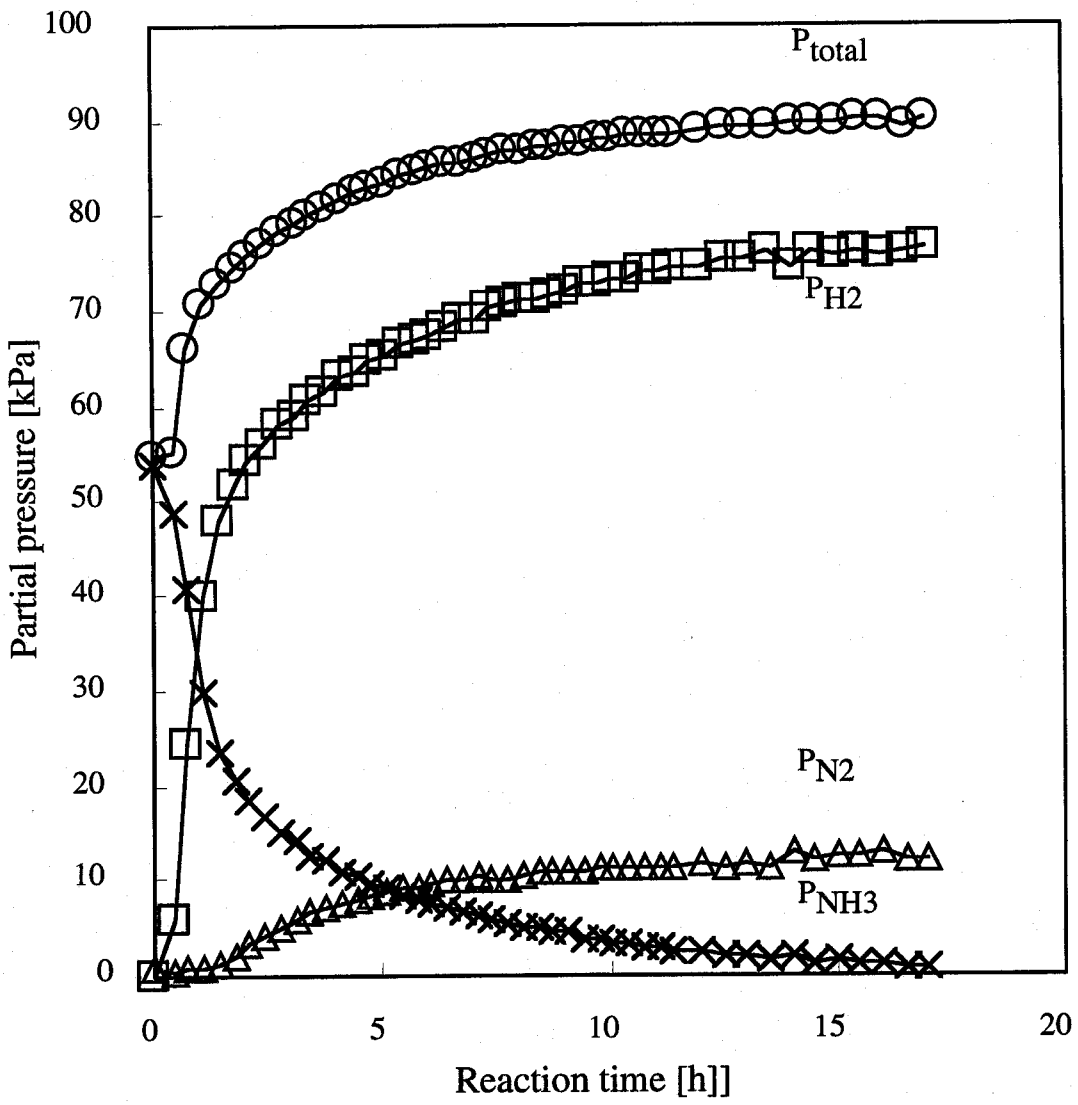

Fig. 2.3 Time variation of the total pressure and partial pressures of NH_3, N_2 and H_2 during the reaction of lanthanum with static NH_3 gas at 500°C

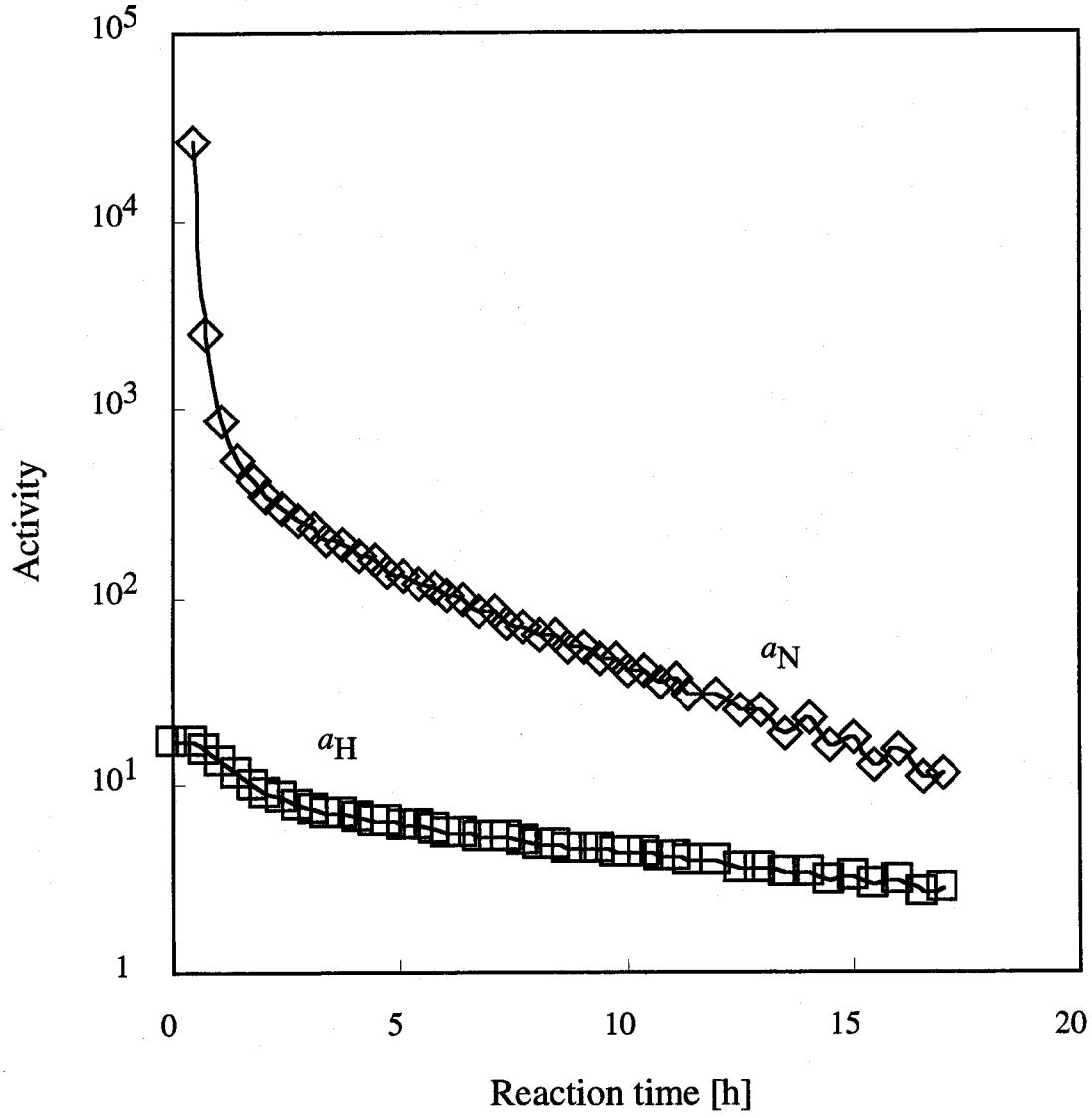

Fig. 2.4 Variation of nitrogen activity, a_N, and hydrogen activity, a_H, during the reaction of lanthanum with NH_3 at 500°C

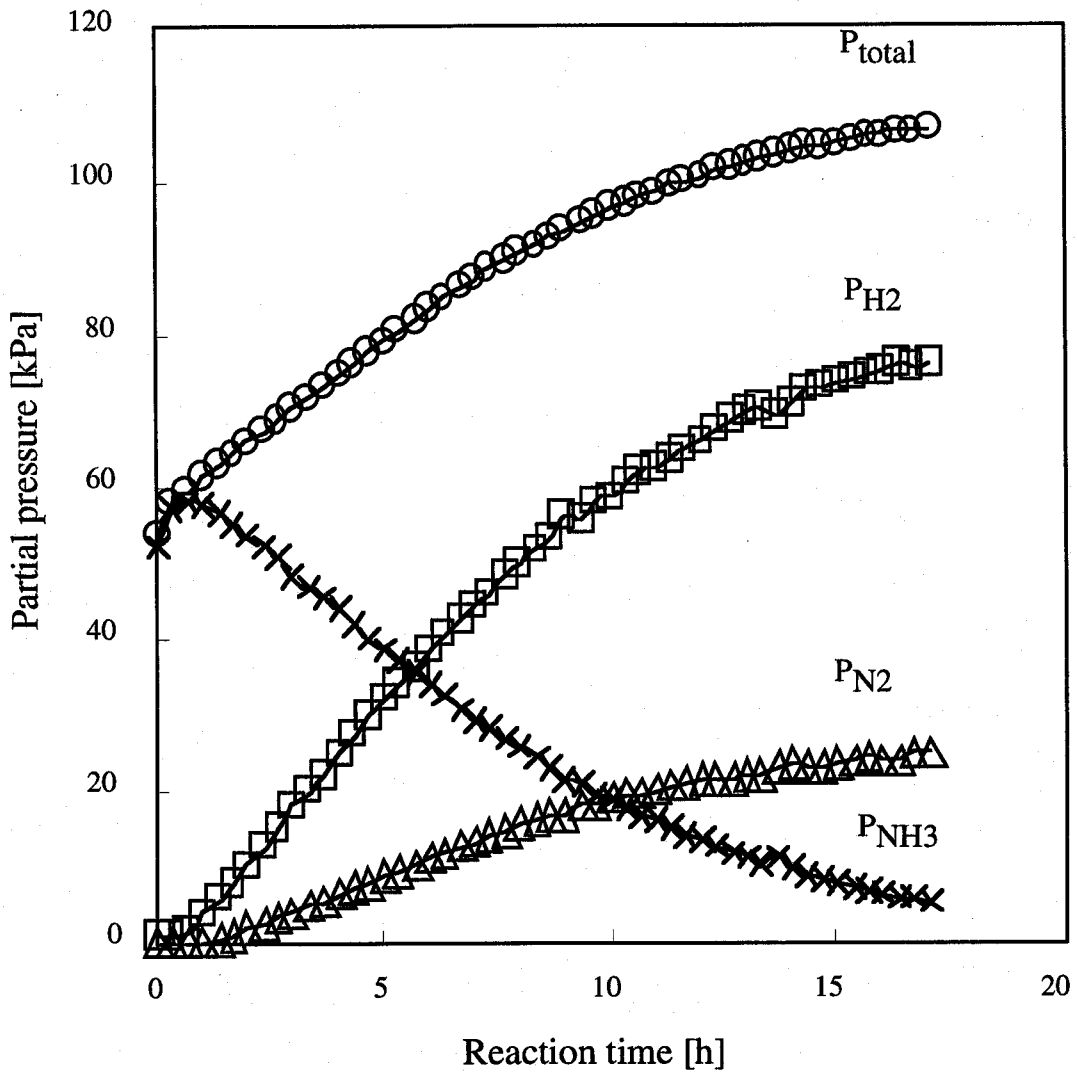

Fig. 2.5 Time variation of the total pressure and partial pressures of NH_3, N_2 and H_2 during the reaction of neodymium with static NH_3 gas at 700°C

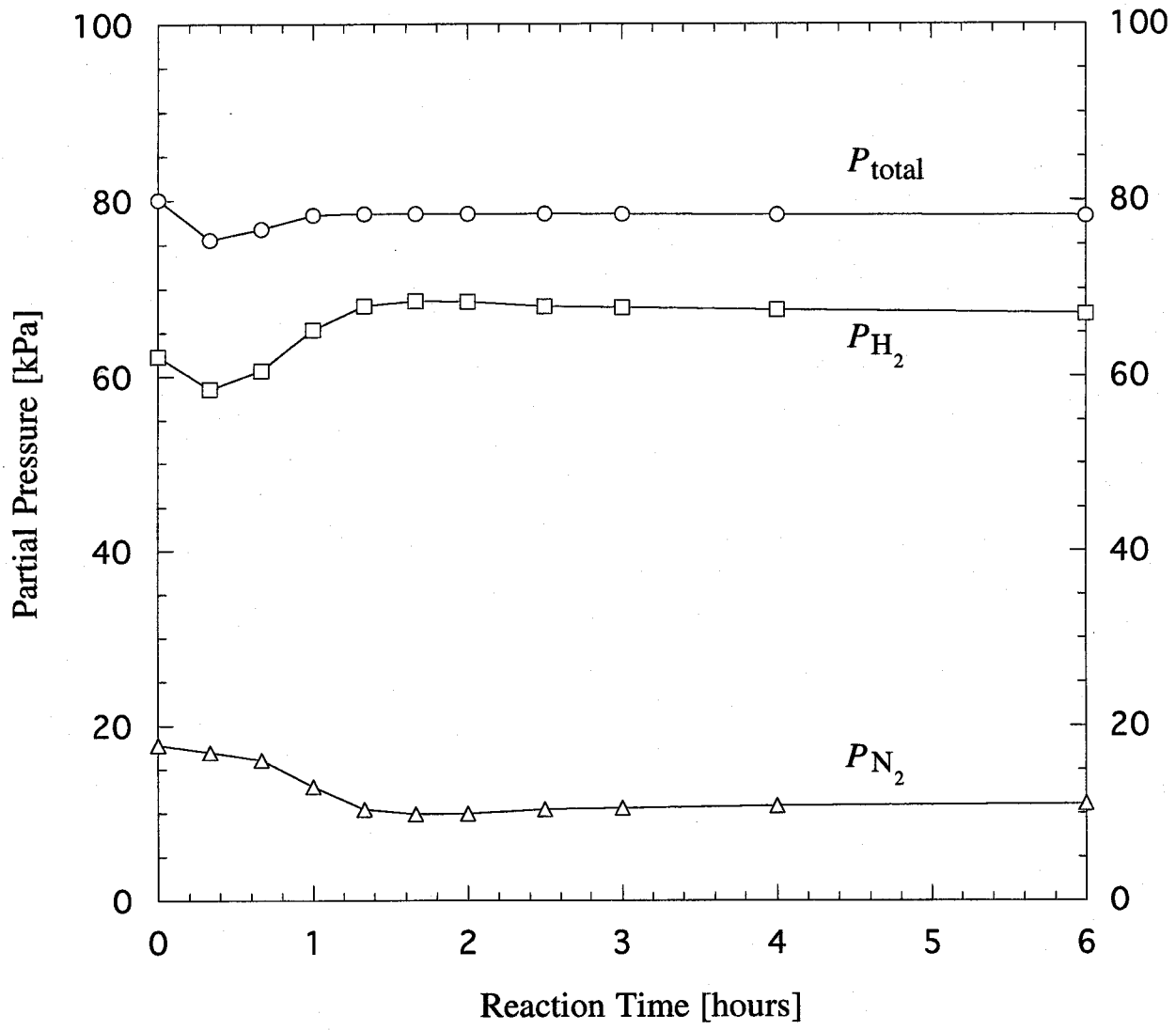

Fig. 2.6 Time variation of the partial pressures of N_2 and H_2 and the total pressure during the reaction of Nd with a mixture of N_2 and H_2 at 700°C

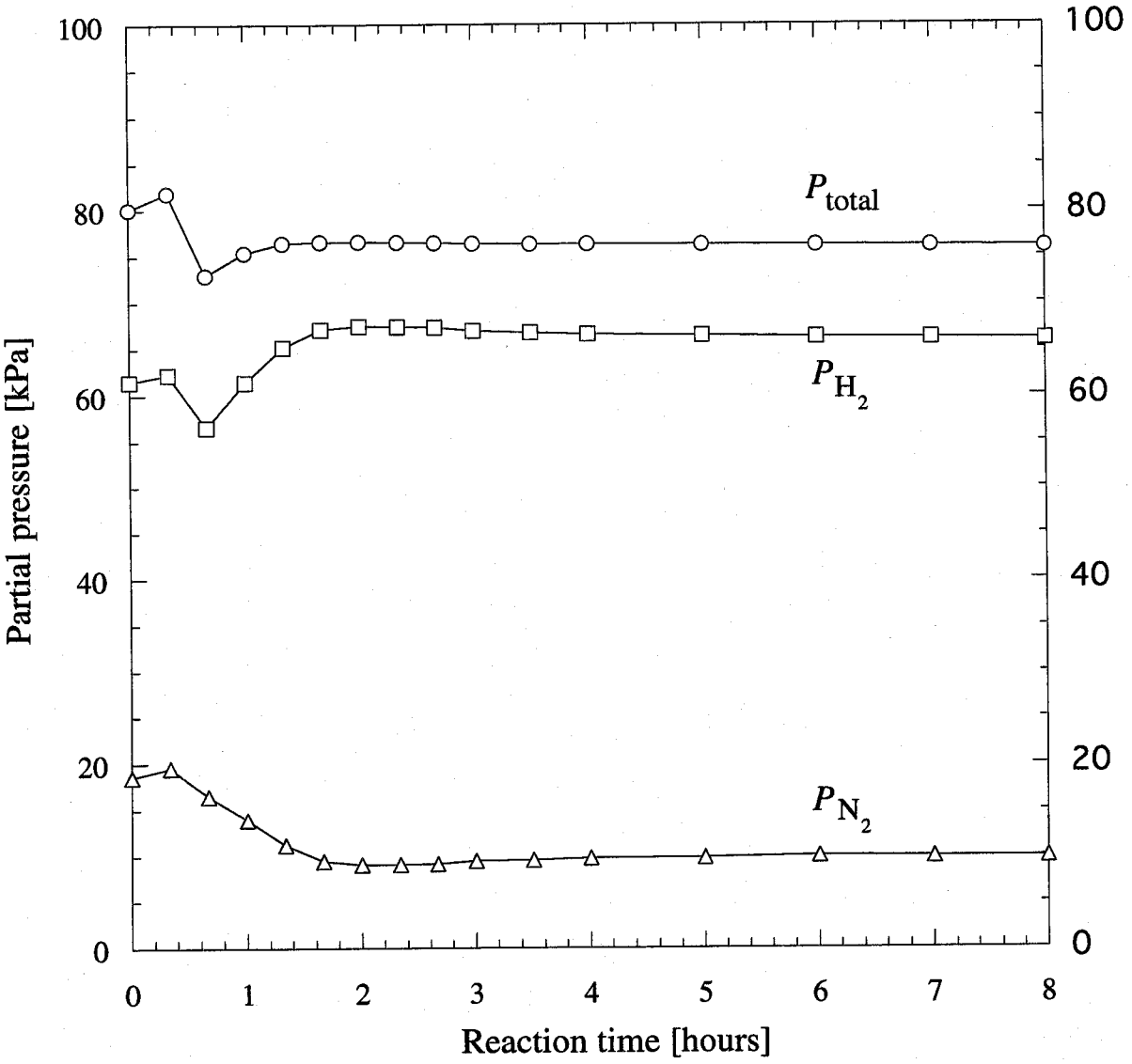

Fig. 2.7 Time variation of the partial pressures of N_2 and H_2 and the total pressure during the reaction of Pr with a mixture of N_2 and H_2 at 600°C

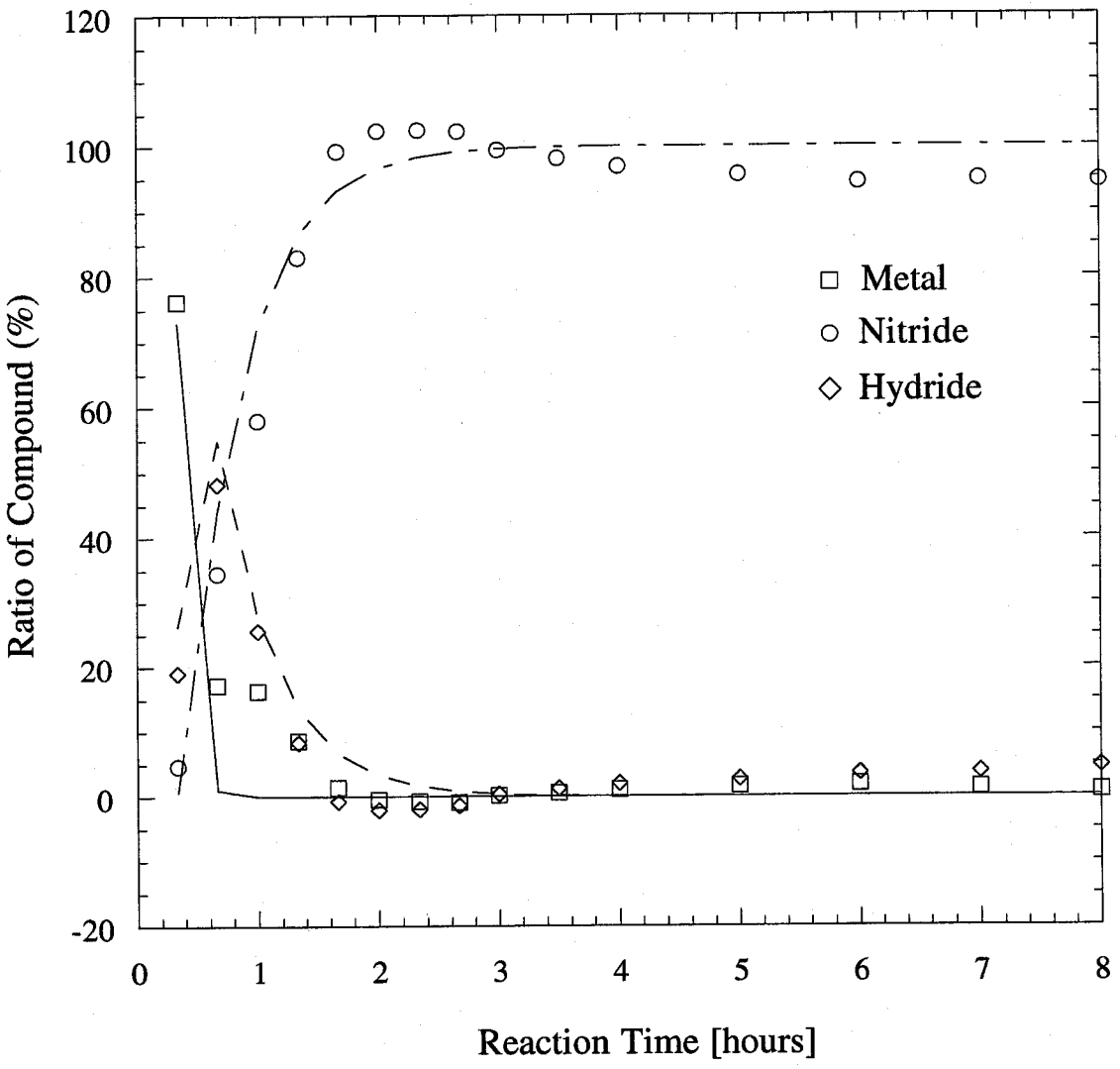

Fig. 2.8 The variation of Pr, PrN and PrH_2 ratios in solid phase during the reaction of Pr with the gaseous mixture of N_2 and H_2 at 600°C.

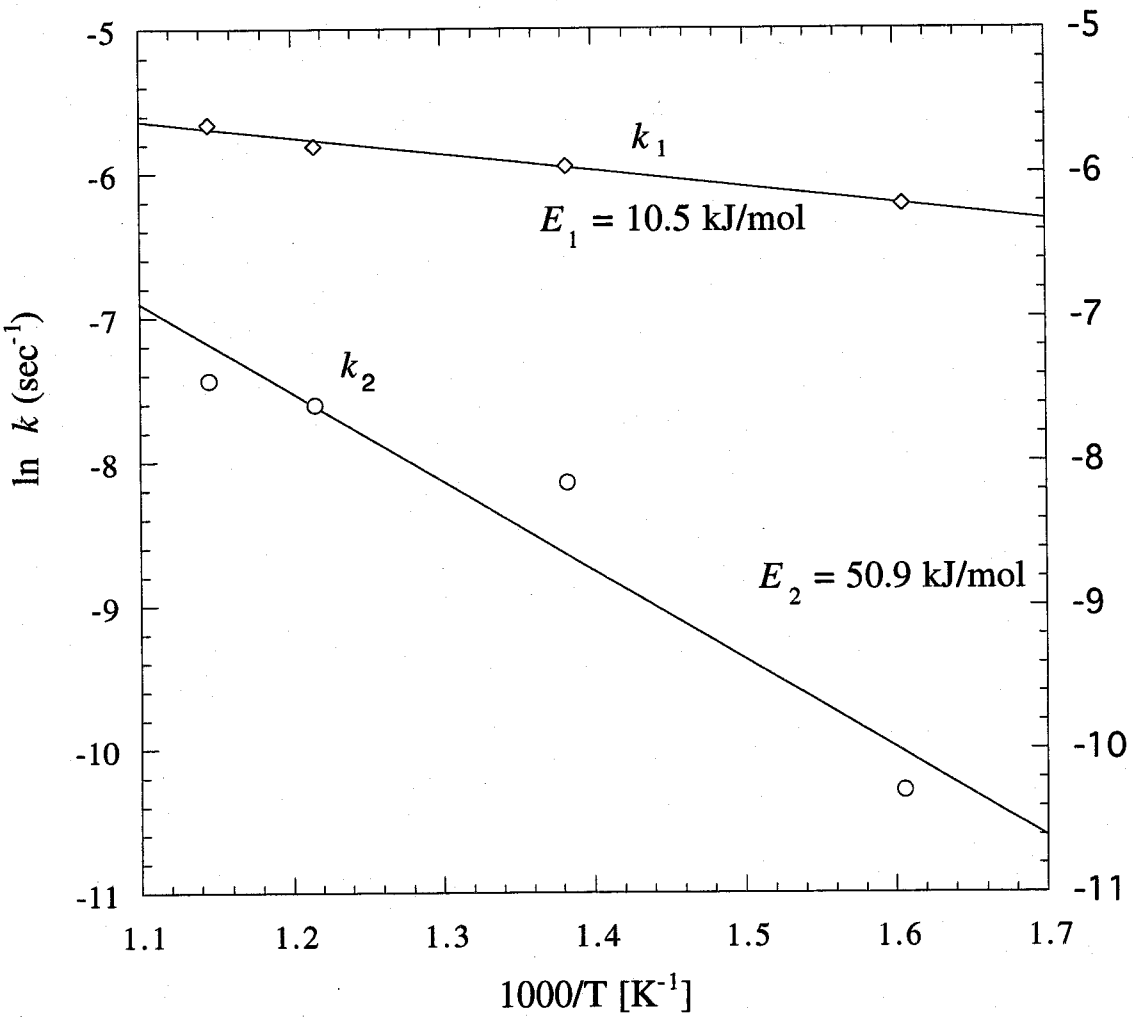

Fig. 2.9 The Arrhenius plots of logarithmic k_1 and k_2 against the reciprocal of the reaction temperature of Pr with the mixture of N_2 and H_2.

Chapter 3

Reactions of NH_3 and rare earth carbides prepared by carbothermic reduction

3.1 Introduction

The methods in which rare earth metals are nitrided at low temperatures have been described in the previous chapter. However, careful attention must be received in treating rare earth metals because they are sensitive to oxygen or moisture. Therefore, it may be desirable to develop a method of rare earth nitride formation from the stable compounds like oxides. Although actinide nitrides could be formed by the carbothermic reduction of oxides under NH_3 or a mixture of H_2 and N_2 atmosphere [1-8], no report regarding rare earth nitride formation from oxides via carbides is found. Thus, the preparation of rare earth nitrides starting from oxides, which are stable compounds in air, has been studied in this work.

Carbothermic reduction is one of the most popular methods of the carbide syntheses. Since Petterson first prepared the dicarbides of lanthanum and yttrium in an electric arc furnace by carbothermic reduction of the oxides [9], most subsequent investigators have employed this method or the modifications to prepare the rare earth carbides. A great deal of investigations on the rare earth carbides has been summarized by Adachi *et al* [10]. The existence of Ln_2C_3 and LnC_2 (Ln : rare earth elements) has been known in the binary systems between respective rare earth elements and carbon. Ln_2C_3 has a Pu_2C_3 type crystal structure [11, 12]. The room temperature forms of LnC_2 possess a body centered tetragonal CaC_2 type structure and they transform to a face centered cubic at a high temperature [13]. The transition temperatures of LnC_2 increase with increasing atomic numbers, roughly following a straight line [13]. Existence of LnC_6 type compounds, in which rare earth atoms are located on centers of graphite hexagons and form a triangular lattice with an atomic distance three times the unit vector of

graphite, are confirmed only in Sm-, Eu-, and Yb-C systems [14-16]. These carbides are referred to as the first-stage intercalation compounds.

Although a number of processes are known for the preparation of the rare earth nitrides [17], no investigation is reported on the conversion of the rare earth carbides to their nitrides. If metal carbides are converted to nitrides, free carbon is liberated. Presence of the free carbon in solid phase causes a quite serious problem for the pure nitride synthesis. Katsura estimated, thermodynamically, nitrogen and hydrogen activities of a gas phase containing NH_3, N_2 and H_2, and showed that if the extent of dissociation of NH_3 was maintained lower than the equilibrium dissociation degree, extremely high nitrogen and hydrogen activities were obtained.[18] In this work NH_3 stream is employed with the aim of nitridation of carbides and removal of free carbon liberated in solid phase, since NH_3 works as both a nitriding agent and a hydriding agent.

3.2 Experimental

3.2.1 Materials

Powders of CeO_2 (99.999%), Pr_6O_{11} (99.999%), and Nd_2O_3 (99.999%) were supplied from The Nilaco Corporation. Sm_2O_3 (99,99%), Eu_2O_3 (99,99%), Gd_2O_3 (99.99%) and Tb_4O_7 (99.9%) powders from Rare Metallic Co., Ltd. Carbon material which was used to reduce the rare earth oxides was powdered amorphous carbon (non-graphitic carbon, E.EERCK AG Darmstadt, Germany). The reactant gases used in this work were NH_3 (99.998%), H_2 (99.999%), and N_2 (99.999%).

3.2.2 Apparatus

Experimental apparatus consisted of a vacuum system, a gas supply system, a reaction tube, and a gas analysis system. The vacuum system, which was composed of two rotary pumps and an oil diffusion pump, could evacuate the reaction system up to the order of 10^{-5} Pa. The reaction tube made from alumina was fitted into a cylindrical resistance furnace. It could be used safely even over 1450°C, and an alumina boat, onto which a sample was loaded, was placed in it. The furnace was controlled by an

on-off type thermoregulator activated by P.R. thermocouple attached to the surface of the reaction tube. Temperature of the sample was measured by the P.R. thermocouple placed close to the sample. A gas chromatograph (type GC-8APT, Shimadzu & Co. Ltd., Japan) equipped with a thermal conductivity detector and columns packed with Chromosorb and Molecular Sieve, an integrator (type C-R6A, Shimadzu & Co. Ltd., Japan), and a gas sampler with two sampling loops constituted the gas analysis system. Helium gas (99.999%) was used as carrier gas. Another rotary pump was employed to prevent carrier gas from intruding into the reaction system.

3.2.3 Procedure

The powders of rare earth oxide and amorphous carbon were weighed so as to arrange the molar ratio of C/Ln (Ln = Ce, Pr, Nd, Sm, Eu, Gd, and Tb) at 4.5. They were thoroughly mixed in an agate mortar with an agate pestle after polyvinylalcohol was added as a binder. Then, they were pressed under 250 MPa into pellets, 10 mm in diameter and 1.2 mm in height. The pellet was placed in the alumina boat and the boat was put into the reaction tube. The system was evacuated to the order of 10^{-5} Pa and heated up to 1450°C and the temperature of the sample was kept at this temperature for 12 hours. During this carbothermic reduction, the pressure in the reaction system gained up to the order of 10^{-3} Pa presumably due to the generation of CO according to the reaction equation; $Ln_xO_y + (2x + y)C = xLnC_2 + yCO$. Re-establishment of the initial pressure (10^{-5} Pa order) in the reaction system was regarded as the completion of carbothermic reduction. After carbothermic reduction, the sample was quenched to room temperature and the reaction tube was filled with Ar gas to avoid oxygen contamination. The reaction product was separated into two portions. One was subjected to the X-ray diffraction (XRD) at room temperature in order to identify the solid product. The other was put on a reaction boat and inserted into the reaction system again to be reacted with a NH_3 stream. The reaction system was evacuated to 10^{-5} Pa order. Thereafter, NH_3 was introduced in it at a flow rate of 200 ml/min. and the temperature of specimen was elevated to the pre-determined temperature. The total pressure, P_{total}, and the partial pressures of NH_3 and N_2, P_{NH3} and P_{N2}, were measured at intervals: P_{total} by a capacitance manometer and P_{NH3} and P_{N2} by a gas chromatograph. The partial pressure of H_2, P_{H2}, was estimated by the relation of P_{total} =

$P_{NH3} + P_{N2} + P_{H2}$. After the stationary state was established, the specimen was quenched to room temperature and pulverized for XRD in Ar atmosphere. As to Ce, Pr, and Nd compounds, parts of the solid products were leached in 10N HNO_3 to dissolve the lanthanide nitrides. The solution was filtered off through the glass filter to check whether insoluble residue (free carbon) was present or not. For comparison of hydriding ability of NH_3 with that of H_2, the similar experiments were conducted for the reactions of cerium, praseodymium, and neodymium carbides with stream of 25%N_2-75%H_2.

X-ray diffraction powder patterns of the solid products were obtained at room temperature with diffractometer (Rigaku Denki, Geiger Flex RAD-rA) using Cu K_α radiation monochromatized by graphite. Each reaction product was embedded in a glass plate with silicon grease in order to minimize oxidation during XRD because lanthanide carbides and nitrides were very sensitive to oxygen or moisture in air. Operation to prepare the samples for XRD was carried out in Ar atmosphere.

3.3 Results and Discussion

3.3.1 Catbothermic reduction of the rare earth oxides

The X-ray diffraction patterns of the products obtained by the reaction of rare earth oxides with amorphous carbon show in Fig 3.1. As for Ce, Pr, Nd, Gd and Tb, these profiles indicate the formation of rare earth dicarbides, LnC_2, with CaC_2 type crystal structure. However, SmC_2 and EuC_2 were not obtained even under the condition similar to the other rare earth dicarbide formation. The profiles obtained with Sm and Eu indicate the diffraction pattern of graphite only. During this carbothermic reduction of CeO_2, Pr_6O_{11}, Nd_2O_3, Gd_2O_3 and Tb_4O_7, the pressure in the reaction system increased up to the order of 10^{-2} Pa presumably due to the generation of CO in the following chemical equation;

$$Ln_xO_y + (2x + y)C = xLnC_2 + yCO. \qquad (3.1)$$

The initial pressure (10^{-5} Pa order) was re-established at the end of the runs. Sharp increase in the pressure was observed at a temperature range between 1200°C and 1300°C, which indicates the carbothermic reduction begins at temperatures in the range. Table 3.1 summarizes the lattice parameters of rare earth dicarbides obtained in this

work. The lattice parameters of LnC_2 calculated from the X-ray diffraction patterns are in good agreement with the values previously reported [13].

3.3.2 Graphitization of amorphous carbon

As mentioned above graphite was obtained by heat-treatment of a mixture of, Sm_2O_3 or Eu_2O_3, and amorphous carbon (mixing ratio C/Ln = 4.5) at 1450°C in vacuum for 12 hours. Mixtures of oxide and amorphous carbon with mixing ratios, C/Ln =3.5 and 5.5, were also annealed at 1450°C in vacuum for 12 hours. In any case examined, amorphous carbon was converted to graphite and no carbide was formed as shown in Fig. 3.2. For comparison, a pellet of amorphous carbon annealed at 1450°C in vacuum. It was not graphitizated, however. Therefore, it is conceivable from these results that Sm, Eu, or their compounds play an important role in graphitization of amorphous carbon. Then, mixtures of Sm_2O_3 and amorphous carbon (mixing ratio C/Sm = 4.5) were heated at various temperatures in vacuum for 12 hours. Fig. 3.3 shows the X-ray diffraction patterns of the starting material (Sm_2O_3 + amorphous carbon) and the products obtained at 1100°C, 1200°C and 1300°C. As can be seen in Fig 3.3, X-ray diffraction profiles of the mixtures heat-treated below 1200°C still show existence of Sm_2O_3, but at 1300°C or higher Sm_2O_3 disappeared and the graphite was formed. It is obvious that the graphitization of amorphous carbon in the mixture occurs between 1200°C and 1300°C. Since in this temperature range other rare earth oxides are reduced by carbon, samarium carbide would have participated in the graphitization of amorphous carbon. No samarium compounds was found in the boat after the annealing, which indicates all samarium was vaporized in the reaction. Seiver *et al.* [19] have reported that SmC_2(s) decomposed into Sm(g) and graphite(s) at temperatures higher than 1400 K and the equilibrium vapor pressure of Sm(g) is expressed by

$$\ln P_{Sm}(\text{atm}) = \{(-31.5 \pm 3)/T\} + (8.1 \pm 0.2) \qquad (T = 1400 - 2080\text{K}). \quad (3.2)$$

Equilibrium vapor pressure of Sm at 1450°C is 3.93×10^{-5} atm (3.98 Pa) according to this equation. This value is much higher than the inner pressure of the reaction tube during the heat treatment (10^{-2}–10^{-5} Pa). If SmC_2 formed by the reaction of Sm_2O_3 with amorphous carbon, it decomposed to samarium vapor and graphite. The formation of SmC_2 was not confirmed in this work. Thus, this process has not been proved yet. Seiver *et al.* have not pointed out the reason why hexagonal graphite formed by decomposition of tetragonal samarium dicarbide. Samarium and europium formed the

graphite intercalation compound, SmC_6 and EuC_6. Intercalation compounds of the other rare earth metals except for ytterbium have not been reported yet. Thus, it is thought that the intercalation compounds, SmC_6 and ErC_6, were formed and decomposed to, Sm and Er, and graphite in the process of the graphitization of amorphous carbon by heat treatment of a mixture of amorphous carbon and, Sm_2O_3 or Er_2O_3. Further work is now in progress to clarify this process.

3.3.3. Reactions of the rare earth carbides with NH_3 gas

The rare earth dicarbides prepared by carbothermic reduction below mentioned were reacted with NH_3 stream. Conditions and results of nitridation of the carbides are shown in Table 3.2. All dicarbides were found to be converted into mononitrides by stream of NH_3. X-ray diffraction patterns of the respective rare earth nitrides obtained by runs 3.3.1–3.3.5 are given in fig. 3.4. Figure 3.5 shows the change in the total pressure and partial pressures of NH_3, N_2, H_2, and CH_4 in run 3.3.2. Methane was detected at the period from 2 to 4.5 hours, which indicates the nitridation of PrC_2 began around 2 hours and then free carbon liberated during nitridation of carbide reacts with NH_3. The reaction product in this run was leached in 10N HNO_3 to find no insoluble residual. For comparison, CeC_2, PrC_2 and NdC_2 were also reacted with a 75%H_2-25%N_2 gas. Conditions and results of the reaction of these three dicarbides with H_2 and N_2 mixture are also summarized in Table 3.2. Figure 3.6 shows changes in the total pressure and partial pressures of N_2 and H_2 in run 3.3.7. X-ray diffraction pattern of the solid phase of this run indicated the PrN formation. Methane was not detected all through the run, and insoluble residual was found in nitric acid in which this product was leached. These facts indicate that PrC_2 also reacts with N_2 to form PrN and the liberated carbon is amorphous carbon. Moreover, the liberated carbon was not reacted with H_2 at 900°C. Katsura derived nitrogen and hydrogen activities, a_N and a_H, exhibited by an unstable gaseous mixture of NH_3, N_2 and H_2 [18]. These activities are represented by the following equations.

$$a_N = \frac{1}{K_P}\frac{P_{NH3}}{P_{H2}^{3/2}} \quad , \tag{3.3}$$

$$a_H = \left(\frac{1}{K_P}\frac{P_{NH3}}{P_{N2}^{1/2}}\right)^{1/3} \quad . \tag{3.4}$$

Here K_P is the equilibrium constant of the reaction $\frac{1}{2}N_2 + \frac{3}{2}H_2 = NH_3$ and P means a partial pressure. The values of a_N and a_H at the end of each run are given in Table 3.2. As seen this table, extremely higher nitrogen and hydrogen activities are obtained by use of NH_3 stream compared to use of a 25%N_2-75%H_2 mixture. In spite of large difference of nitrogen activity between NH_3 and N_2/H_2 mixture, only mononitrides were obtained by the reaction of dicarbides either with NH_3 or with N_2-H_2 mixture. This indicates that no nitrides higher than mononitrides are existence in Ce-N, Pr-N, Nd-N, Gd-N and Tb-N systems. As shown in Table 3.2, only NH_3 stream, which shows high hydrogen activity, leads to formation of CH_4. Thus, higher hydrogen activity possesses an ability of proceeding the hydride reaction faster or decreasing the activation energy of hydridation. Figure 3.7 shows the change in the total pressure and partial pressures of NH_3, N_2 and H_2 during run 3.3.4. In this run, CH_4 was not detected because the partial pressure of CH_4 becomes lower as temperature increases. The reaction of GdC_2 with NH_3 at 900°C did not complete although the experiment was continued for 40 hours. The GdC_2 and GdN phases were observed in the product of this reaction. Single GdN phase was obtained by the reaction at 1000°C. However, single TbN phase was not formed successfully even at 1100°C for 40 hours. These facts suggest that heavier rare earth dicarbide is more stable against NH_3. At 1200°C, TbC_2 could be converted to TbN using NH_3 stream. As most of NH_3 was decomposed to N_2 and H_2 at this high temperature in spite of at a higher flow rate (250ml/min.) and partial pressure of NH_3 decreased below detection level (5 Pa), nitrogen and hydrogen activities could not be estimated during this reaction.

In run 3.3.9, graphite was used as a starting material to prepare CeC_2. CeC_2 could be formed from either amorphous carbon or graphite. X-ray diffraction pattern of the solid product of run 3.3.9 shown in Fig. 3.8 indicates the formation of CeN and presence of graphite. This graphite was not carbon liberated in the nitridation of carbide and was the excess carbon added at carbide formation. This fact indicates graphite is difficult to be removed even by flowing ammonia at 900°C. To confirm this point, amorphous carbon and graphite were reacted with flowing NH_3. For comparison, amorphous carbon was also reacted with a mixture of N_2 and H_2. As shown in table 3.3, during the runs 3.3.13 and 14 the gaschromatogram did not reveal the presence of CH_4, whereas, in runs 3.3.10–12, the amount of CH_4 continued to

decrease with time until it fell well below the detection limit. The visual observation of the carbon sample made at intervals clearly showed that the amount of the sample continued to decrease and eventually almost all the carbon sample was removed from the boat. However, after run 3.3.12 (the initial carbon:0.50 g), a small amount of solid remained in the boat and this was identified to be graphite by XRD analysis. Although a solid material was present in the boat after runs 3.3.10 and 11 (the initial amount of carbon: 0.048g), the amounts were too little to make significant diffraction. In other words, the amorphous carbon includes a small amount of graphite. These results show that only the combination of the amorphous carbon and a stream of NH_3 may lead to the formation of CH_4 and neither the combination of graphite and NH_3 and nor that of amorphous carbon and a stream of H_2 can produce CH_4 at 900°C. These experimental facts may suggest that both high hydrogen activity $a_{H,}$ exhibited by a stream of NH_3 and high carbon activity, a_C, of the active carbon play key roles in the formation of CH_4. This can be considered thermodynamically as follows.

The reaction between the carbide and NH_3 may consist of two steps. In the first step, NH_3 reacts with the carbide to form the nitride and free carbon. This is followed by the formation of CH_4 by the reaction of the free carbon with NH_3, resulting in the removal of the free carbon from the reaction products. This reaction may be expressed as

$$\mathrm{C(s)} + \frac{4}{3}\mathrm{NH_3(g)} = \mathrm{CH_4(g)} + \frac{2}{3}\mathrm{N_2(g)}. \tag{3.5}$$

When carbon reacts with NH_3 according to eqn. 3.5, the following relation must hold

$$\mu(\mathrm{C}) + \frac{4}{3}\mu(\mathrm{NH_3}) = \mu(\mathrm{CH_4}) + \frac{2}{3}\mu(\mathrm{N_2}), \tag{3.6}$$

where μ denotes the chemical potential. It is easily shown that eqn. 3.6 leads to the following equation

$$\frac{4}{3}\Delta G_{\mathrm{f}}^{\circ}(\mathrm{NH_3}) - \Delta G_{\mathrm{f}}^{\circ}(\mathrm{CH_4}) = RT\ln\frac{P_{\mathrm{CH4}}}{a_c}\left(\frac{P_{\mathrm{N2}}^{1/2}}{P_{\mathrm{NH3}}}\right)^{4/3}. \tag{3.7}$$

where P is the partial pressure, a_C is carbon activity, $\Delta G^{\circ}_{\mathrm{f}}$ is standard free energy of formation, R is gas constant and T is temperature. Using the relation $\Delta G_{\mathrm{f}}^{\circ} = -RT\ln K_p$, one obtains

$$P_{CH4} = a_C K_{p,CH4} \left(\frac{P_{NH3}}{K_{p,NH3} P_{N2}^{1/2}} \right)^{4/3} . \quad (3.8)$$

where $K_{p,NH3}$ is the equilibrium constant for $\frac{1}{2}N_2 + \frac{3}{2}H_2 = NH_3$ and $K_{p,CH4}$ is that for $C+2H_2=CH_4$. Substitution of eqn. 3.4 into eqn. 3.8 yields

$$P_{CH4} = a_C K_{p,CH4} a_H^4 . \quad (3.9)$$

Since a_c, $K_{p,CH4}$ and $K_{p,NH3}$ are constant at a given temperature, P_{CH4} depends only on $P_{NH3} / P_{N2}^{1/2}$ and consequently on hydrogen activity a_H. The total pressure of ammonia, nitrogen and hydrogen is kept constant. Partial pressure of methane never reached the equilibrium one because the methane produced in the reaction tube is soon swept away by flowing ammonia gas and thus is at a pressure well below 1 bar as shown in fig. 3.5. However, equilibrium partial methane pressure can be estimated using eqn. 3.8. When partial pressures of ammonia and nitrogen are expressed in terms of dissociation degree, α, of ammonia, the eqn. 3.9 is rewritten by

$$P_{CH_4} = a_c K_{p,CH_4} K_{p,NH_3}^{-4/3} \left(\frac{\sqrt{2 \cdot P_{total}} \cdot (1-\alpha)}{\sqrt{\alpha(1+\alpha)}} \right)^{4/3} . \quad (3.10)$$

Assuming that total pressure ($P_{total} = P_{NH3} + P_{N2} + P_{H2}$) maintains at 1 bar and activity of free carbon is unity, the equilibrium partial pressure of methane becomes enormously high as shown in Fig. 3.9. The equilibrium methane pressure increases with decreasing dissociation degree of ammonia and decreasing temperature. Under 1 bar H_2 atmosphere at 900°C, CH_4 of 1920 Pa equilibrates carbon, of which activity is unity [20]. When the largest value of the dissociation degree of NH_3 obtained in the run 3.3.2 is substituted in eqn. 3.10, the equilibrium partial pressure of CH_4 becomes 104 bars. Suppression of dissociation degree of NH_3 leads to high equilibrium partial pressure of CH_4.

Generally, it is said that HCN is generated during nitridation by carbothermic reduction, which is carried out in N_2 and H_2 mixture atmosphere [1, 21]. However, in this work, HCN was not detected all through the experiments. Figure 3.10 shows the composition of gas phase by the reaction of C + NH_3 at several temperatures where equilibrium is established under 1 bar. Partial pressure of CH_4 is higher than that of HCN in the temperature range at which the experiments were performed in this work. Therefore, CH_4 was formed by the reaction of liberated carbon with NH_3 in this work.

Thus, preparation of nitrides by carbothermic reduction should be carried out below 1200°C to refrain from generating toxic HCN.

3.3.4 Preparation of rare earth mixed nitrides

Carbothermic reduction and ammonia nitridation methods above mentioned seem to be applicable to prepare rare earth mixed carbides and nitrides. First, the solubilities between two kinds of rare earth oxides were examined for preparation of the rare earth mixed carbides and nitrides. CeO_2 and Pr_6O_{11} powders were mixed in an agate mortar at a given ration and the mixture powder was pressed into the pellets. Then the pellets were sintered at 1400°C in air for 12 hours. The X-ray diffraction patterns of sintered mixtures of Ce and Pr oxides indicate the presence of a single phase of cerium-praseodymium mixed dioxide $(Ce, Pr)O_2$ (CeO_2 type) up to a Pr_6O_{11} content of 40 mol%, and two phases of $(Ce, Pr)O_2$ and $(Pr, Ce)_6O_{11}$ (Pr_6O_{11} type) within the range of $0.10 \leq x \leq 0.55$ (x denotes the ratio of cerium to metal). Fig. 3.11 shows the X-ray diffraction patterns of the sintered oxide mixtures of CeO_2 and Pr_6O_{11} with the mixing ratios, Ce/(Ce+Pr) = 0.55 and 0.60. Table 3.4 summarizes the results and conditions of sintering oxide mixture. These results are similar to those reported by Nauer *et al.* [22], but they are inconsistent with those reported by Takasu *et al.* [23]. However, the obtained data agree with the latter in that two fluorite phases coexist even at low CeO_2 contents. Figure 3.12 shows the relation between lattice parameters of sintered oxide mixtures and mixing ratio. Lattice parameter of $(Ce, Pr)O_2$ changes linearly over a domain of single phase. In the two-phase domain lattice parameters of both $(Ce, Pr)O_2$ and $(Pr, Ce)_6O_{11}$ are constant and the respective values are 0.5403 and 0.5466 nm. This lattice parameter of $(Ce, Pr)O_2$, 0.5403 nm, corresponds to x=0.58, which is the terminal composition of the single phase domain.

The similar experiments were carried out for CeO_2 and Tb_4O_7. Single phase Ce-Tb mixed oxide was obtained by sintering the oxide mixture at 1400°C in air for 12 hours only in the case that the mixing ratio Ce/(Ce+Tb) was 0.90. Two oxide phases were observed in the sintered oxide mixtures in the other mixing ratio (0.10~0.80). The XRD patterns of the sintered mixtures in the mixing ratios of 0.90 and 0.80 are given in Fig. 3.13. These results indicate that the CeO_2 and Tb_4O_7 are partially miscible within a very narrow range.

Single phase of cerium-praseodymium mixed dicarbide, $Ce_xPr_{1-x}C_2$ (bct structure), was obtained by carbothermic reduction of the sintered oxide mixture above mentioned for several selected values of x (x=0~1). The similar results were obtained from carbothermic reduction of as-blended oxide mixtures. The results of XRD suggest that if compared at the same x value, the heat treatment of oxide mixture has no effect in the final results. It is also found from these results that cerium dicarbide and praseodymium dicarbide are completely miscible, as suggested by Adachi *et al.* [10]. They pointed out that lattice parameters of cerium-praseodymium mixed dicarbide followed Vegard's law over the whole range. However, the results in this work show clearly a negative deviation from Vergard's law. The relation between lattice parameters and cerium to metal ratio is given in Fig. 3.14. The lattice parameters of CeC_2 and PrC_2 prepared by carbothermic reduction in this work are a=0.3883nm and c=0.6495nm, and a=0.3854nm and c=0.6434nm, respectively, and these values are in good agreement with those reported previously (a=0.388nm and c=0.649nm for CeC_2 and a=0.3855nm and c=0.6434nm for PrC_2) [13, 25]. The smooth variation of lattice parameters a and c value and of tetragonality c/a value may suggest that cerium and praseodymium atoms are distributed at random. It is observed that the dicarbides are easily formed irrespective of whether the mixtures of CeO_2 and Pr_6O_{11} have been heat-treated or not. This fact may suggest that CeC_2-PrC_2 mixed carbides are thermodynamically considerably stable compared with their simple mixtures. However, it is not clear in what stage of the carbothermic reduction the mixing of Ce and Pr atoms occur. Further work is now in progress to clarify this point.

Ce-Tb mixed dicarbides were also prepared by carbothermic reduction of oxide mixtures of CeO_2 and Tb_4O_7. Single phase dicarbides, $Ce_xTb_{1-x}C_2$, were obtained at any mixing ratios examined in this work. This indicates that CeC_2 and TbC_2 are also soluble in each other at any ratios. The plot of the lattice parameters of Ce-Tb mixed dicarbides versus cerium to metal ratio is given in Fig. 3.15. Contrary to the case of Ce-Pr mixed dicarbides, the lattice parameters of Ce-Tb mixed dicarbides varies linearly as the mixing ratio increases.

The thus prepared Ce-Ln (Ln=Pr and Tb) mixed dicarbides were also reacted with flowing NH_3. The conditions and results are summarized in Table 3.5. The relationship between the lattice parameters and composition of $Ce_xLn_{1-x}N$ is given in Fig.

3.16. Single phase mixed nitride (NaCl type) is obtained for all the x-values examined, indicating that CeN and LnN are completely miscible. When the plot of the lattice parameters of lanthanide mononitrides versus the radii of lanthanide trivalent ions is drawn, the lattice parameter of CeN deviates largely from the plot (Fig. 3.17) [17]. Cations in all lanthanide mononitrides except for CeN are trivalent. Cerium in its mononitride has, however, a valence higher than+3 (almost +4) [17]. Only Ce, Pr and Tb among lanthanide elements take tetravalent in their compounds. The radii of lanthanide tetravalent ions are smaller than those of trivalent ions [26]. If the valence of Pr or Tb in $Ce_xLn_{1-x}N$ becomes higher than +3, the lattice parameters of $Ce_xLn_{1-x}N$ take negative deviation from Vegard's law. On the other hand, if Ce in $Ce_xLn_{1-x}N$ has a smaller valence than that in CeN monophase, a positive deviation from Vegard's law would be observed. The lattice parameters of both Ce-Pr and -Tb mixed nitrides obey Vegard's law as shown in Fig. 3.16. This indicates the valence of Pr, Tb and Ce does not change in $Ce_xLn_{1-x}N$. In other words, Ce in mixed nitrides remains to be the tetravalent cation, and Tb and Pr the trivalent cations.

3.4 Conclusions

Rare earth dicarbides (CeC_2, PrC_2, NdC_2, GdC_2, and TbC_2) were prepared by carbothermic reduction of their oxides at 1450°C in vacuum. Graphite was formed by heat-treatment of mixtures of, Sm_2O_3 and Er_2O_3, and amorphous carbon (C/Ln = 4.5) at 1450°C in vacuum. The experiments of heat-treatment of the mixtures with different mixing ratios lead to the same results. Graphitization of amorphous carbon in the case of heat-treatment of mixture of Sm_2O_3 and amorphous carbon proceeds at the temperature range from 1200°C to 1300°C. This temperature just corresponds to the temperature at which carbothermic reduction of the other rare earth oxides proceeds.

The rare earth dicarbides (CeC_2, PrC_2, NdC_2, GdC_2 and TbC_2) react either with NH_3 stream or with N_2-H_2 mixture to form mononitrides (CeN, PrN, NdN, GdN and TbN). The rare earth dicarbides are more stable against NH_3 as mass number of rare earth element increases. No higher nitrides than mononitride are present in Ce-N, Pr-N Nd-N, Gd-N and Tb-N systems. Only the combination of amorphous carbon and NH_3 can

form CH_4. This may be ascribed to high hydrogen activity exhibited by a stream of NH_3 and high carbon activity of the active carbon. The reaction of free carbon with NH_3 below 1200°C does not result in the formation of HCN but results in CH_4.

Single (Ce, Pr)O_2 phase was obtained by sintering the mixture of CeO_2 and Pr_6O_{11} up to Pr_6O_{11} contents 40 mol% and two fluorite phases, (Ce, Pr)O_2 and (Pr, Ce)$_6O_{11}$, were obtained within $0.10 \leq x \leq 0.55$ (x is a cerium ratio to metal). Lattice parameters of (Ce, Pr)O_2 change linearly with composition in a region of cerium richer single phase. In a two-phase region, the values of lattice parameters of (Ce, Pr)O_2 and (Pr, Ce)$_6O_{11}$ are constant and they are 0.5403nm and 0.5466nm, respectively. The former corresponds to that of $(Ce_{0.58}Pr_{0.42})O_2$. CeO_2 and Tb_4O_7 are miscible within a very narrow range (Ce/(Ce+Tb)≥0.9). The mixed dicarbides $Ce_xLn_{1-x}C_2$ (Ln = Pr and Tb) were obtained by carbothermic reduction of sintered oxide mixtures as well as non-sintered ones. It is confirmed that CeC_2 and LnC_2 are completely miscible. The results of XRD of $Ce_xPr_{1-x}C_2$ indicate a negative deviation from Vegard's law. On the other hand, the lattice parameter of Ce-Tb mixed dicarbide varies linearly increasing with mixing ratio, Ce/(Ce+Tb). $Ce_xLn_{1-x}N$ were also prepared by reactions of $Ce_xLn_{1-x}C_2$ with NH_3. This is the first report of $Ce_xPr_{1-x}N$ and $Ce_xTb_{1-x}N$ formation. CeN and LnN are completely miscible and their lattice parameters obey Vegard's law.

References

[1] T. Ogawa, Y. Shirasu, M. Kazuo and H. Serizawa, *J. Nucl. Mater.* **247**(1997)151.

[2] T. Muromura and H. Tagawa, *J. Nucl. Mater.* **80**(1979)330.

[3] R. D. Shoup, *J. Am. Ceram. Soc.* **60**(1977)332

[4] G. Pautasso, K. Richter and C. Sari, *J. Nucl. Mater.* **158**(1988)12

[5] Y. Arai, S. Fukushima, K. Shiozawa and M. Handa, *J. Nucl. Mater.* **168**(1989)280.

[6] Y. Arai, C. Sari and J. C. Spirlet, *J. Nucl. Mater.* **185**(1991)159.

[7] P. Bardelle and D. Warin, *J. Nucl. Mater.* **188**(1992)36

[8] T. Ogawa, T. Ohmichi, A. Maeda, Y. Arai and Y. Suzuki, *J. Alloys Comp.* **224**(1995)55.

[9] O. Petterson, *Chem Ber.* **28**(1895)2419.

[10] G. Adachi, N. Imanaka and Z. Fuzhong, "Handbook on the Physics and Chemistry of Rare Earth," K. A. Gschneidner, Jr. and L. Eyring, ed., Elsevier Science Publishers B.V. (1991) Vol. 15, Chpt. 99, p. 62.

[11] L. Brewer and O. Krikorian, *J. Electrochem. Soc.* **103**(1956)38.

[12] W. H. Zachariasen, *Acta Cryst.* 5(1952)17.

[13] K. A. Gschneidner, Jr, and F. W. Calderwood, *Bull. Alloy Phase Diagrams*, **7**(1986)564.

[14] M. El-Makrini, D. Guérard, P. Lagrange and A. Hérold, *Physica B*, **99**(1980)481.

[15] H. Suematsu, K. Ohmatsu and R. Yoshizaki, *Solid State Commun.* **38**(1981)1103.

[16] M. Inagaki and Y. Maeda, "Introduction of Carbon Materials," Tanso-Zairyou-Gakkai, Tokyo (1984), Chpt. 8, p. 87. in Japanese.

[17] F. Hulliger, "Handbook on the Physics and Chemistry of Rare Earth," K.A.Gschneidner, Jr. And L. Eyring, ed., Elsevier Science Publishers B.V.(1979) **Vol.4**, Chpt.33, P.160 and P168.

[18] M. Katsura, *J. Alloys Comp.* **182**(1992)91.

[19] R. L. Seiver and H. A. Eick, *High Temp. Sci.* **3**(1971)292.

[20] M.W.Chase, Jr., C.A.Davies, J.R.Downey, Jr., D.J.Frurip, R.A.McDonald, and A.N.Synerud, "JANAF Thermochemical Tables, 3rd Ed.," J. Phys. Chem. Ref. Data, Vol. 14, suppl. 1, 1985, p600.

[21] A. W. Weimer, "carbide, nitride and boride materials synthesis and processing," A. W. Weimer, ed., Chapman & Hall, London (1997), pp. 79.

[22] M. Nauer, C. Ftikos and B. C. H. Steele., *J. Euro. Ceram. Soc.* **vol.14**(1994)493.

[23] Y. Takasu, T. Sugino and Y. Matsuda, *J. Appl. Electrochem.* **14**(1984)79.

[24] J. O. Sawyer, B.G Hyde and L. Eyring, *Bull. Soc. Chim. France*, (1965), pp. 1190.

[25] Spedding, *J. Am. Chem. Soc.* **80**(1958)4499.

[26] L. Eyring, "Handbook on the Physics and Chemistry of Rare Earth," K.A.Gschneidner, Jr. And L. Eyring, ed., Elsevier Science Publishers B.V.(1979) **Vol.3**, Chpt.27, pp. 340.

Table 3.1 Results of carbothermic reduction of lanthanide oxides[#].

Run	Starting material	Product*	Lattice parameters [nm]**	
			a	c
3.1.1	CeO_2	CeC_2	0.3883	0.6495
3.1.2	Pr_6O_{11}	PrC_2	0.3857	0.6441
3.1.3	Nd_2O_3	NdC_2	0.3826	0.6410
3.1.4	Gd_2O_3	GdC_2	0.3714	0.6277
3.1.5	Tb_4O_7	TbC_2	0.3693	0.6204

reaction temperature : 1450°C, reaction time : 12 hours

* containing a few weight percent of excess carbon

** crystal structure : CaC_2 type (body centered tetragonal)

Table 3.2 Conditions and results of nitridation of lanthanide dicarbides.

Run	Starting material*	Reactant gas	Temperature[°C]	Time [h]	Product§	Lattice parameter[nm]	Nitrogen activity	Hydrogen activity
3.3.1	CeC_2	NH_3#	900	20	CeN	0.5026	3.01×10^3	14.3
3.3.2	PrC_2	NH_3#	900	20	PrN	0.5169	3.04×10^3	14.5
3.3.3	NdC_2	NH_3#	900	20	NdN	0.5132	2.64×10^3	13.9
3.3.4	GdC_2	NH_3#	1000	40	GdN	0.4981	1.04×10^2	4.98
3.3.5	TbC_2	NH_3##	1200	40	TbN	0.4926	-†	-†
3.3.6	CeC_2	N_2+H_2###	900	20	CeN + C	0.5027	0.5	0.87
3.3.7	PrC_2	N_2+H_2###	900	20	PrN + C	0.5168	0.5	0.87
3.3.8	NdC_2	N_2+H_2###	900	20	NdN + C	0.5173	0.5	0.87
3.3.9	CeC_2**	NH_3#	900	20	CeN + C	0.5024	1.61×10^3	11.7

* containing a few weight percents of free carbon

** prepared by the reaction of CeO_2 with graphite at 1450°C in vacuum for 12 hours

§ crystal structure of nitride : NaCl type

flow rate : 200 ml/min.

flow rate : 250 ml/min.

flow rate : N_2 50 ml/min., H_2 150 ml/min.

† Activity could not be estimated because ammonia partial pressure was below detection level of gas chromatograph.

Table 3.3 Experimental results of reaction of carbon with a stream of NH_3 or H_2 at 900°C.

Run	Reaction	Time [h]	a_H	Detection of CH_4	Removal of carbon
3.3.10	Active carbon (0.048 g) +NH_3 (200 ml/min)	19	19	Detected	Removed
3.3.11	Active carbon (0.048 g)+NH_3 (200 ml/min)	9	21	Detected	Removed
3.3.12	Active carbon (0.50 g) +NH_3 (200 ml/min)	23	17	Detected	Removed
3.3.13	Graphite (0.048 g) +NH_3 (200 ml/min)	20	18	Not Detected	Not Removed
3.3.14	Active carbon (0.048 g) +H_2 (200 ml/min)	21	1	Not Detected	Not Removed

Table 3.4 The results and conditions of sintering mixture of CeO_2 and Pr_6O_{11}.

run	mass of starting material [g]		x (Ce to Ce + Pr ratio)	products	lattice parameter [nm]
	CeO_2	Pr_6O_{11}			
3.4.1	0.1048	0.9389	0.10	$(Ce,Pr)O_2$ $(Pr,Ce)_6O_{11}$	0.5405 0.5468
3.4.2	0.2109	0.8356	0.20	$(Ce,Pr)O_2$ $(Pr,Ce)_6O_{11}$	0.5399 0.5467
3.4.3	0.1820	0.4183	0.30	$(Ce,Pr)O_2$ $(Pr,Ce)_6O_{11}$	0.5402 0.5469
3.4.4	0.2414	0.3586	0.40	$(Ce,Pr)O_2$ $(Pr,Ce)_6O_{11}$	0.5401 0.5470
3.4.5	0.2990	0.3002	0.50	$(Ce,Pr)O_2$ $(Pr,Ce)_6O_{11}$	0.5403 0.5462
3.4.6	0.3314	0.2686	0.55	$(Ce,Pr)O_2$ $(Pr,Ce)_6O_{11}$	0.5403 0.5462
3.4.7	0.3606	0.2398	0.60	$Ce_{0.60}Pr_{0.40}O_2$	0.5406
3.4.8	0.4200	0.1794	0.70	$Ce_{0.70}Pr_{0.30}O_2$	0.5406
3.4.9	0.4808	0.1190	0.80	$Ce_{0.80}Pr_{0.20}O_2$	0.5407
3.4.10	0.5407	0.0598	0.90	$Ce_{0.90}Pr_{0.10}O_2$	0.5409

Table 3.5 The conditions and results of the experiments of mixed nitride formation.

run	reactant*	reaction time [h]	temp. [°C]	product	lattice parameter [nm]
3.4.11	CeC_2	45	900	CeN	0.5021
3.4.12	$Ce_{0.9}Pr_{0.1}C_2$	40	900	$Ce_{0.9}Pr_{0.1}N$	0.5032
3.4.13	$Ce_{0.7}Pr_{0.3}C_2$	25	900	$Ce_{0.7}Pr_{0.3}N$	0.5056
3.4.14	$Ce_{0.5}Pr_{0.5}C_2$	25	900	$Ce_{0.5}Pr_{0.5}N$	0.5101
3.4.15	$Ce_{0.3}Pr_{0.7}C_2$	25	900	$Ce_{0.3}Pr_{0.7}N$	0.5117
3.4.16	$Ce_{0.1}Pr_{0.9}C_2$	40	900	$Ce_{0.1}Pr_{0.9}N$	0.5145
3.4.17	PrC_2	20	900	PrN	0.5165
3.4.18	$Ce_{0.7}Tb_{0.3}C_2$	40	1200	$Ce_{0.7}Tb_{0.3}N$	0.4998
3.4.19	$Ce_{0.5}Tb_{0.5}C_2$	40	1200	$Ce_{0.5}Tb_{0.5}N$	0.4981
3.4.20	$Ce_{0.3}Tb_{0.7}C_2$	40	1200	$Ce_{0.3}Tb_{0.7}N$	0.4958
3.4.21	TbC_2	40	1200	TbN	0.4926

* containging a few weight percents of amorphous carbon

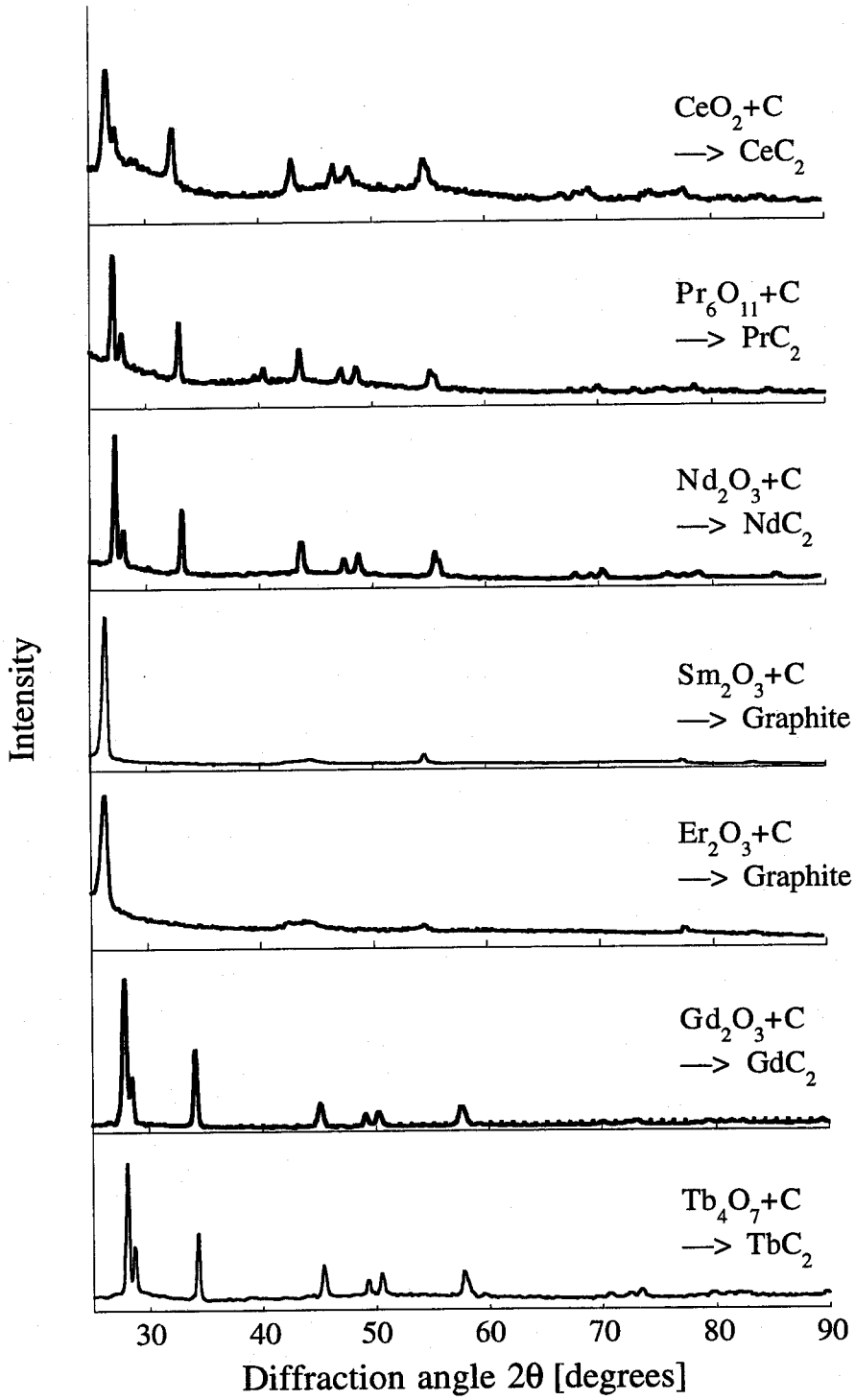

Fig. 3.1 X-ray diffraction patterns of the products obtained by the reactions of rare earth oxides with amorphous carbon in vacuum at 1450°C for 12 hours

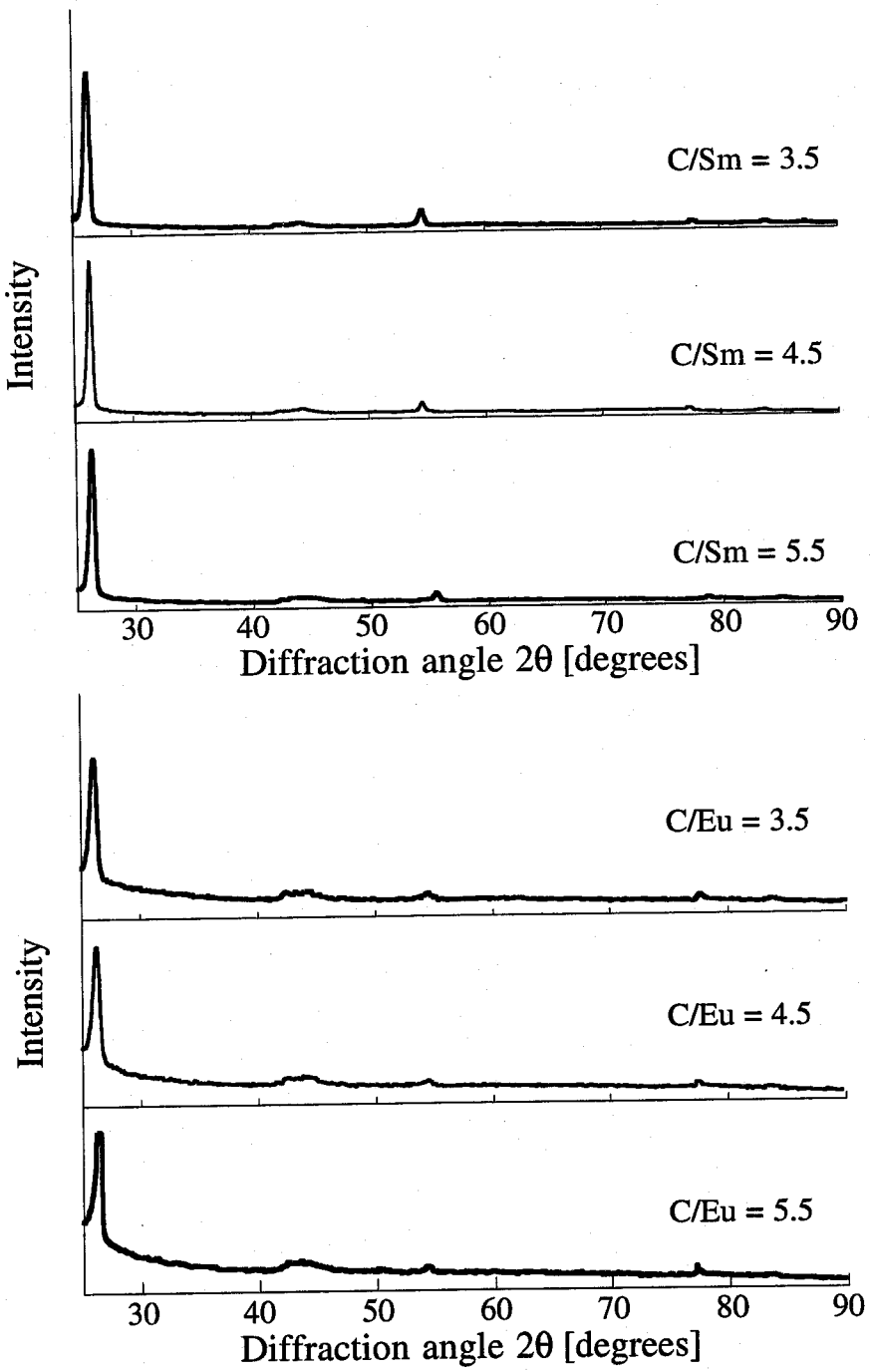

Fig. 3.2 X-ray diffraction patterns of the products obtained by the reactions of Sm_2O_3 and Eu_2O_3 with amorphous carbon at various mixing ratios (C/M = 3.5, 4.5 and 5.5) in vacuum at 1450°C for 12 hours

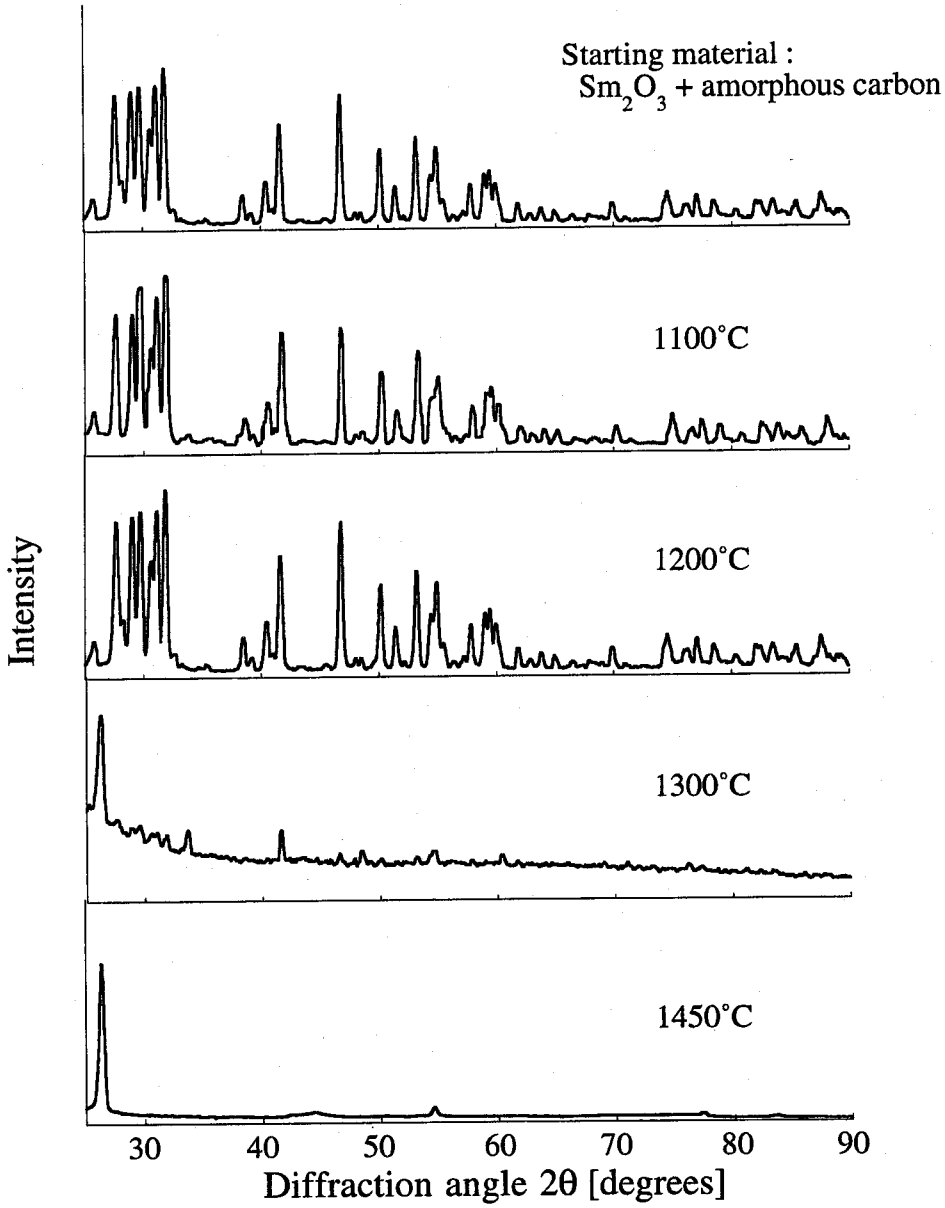

Fig. 3.3 X-ray diffraction patterns of the products obtained by the reactions of Sm_2O_3 with amorphous carbon in vacuum at several temperatures for 12 hours

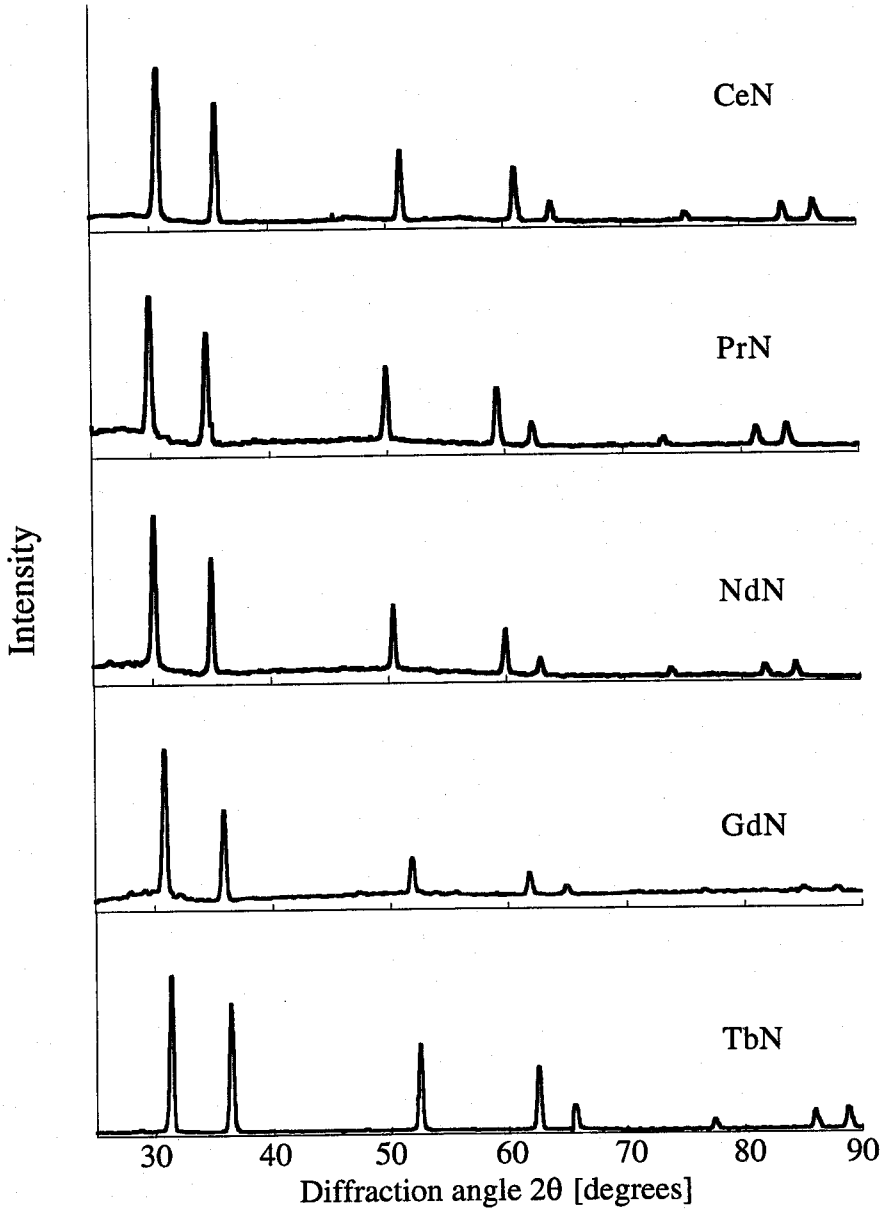

Fig. 3.4 X-ray diffraction patterns of the products obtained by the ractions of rare earth dicarbides with flowing NH_3

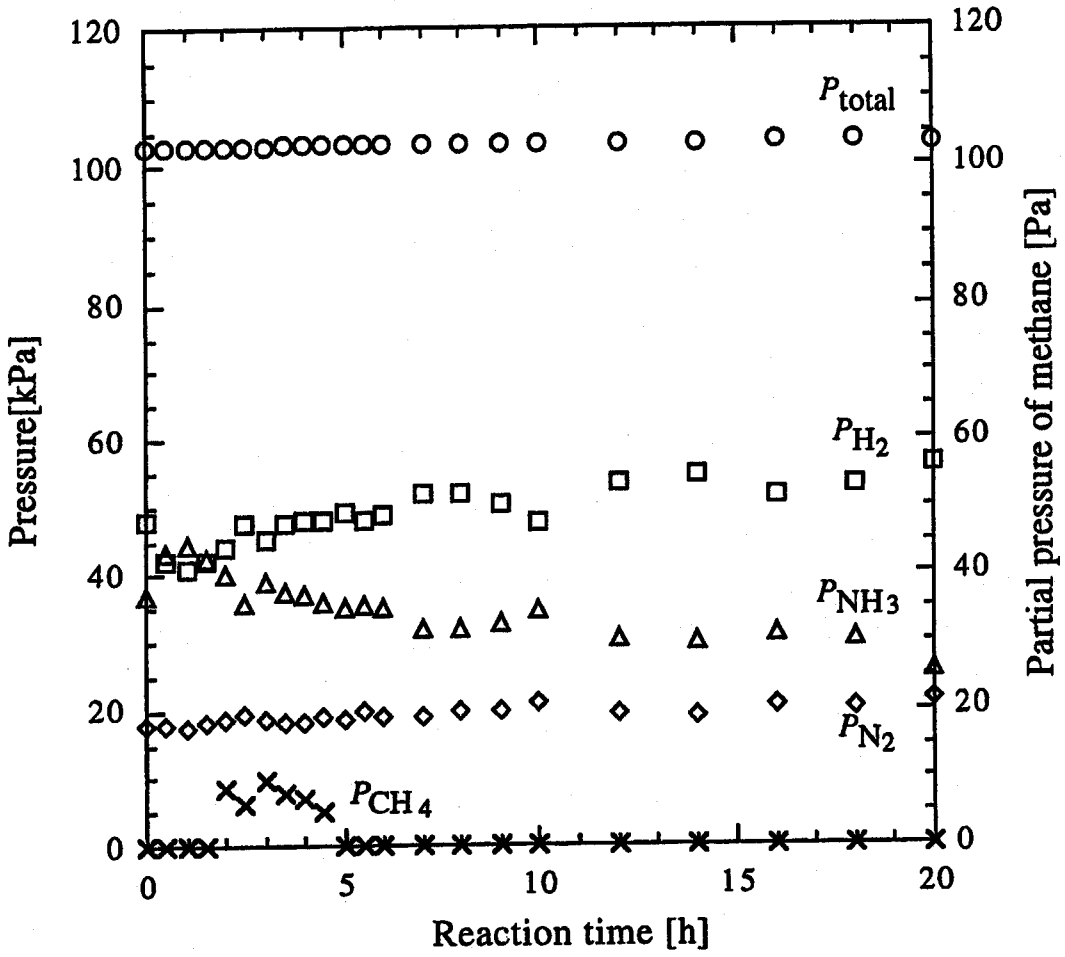

Fig. 3.5 Time variation of the partial pressures of NH_3, N_2, H_2 and CH_4 and the total pressure during the run 3.3.2

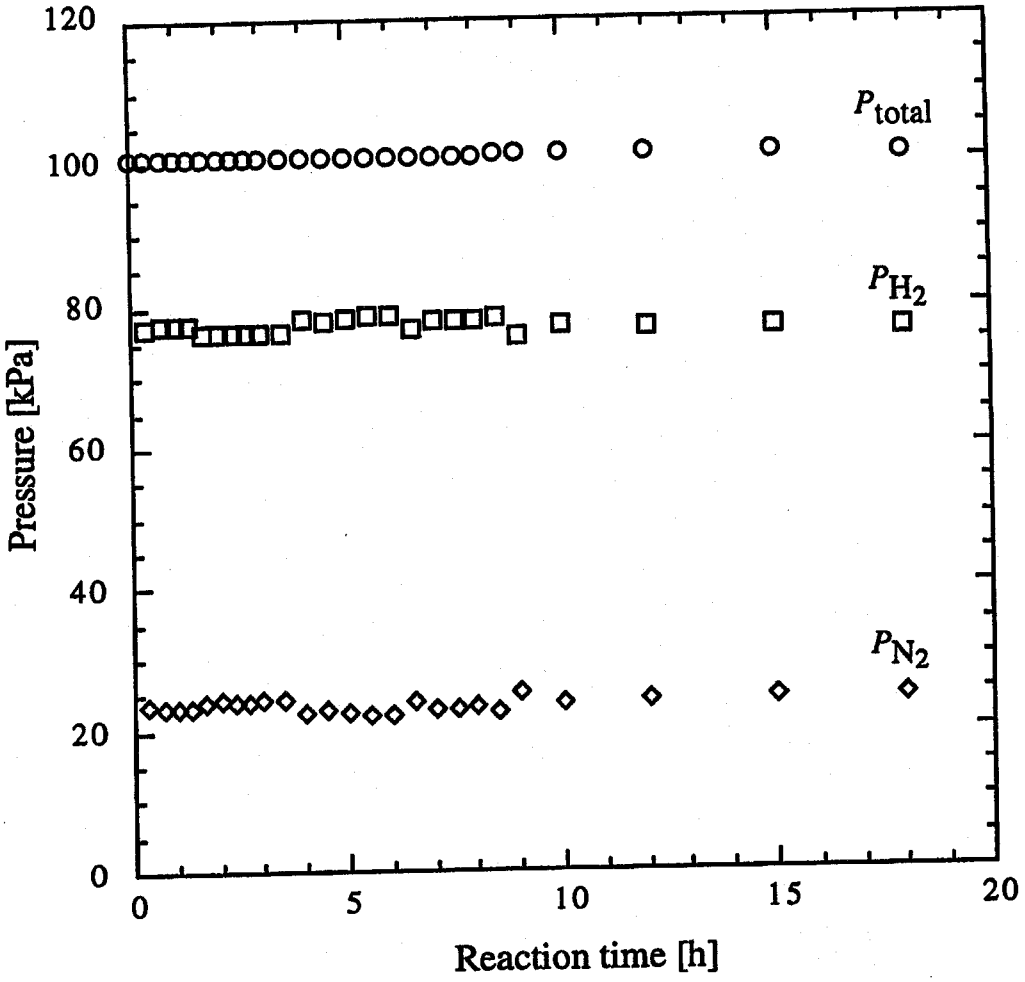

Fig. 3.6 Time variation of the partial pressures of N_2 and H_2 and the total pressure during the run 3.3.7

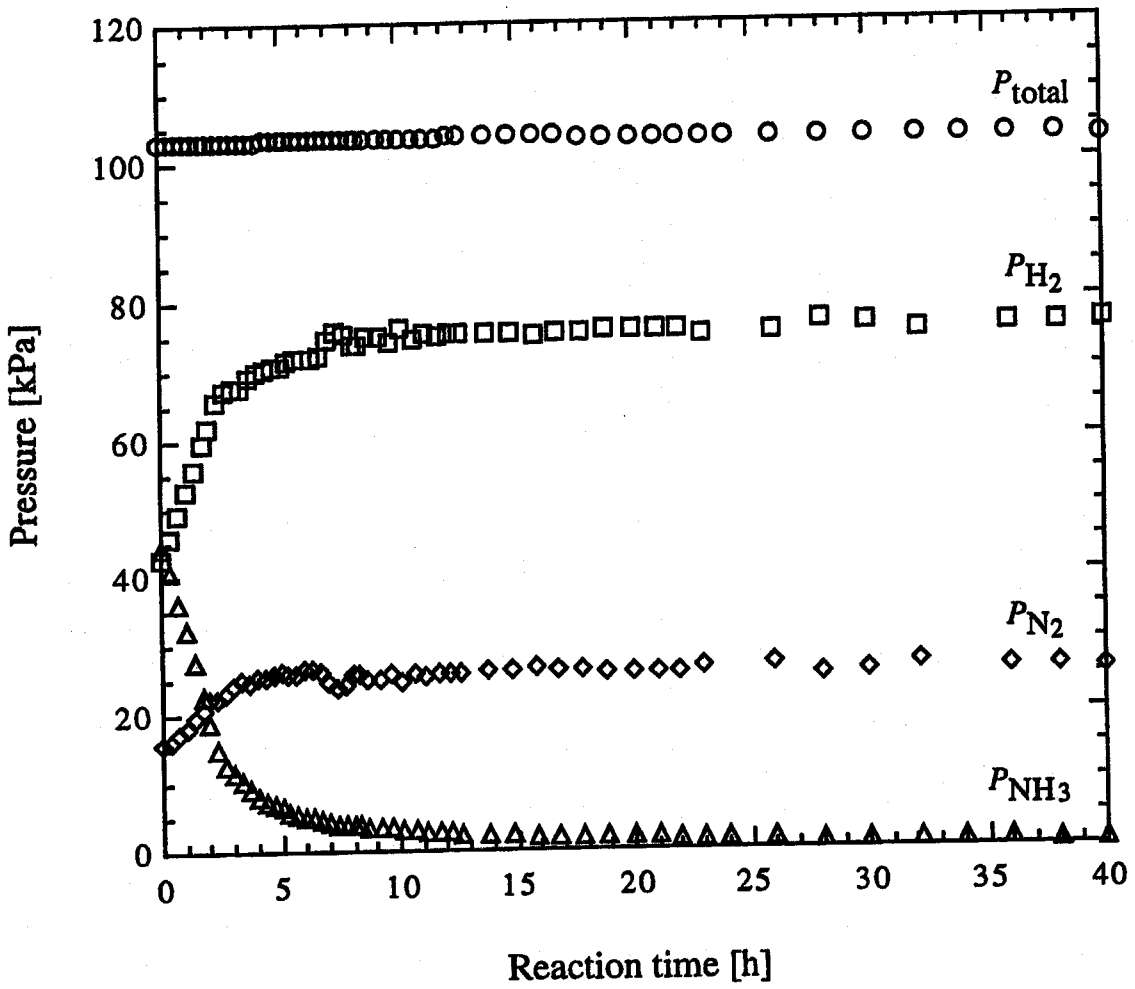

Fig. 3.7 Time variation of the partial pressures of NH_3, N_2 and H_2 and the total pressure during the run 3.3.4

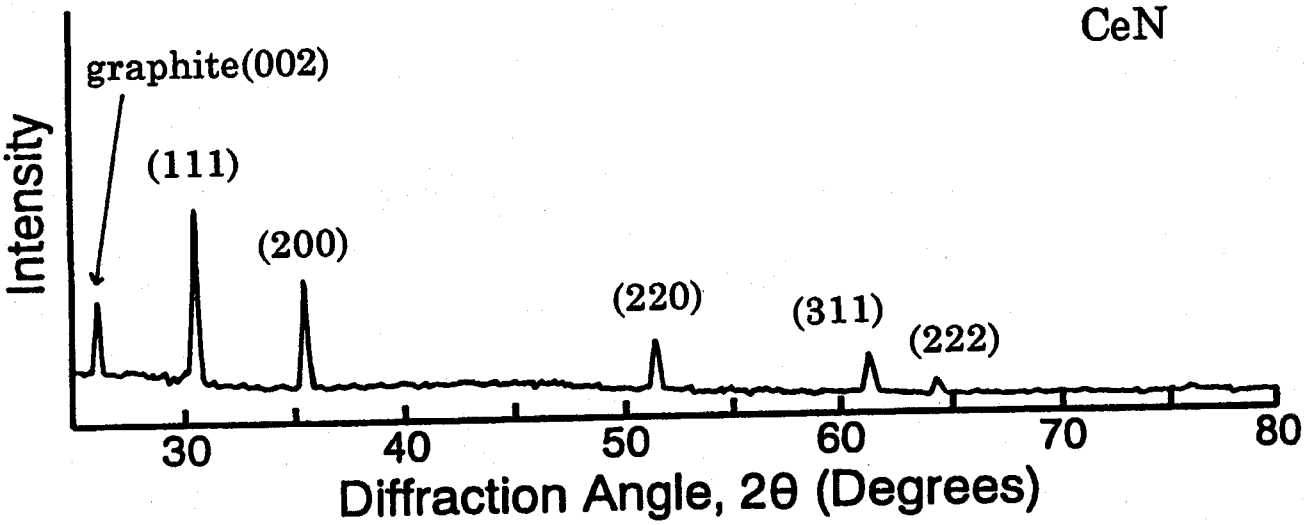

Fig. 3.8 X-ray diffraction pattern of the solid phase obtained by the reaction of flowing NH_3 with CeC_2 which was synthesized by carbothermic reduction of CeO_2 with graphite

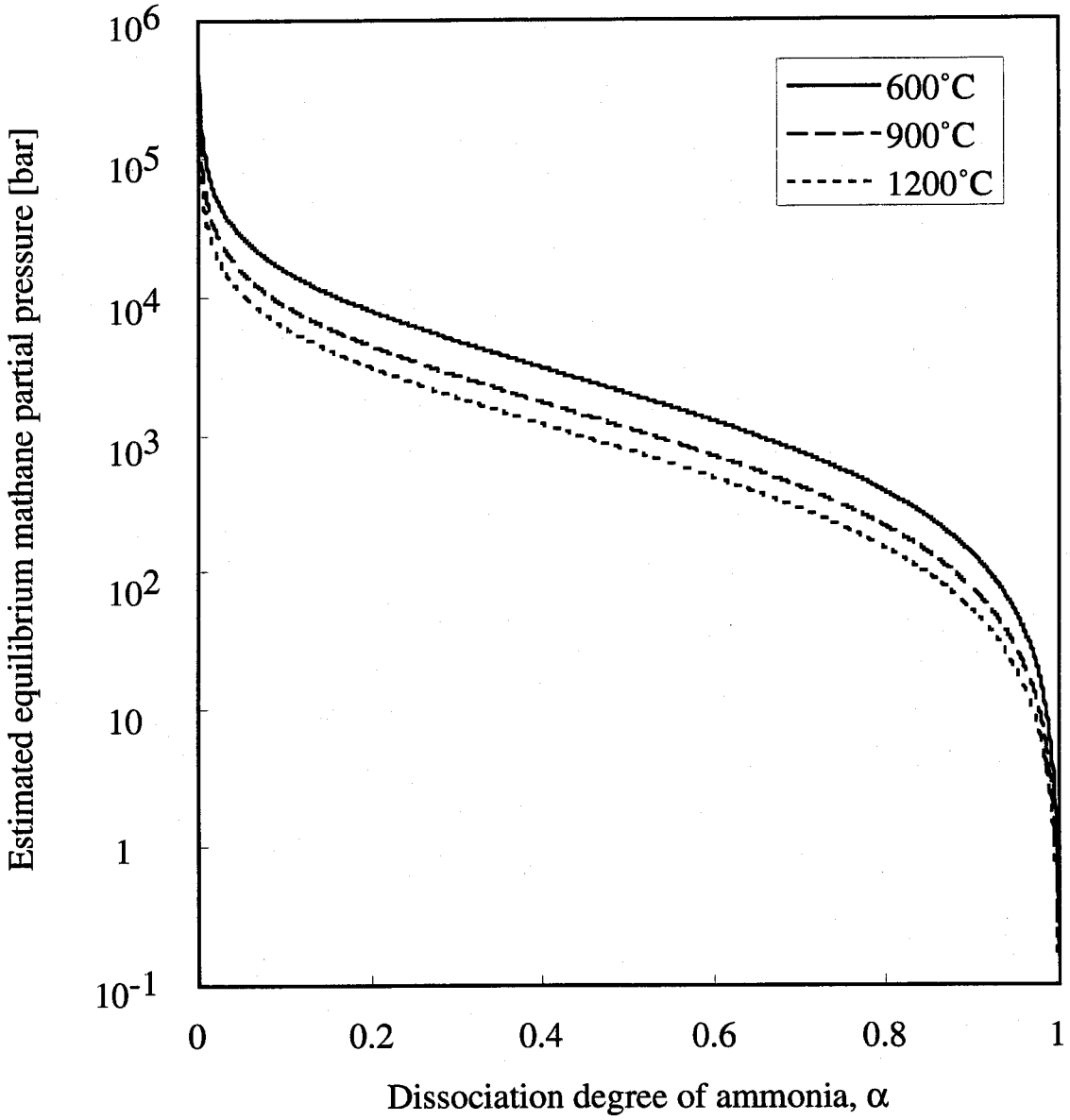

Fig. 3.9 Estimated equilibrium methane pressure as a function of dissociation degree of ammonia

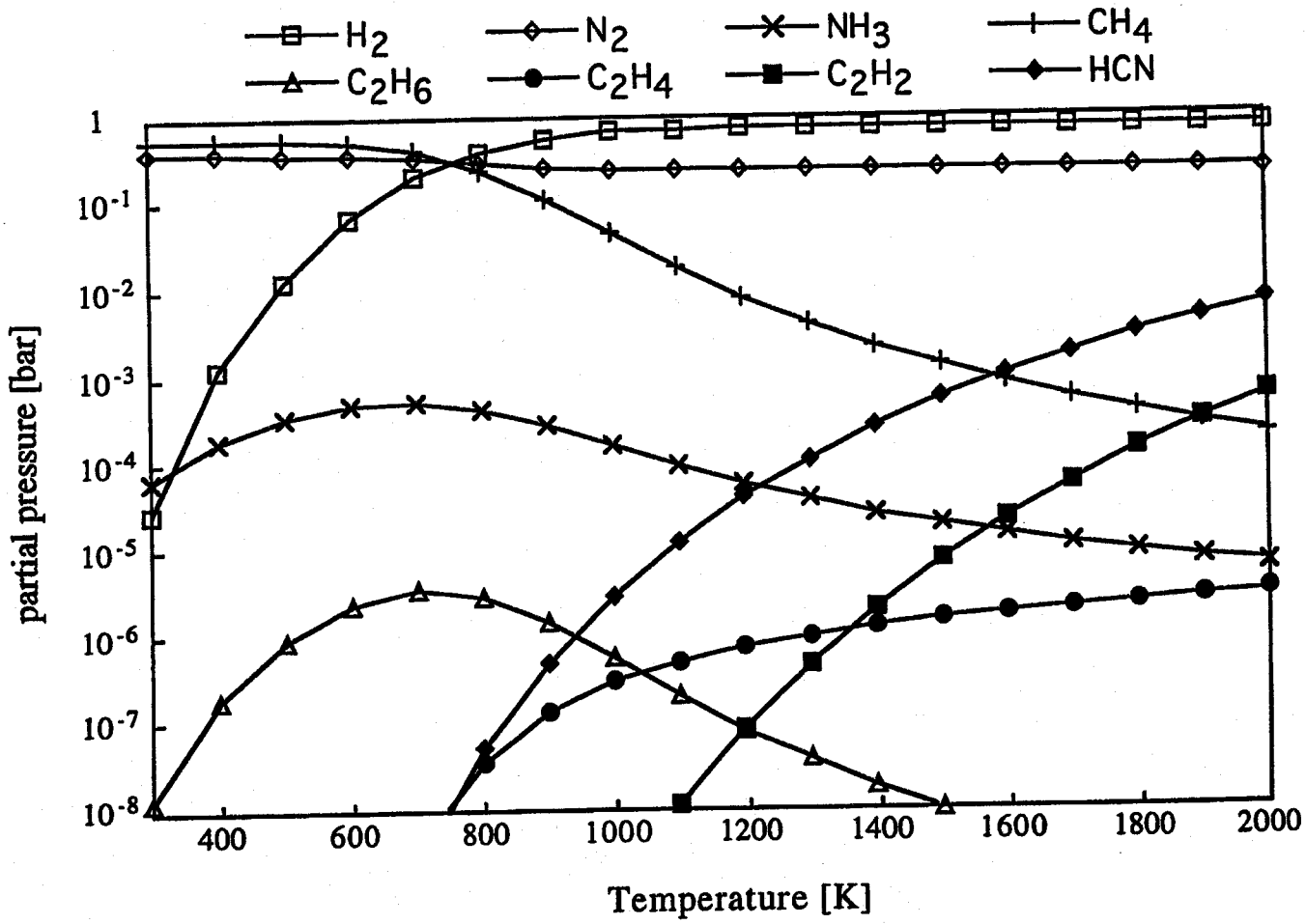

Fig.3.10 Equilibrium partial pressures of respective gases as a function of temperature by the raction of C with NH_3 under 1 bar

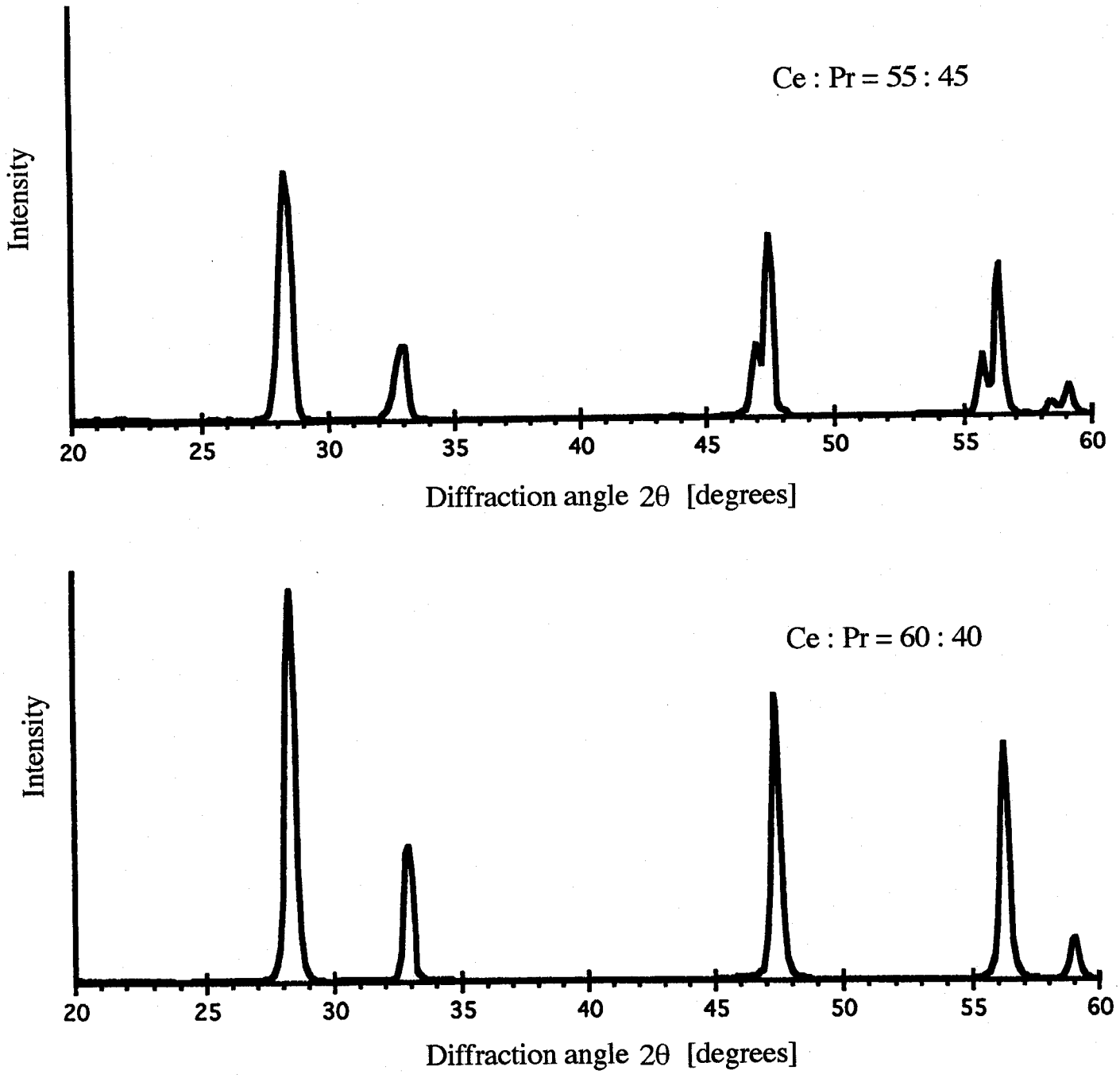

Fig. 3.11 X-ray diffraction pattern of the sintered oxide mixtures of CeO_2 and Pr_6O_{11} at the mixing ratios (Ce/Pr=55/45 and Ce/Pr=60/40)

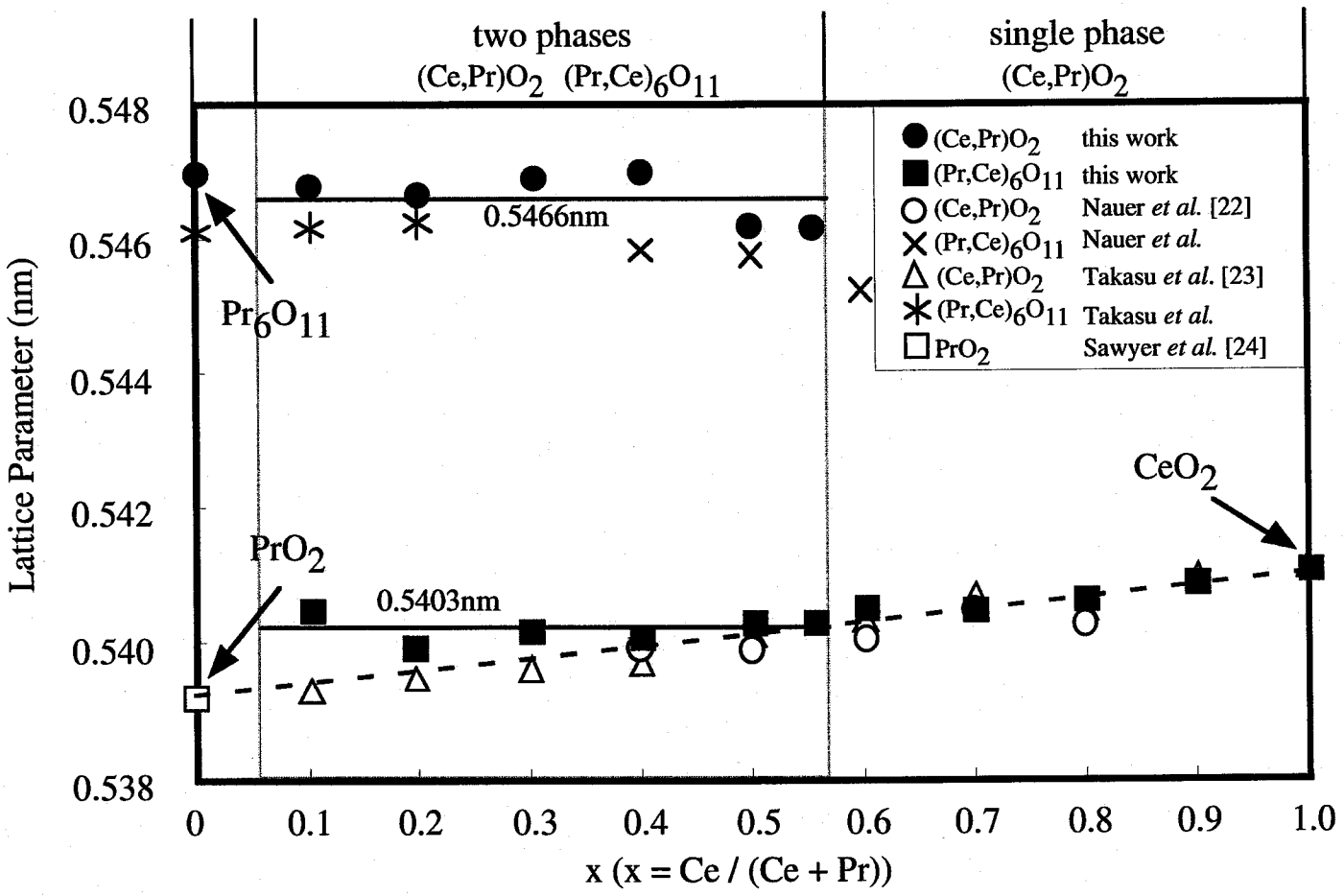

Fig. 3.12 Relationship between lattice parameters of obtained products and mixing ratio of CeO_2 and Pr_6O_{11}

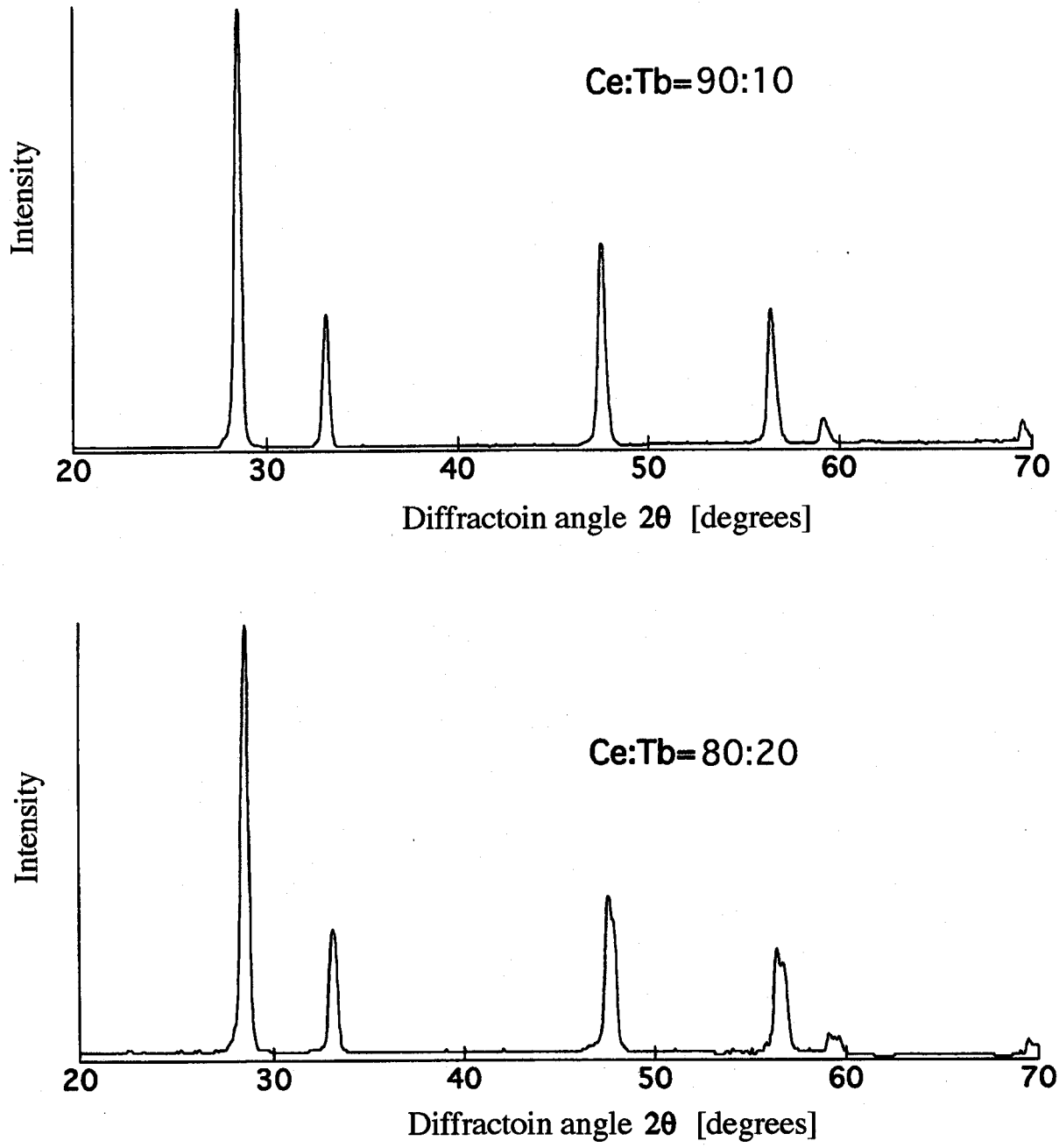

Fig. 3.13 X-ray diffraction patterns of the products obtained by sintering the oxide mixtures (Ce:Tb=90:10 and 80:20) in air at 1400°C for 12 hours

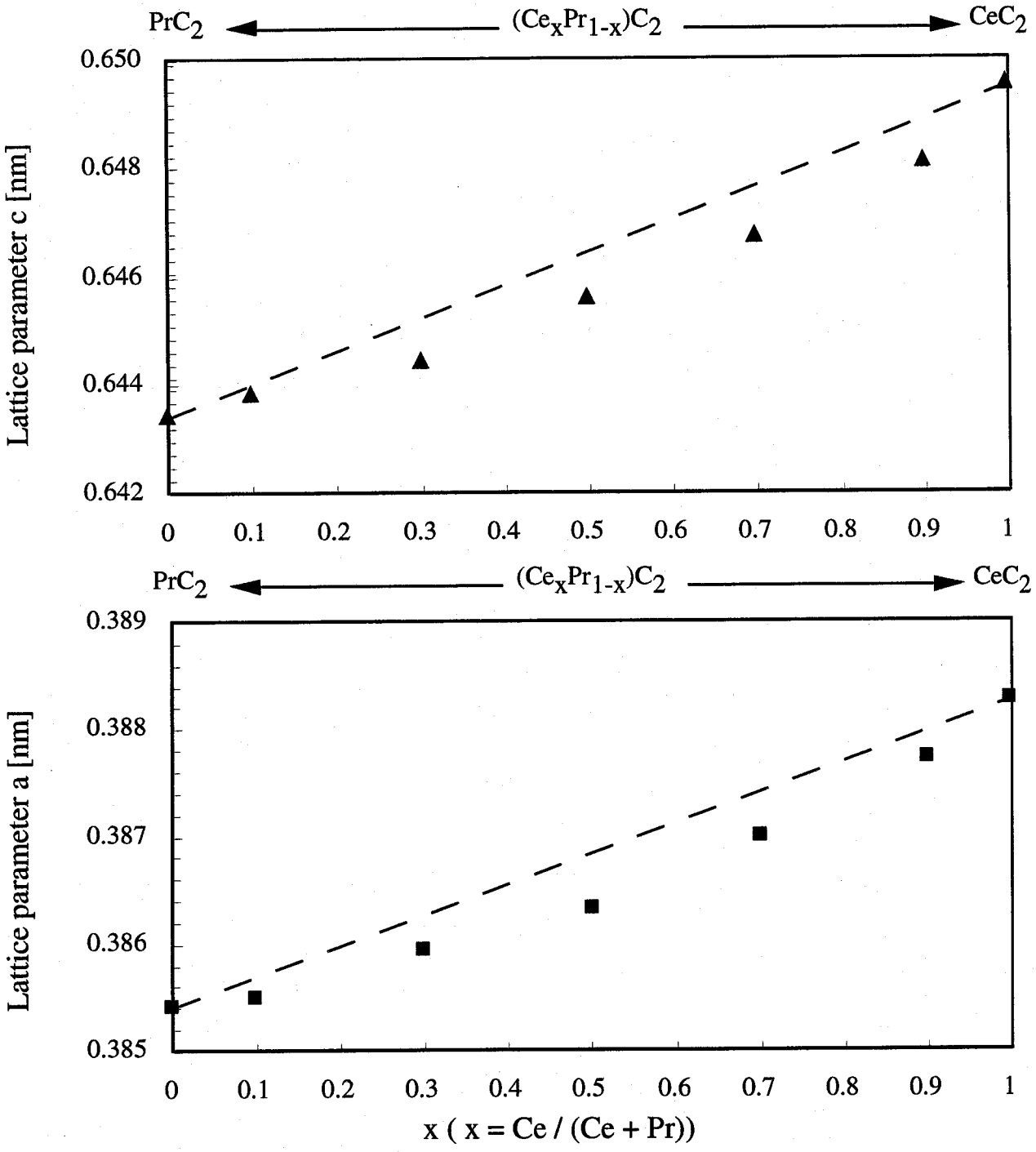

Fig. 3.14 Relationship between lattice parameters of Ce-Pr mixed dicarbides and x

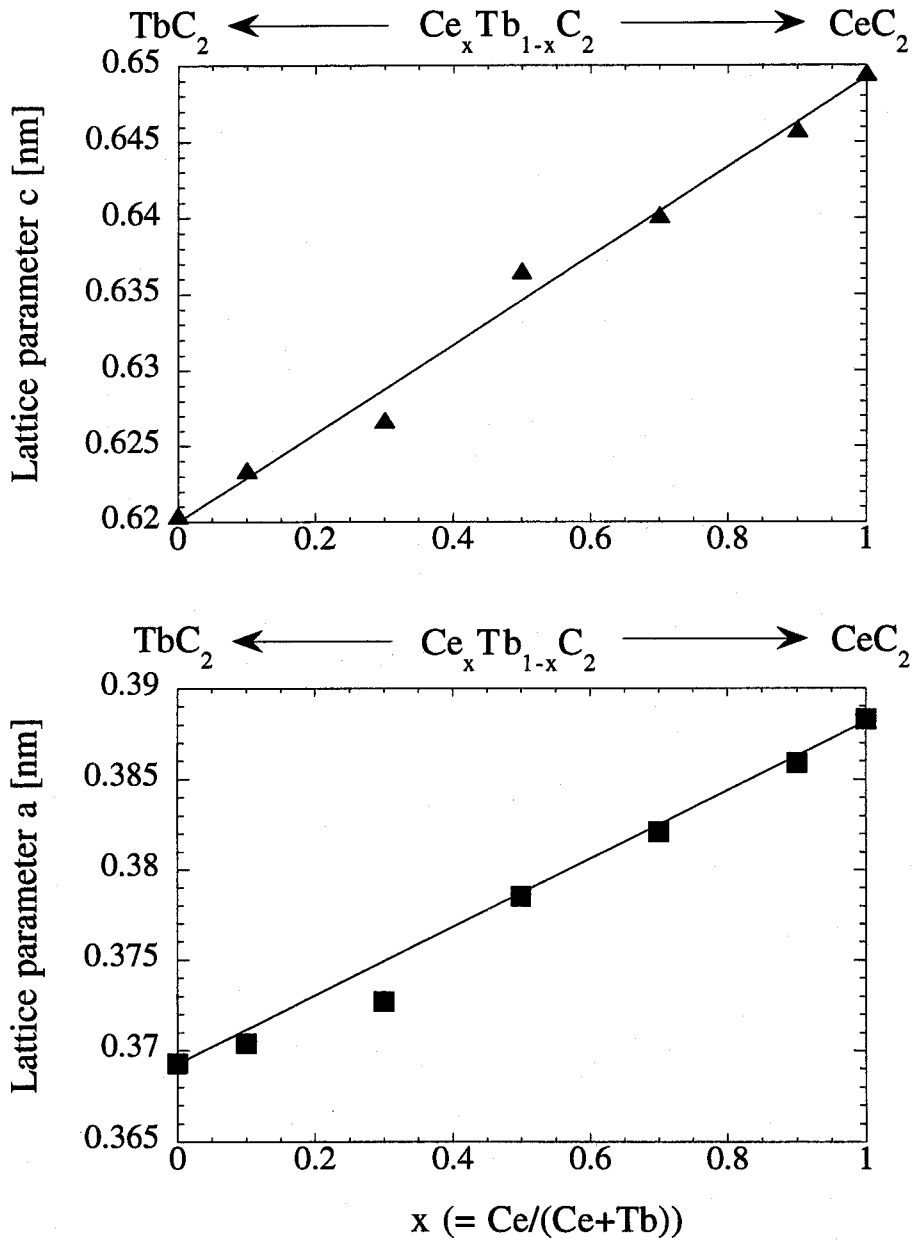

Fig. 3.15 Relationship between lattice parameters of Ce-Pr mixed dicarbes and compostion x

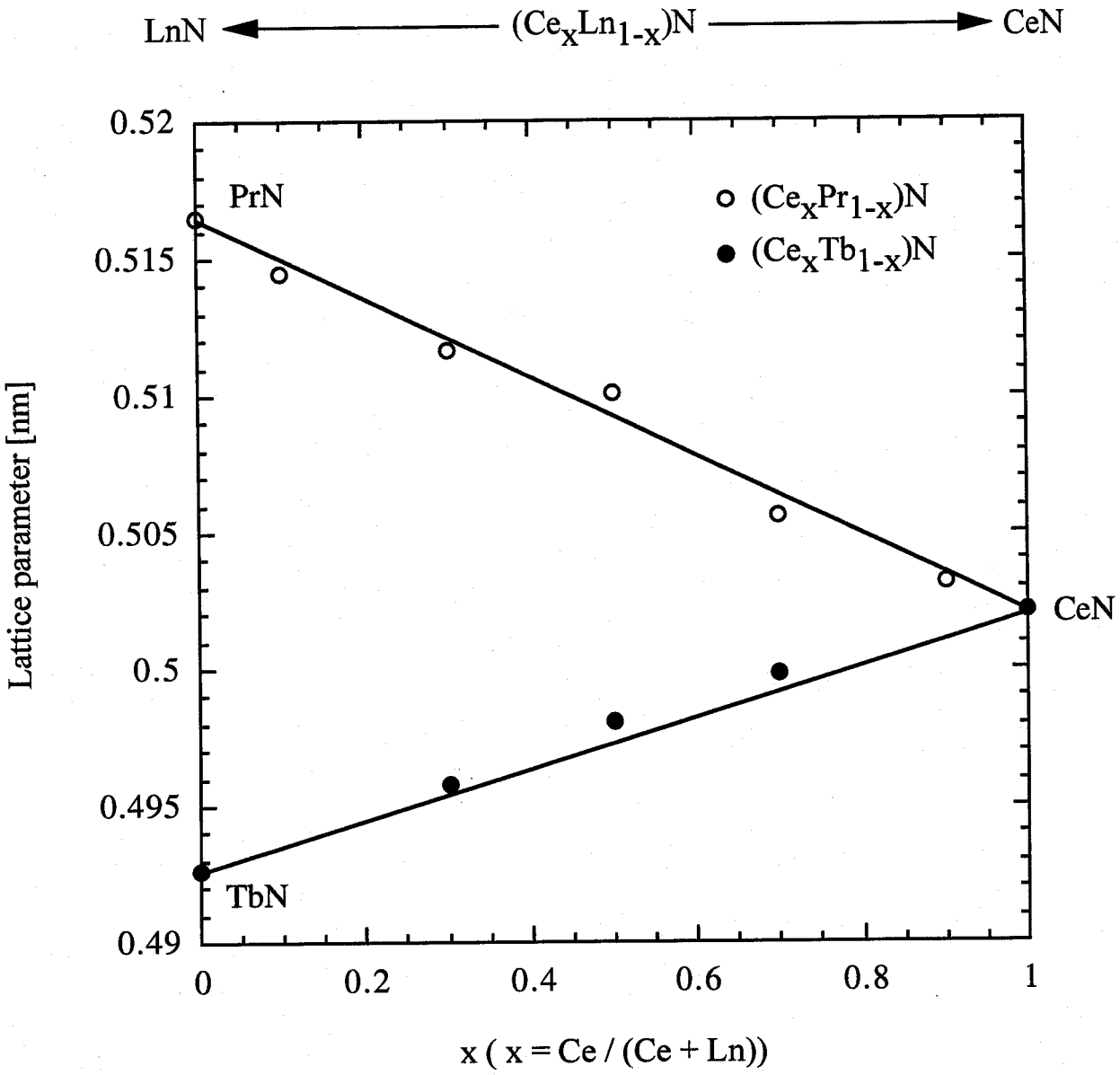

Fig. 3.16 Relationship between lattice parameters of the mixed nitrides and composition x

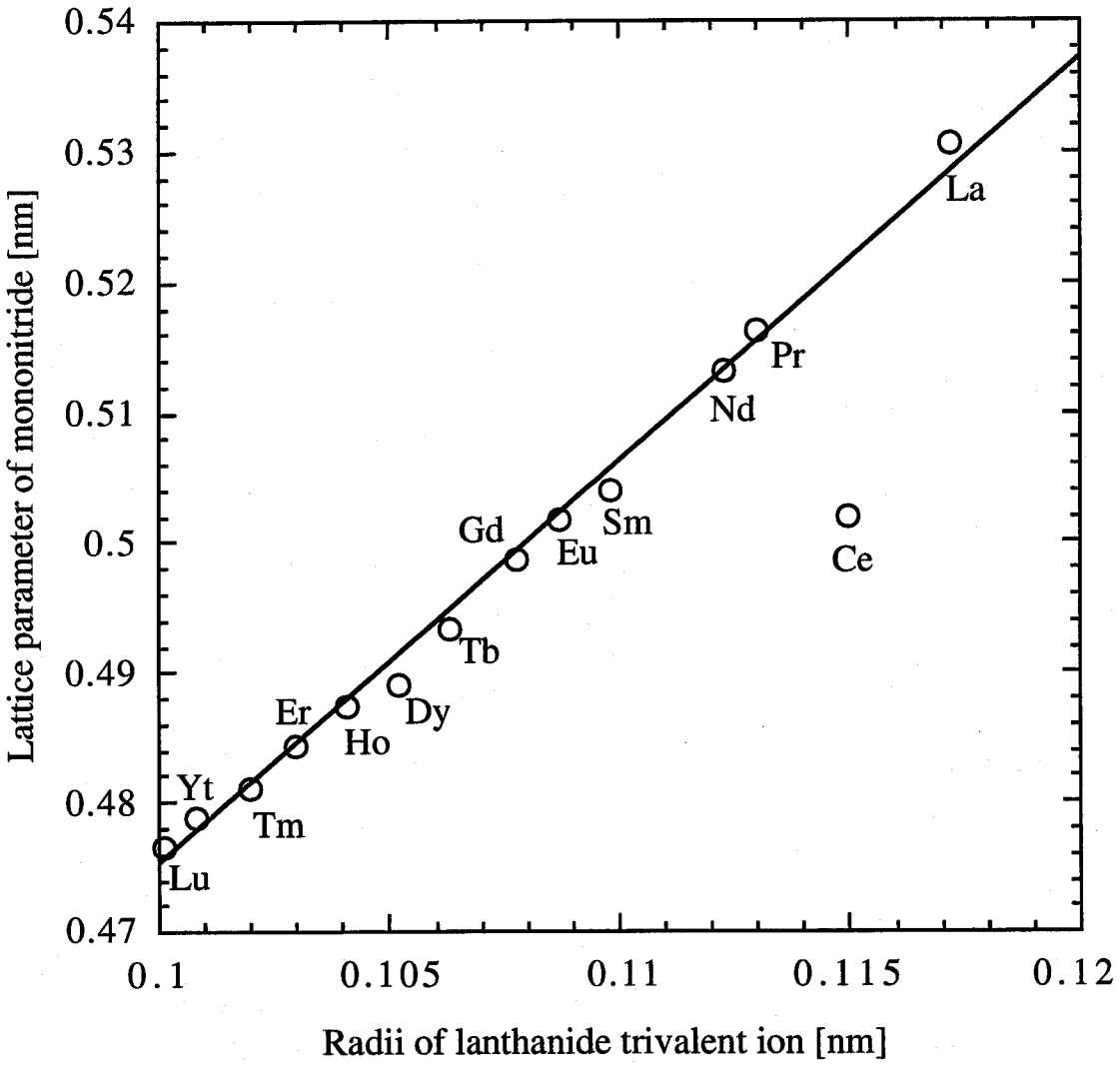

Fig. 3.17 Relationship between lattice parameters of lanthanide mononitrides and trivalent cation radii [17].

Chapter 4

K-edge XAFS study of rare earth elements in the oxides, carbides and nitrides

4.1 Introduction

Since rare earth (RE) elements fill partially 4f orbitals, their properties are similar to each other and gradually vary over a wide range. These similarity and variety have not been fully exploited yet because of some difficulties, for instance, in separating each other out of the natural resource containing many RE elements together. To make full use of their unexploited potential properties from the viewpoints of science and technology, it is necessary to analyze an RE element and its compound without suffering from the presence of other RE elements as impurities.

The x-ray absorption edge energy is distinctive of each element and free from interference of other ones. Energy separation between adjacent rare earth elements' *K*-edges is from 1.5 keV (La-Ce) to 2.0 keV (Yb-Lu). The x-ray absorption spectrum, in the region from the vicinity of the edge to a point several hundreds eV higher than that, involves information on the short range order of the target element in the condensed matter, which is known as extended x-ray absorption fine structure (EXAFS). The data analysis methods of EXAFS were well developed and summarized by Teo [1]. A narrower region, from the vicinity of the edge to several tens eV higher, involves information on electron transitions from the core level to unoccupied levels in bands just higher than the Fermi energy, so that the electronic structure of the matter is reflected in the spectrum. This is known as x-ray absorption near edge structure (XANES) [2]. X-ray absorption fine structure (XAFS) is a general term for EXAFS and XANES. Since XAFS is sensitive only to the target element, it is a powerful analysis tool for studying materials containing RE elements. *K*-edge energies of RE elements were, however, too high to be measured at storage rings installed and

developed in 1980's, for instance, PF-KEK and NSLS-BNL. However, in 1997 SPring8 has been completed, which emits x-ray beams with high brilliance, intensities and energies enough for measuring RE-EXAFS and RE-XANES at *K*-edges [3].

Many *L*-edge XAFS studies of rare earth oxides [4-7] including only a single report on cerium nitride [8] have so far been reported. However, no reports on *K*-edge XAFS of RE nitrides and carbides are found. In this chapter, the author the reports results of *K*-edge XAFS of cerium oxides, carbides and nitrides, measured at SPring8.

4.2 XAFS measurements

Rare earth oxides were supplied from Rare Metallic Co., Ltd. and carbides and nitrides were prepared in the methods mentioned in chapter 3. The room temperature RE *K*-edge XAFS measurements of their oxides, carbides and nitrides were carried out at the beam line L01B1 [3] in SPring8 in a transmission mode with the Si (311) plane of the inclined double-crystal monochrometer. Parallelism of the double-crystal planes was tuned so as to maximize the rocking curve by finely adjusting the monochrometer using a piezo actuator once just before each scan over the required energy region. The incident and transmitted x-ray intensities were monitored by ionization chambers with flowing Ar and Kr gases, respectively. X-ray beam's cross section was 5 mm$\times$1 mm at the sample position. The x-ray energy indicated by the measuring system was carefully calibrated at times by measuring *K*-edge energies of Gd and Tb metal foils.

4.3 Results and discussion

All samples for XAFS measurement were identified as in monophase materials without any impurity diffraction peaks by XRD. After the XAFS measurements, XRD analyses of all samples were carried out again to ascertain that no oxidation of the carbides and nitrides occurred even after the measurements. Rare earth compounds measured in this work are given in table 4.1.

In Fig. 4.1 XAS (X-ray absorption spectra) of CeO_2, CeC_2 and CeN are illustrated,

all of which were normalized to the same edge jump height. Both incident and transmitted x-ray intensities, I_0 and I, have been clearly measured as smooth curves without any discontinuity, which demonstrates that the present measurement system works properly and the present specimens have no problem. Even by glancing at the figure these three compounds are noticed to have different fine structures reflecting their crystal structures (see table 4.1).

Figure 4.2 shows the XANES of these spectra expressed as derivative spectra $d\mu/dE$ as a function of E, where E is x-ray energy and $\mu(E)$ is experimental. The derivative spectrum emphasizes features of the spectrum and makes it easy to investigate the shift of edge energy. It has been pointed out that chemical shifts could not be observed in such high energies of rare earth K-edge because of the much broadened transition peak forced by short lifetimes of excited core levels [2]. There were found, however, significant and clear differences in edge energy depending on chemical states of cerium. The edges of CeC_2, CeN and CeO_2 were located in the increasing order of energy. When peak energy of $d\mu/dE$ vs.E curve in Fig. 4.2, namely, inflection point of edge jump is adopted as the edge energy E_0,

$$E_0(CeC_2) = E_0(CeO_2) - 9.7 \text{ (eV)}$$

$$E_0(CeN) = E_0(CeO_2) - 6.0 \text{ (eV)}.$$

Since the edge energy corresponds to energy gap between electrons in 1s orbital and the Fermi level E_f of each compound, E_0 may be replaced by E_f in these relations by neglecting the dependence of 1s level on the chemical state. The same procedure was done for other data sets of Pr, Nd, Gd and Tb to evaluate the chemical shift in edge energy, and their results are tabulated in Table 4.2.

K-edge measurements are favorable for EXAFS spectroscopy because of the absence of higher absorption. For fine EXAFS analysis, it requires a wide range spectrum (generally more than 1000 eV from E_0). Since three L-edges of rare earth elements appear at intervals of a few hundred eV, data in a wide enough range are never obtainable. Figure 4.3 shows XAFS spectrum of Ce L_{III}-edge in CeO_2 which was measured at BL7C in PF-KEK. The L_{II} absorption edge of Ce at 6170 eV interrupts L_{III}-edge XAS spectra. Although XAS spectra in the range up to 1000 eV above K-edge of cerium were observed as shown in Fig. 4.1, the spectrum in the range only up to 450 eV above could be obtained in L_{III}-edge EXAFS measurements.

In order to extract structural information from EXAFS spectrum, $\chi(E)$ is defined as

$$\chi(E) = \frac{\mu(E) - \mu_0(E)}{\mu_0(E)} \tag{4.1}$$

where E is incident x-ray energy, $\mu(E)$ is experimental XAS and $\mu_0(E)$ is background absorption spectrum of an isolated atom. To relate $\chi(E)$ to structural parameters, it is necessary to convert the energy E into the photoelectron wavevector k by the relation

$$k = \frac{2\pi}{h}\sqrt{2m(E - E_0)} \tag{4.2}$$

where h is Planck's constant and m is the electron mass. From eqns. 4.1 and 4.2 EXAFS function, $\chi(k)$, is obtained. The Fourier transform of the EXAFS function from k space to R space yields the radial distribution function (RDF):

$$\Phi(R) = \frac{1}{\sqrt{2\pi}}\int_{k_{\min}}^{k_{\max}} w(k)k^3\chi(k)e^{-2ikR}\,\mathrm{d}k\,. \tag{4.3}$$

Hanning function is applied as a window function, $w(k)$:

$$w(k) = \begin{cases} \sin^2\left\{\dfrac{\pi(k - k_{\min} - 0.5)}{2}\right\}, & k_{\min} - 0.5 \le k < k_{\min} + 0.5 \\ 1 \qquad\qquad\qquad\quad , & k_{\min} + 0.5 \le k \le k_{\max} - 0.5 \\ \cos^2\left\{\dfrac{\pi(k - k_{\max} + 0.5)}{2}\right\}, & k_{\max} - 0.5 < k \le k_{\max} + 0.5 \end{cases} . \tag{4.4}$$

The factor k^3, used to weight the data according to the value of k, counteracts the rapid damping of $\chi(k)$ with increasing k. The RDFs calculated from the results of K- and L_{III}-edge measurements of CeO_2 are illustrated in Fig. 4.4. For K-edge, k_{min} and k_{max} are 2.5 and 17.5, respectively, and for L_{III}-edge, 2.5 and 7.5. As the Fourier transforms have been produced without consideration of the absorber and scatterer phase shifts for the backscattering atoms, the peaks are not expected to correspond exactly to the true interatomic distances. Although the RDF of L_{III}-edge crumbles for R past 0.5 nm, reasonable peaks clearly appear even for high-R part in the RDF of K-edge. The RDFs obtained by the other rare earth compounds, which were examined in this work, are shown in Figs. 4.5–4.9. Table 4.3 gives results of fitting the nearest distances between Ce and light elements of K-edge measurements to theoretical standards produced by FEFF 7 code [9] by considering phase shifts. The nearest distances calculated from XRD analyses are also given in Table 4.3. These values are in excellent agreement with each other. All the present results obviously indicate that EXAFS data obtained at

SPring8 are reliable and would be useful for further studies on the RE compounds.

4.4 Conclusions

X-ray fine structure spectra of *K* absorption edges of rare earth elements in their oxides, carbides and nitrides were obtained at the beamline BL01B1 of SPring8. Significant chemical shifts were observed around *K*-edges of all rare earth elements (Ce, Pr, Nd, Gd and Tb). The interatomic distances between Ce and the nearest light elements (O, C and N) were calculated from Ce *K*-edge EXAFS of oxide, carbide and nitride and these values are in good agreement with those from XRD, respectively.

Acknowledgement

The authors thank the staff at SPring8 for providing beam time. They are also grateful to Dr. T. Uruga and Dr. H. Tanida for their help in the measurements at beamline BL01B1 of SPring8.

References

[1] B. Teo, "EXAFS : Basic Principles and DATA Analysis," Springer-Verlag, Berlin (1986)

[2] J. C. Fuggle and J. E. Inglesfield, " Unoccupied electronic states : fundamentals for XANES, EELS, IPS and BIS," J. C. Fuggle and J. E. Inglesfield, ed., Springer-Verlag, Berlin (1992), pp. 1--21.

[3] S. Emura, H. Maede and T. Uruga, *SPring-8 Annual Report 1996*, H. Yokomizo, ed., 1997, pp. 82--83.

[4] A. Bianconi, A. Marcelli, H Dexpert, R. Karnatak, A. Kotani and T. jo, *Phys. Rev.*, **B35**(2)1987(806).

[5] N. V. Moghe, V. S. Pai, G. G. Sahasrabudhe and V. B. Sapre, *Pramana - J. Phys.*, **42**(1)(1994)23.

[6] S. N. Gupta, V. P. Vijayavargiya, B. D. Padalia, B. C. Tripathi and M. N. Ghatikar, *Phys. Stat. Sol. (b)*, **82**(1977)603.

[7] V. P. Vijayavaragiya, S, N, Gupta and B. D. Padalia, *Phys. Stat. Sol. (b)*, **80**(1977)83

[8] D. Malterre, C. Brouder, G. Krill, E. Beaurepaire, B. Carrière and D. Chandesris, *Europhysics Let,*. **15**(6)(1991)687.

[9] S.I. Zabinsky, J.J. Rehr, A. Ankudinov, R.C. Albers and M.J. Eller, *Phys. Rev.*, B52 (1995)2995.

Table 4.1 Rare earth compounds of which XAFS measurements were carried out.

	Oxides (crystal type)	Carbides[#]	Nitrides[##]
Ce	CeO_2 (CaF_2)	CeC_2	CeN
Pr	Pr_6O_{11} (Ce_6O_{11})	PrC_2	PrN
Nd	Nd_2O_3 (La_2O_3)	NdC_2	NdN
Gd	Gd_2O_3 (Mn_2O_3)	GdC_2	GdN
Tb	Tb_4O_7 (Tb_4O_7)	TbC_2	TbN

[#] Crystal type : CaC_2
[##] Crystal type : NaCl

Table 4.2 Chemical shifts of K-edge energy of some rear earth carbides and nitrides in reference to their edges of oxides.

Elements	Ce	Pr	Nd	Gd	Tb
Carbides	-9.7	-2.8	-3.5	-3.5	-2.4
Nitrides	-6.0	-2.0	-2.2	-3.5	-2.4

Energy unit : eV

Table 4.3 Distances between cerium and nearest atoms in cerium compounds determined by XRD and *K*-edge EXAFS.

Compounds	CeO_2	CeC_2	CeN
XRD	0.2343	0.2598	0.2515
EXAFS	0.234(3)	0.259(4)	0.251(0)

Length unit : nm

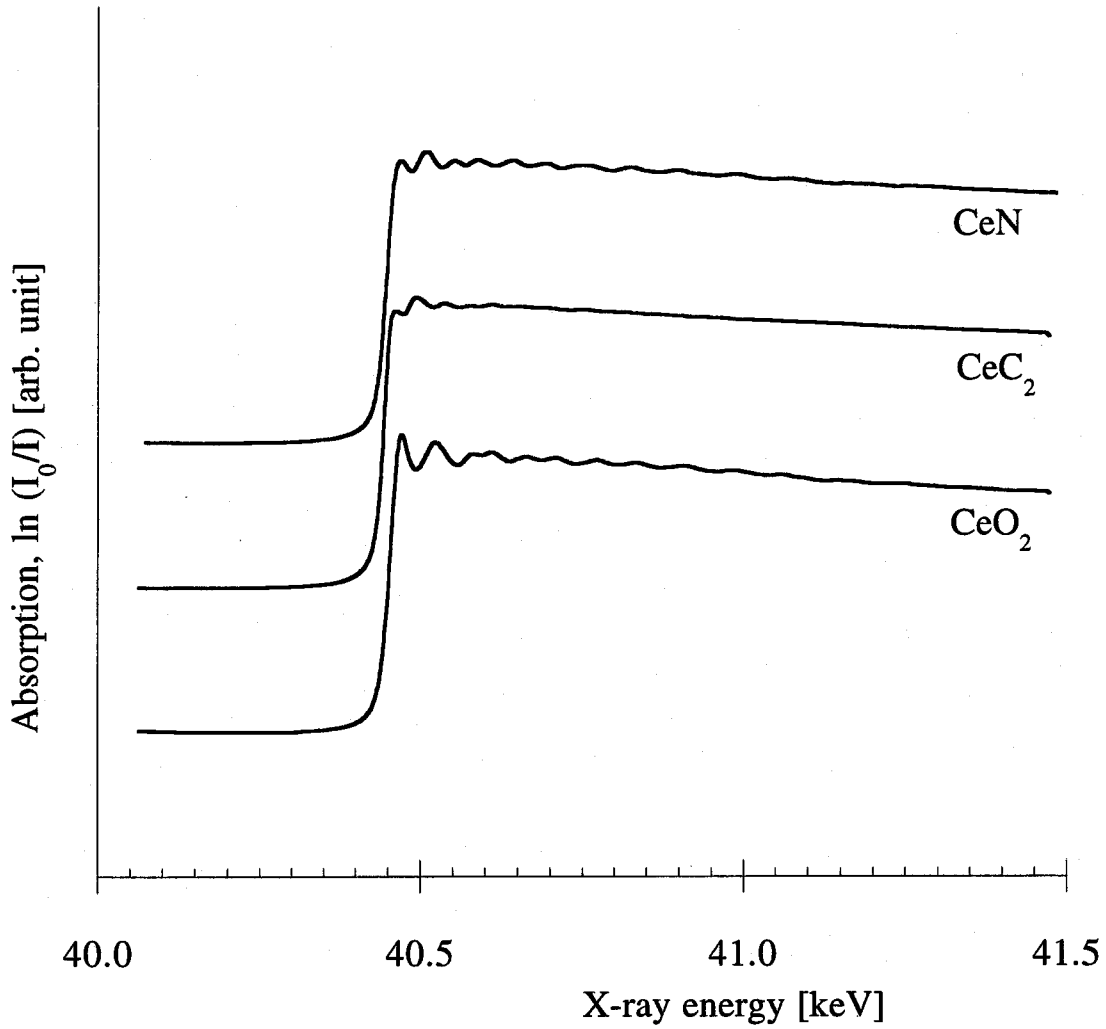

Fig. 4.1 XAFS spectra of K absorption edge of Ce in its compounds

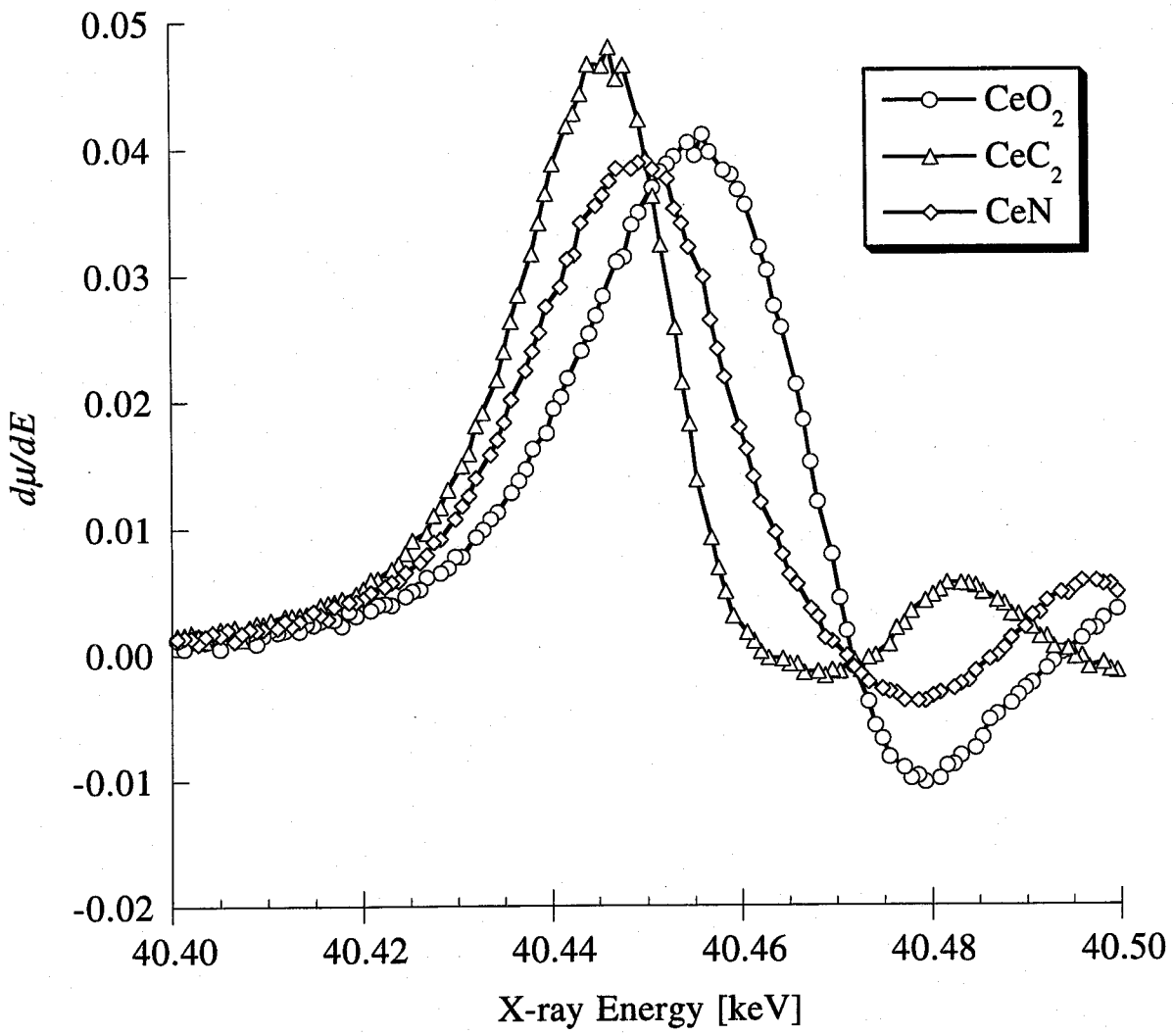

Fig. 4.2 Relationship between the derivative spectra of CeO_2, CeC_2 and CeN and x-ray energy

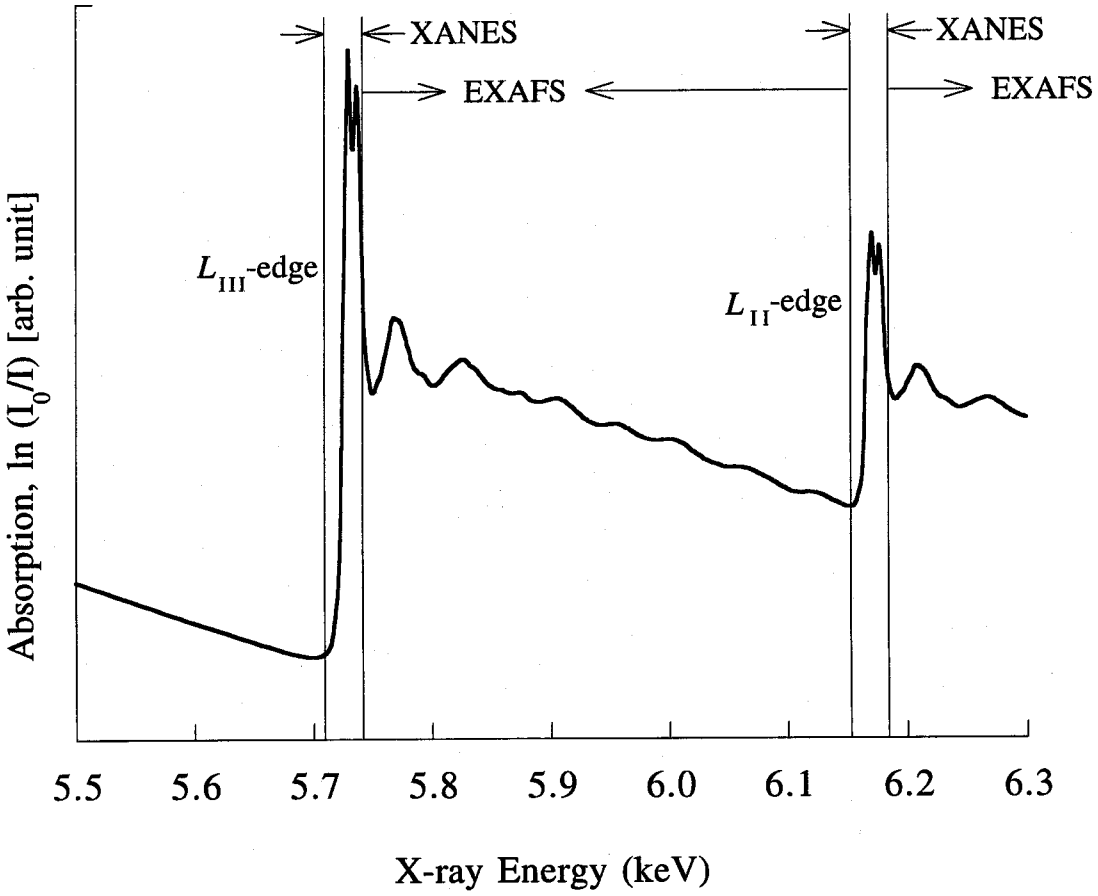

Fig. 4.3 XAFS spectrum of L_{III} edge of CeO_2

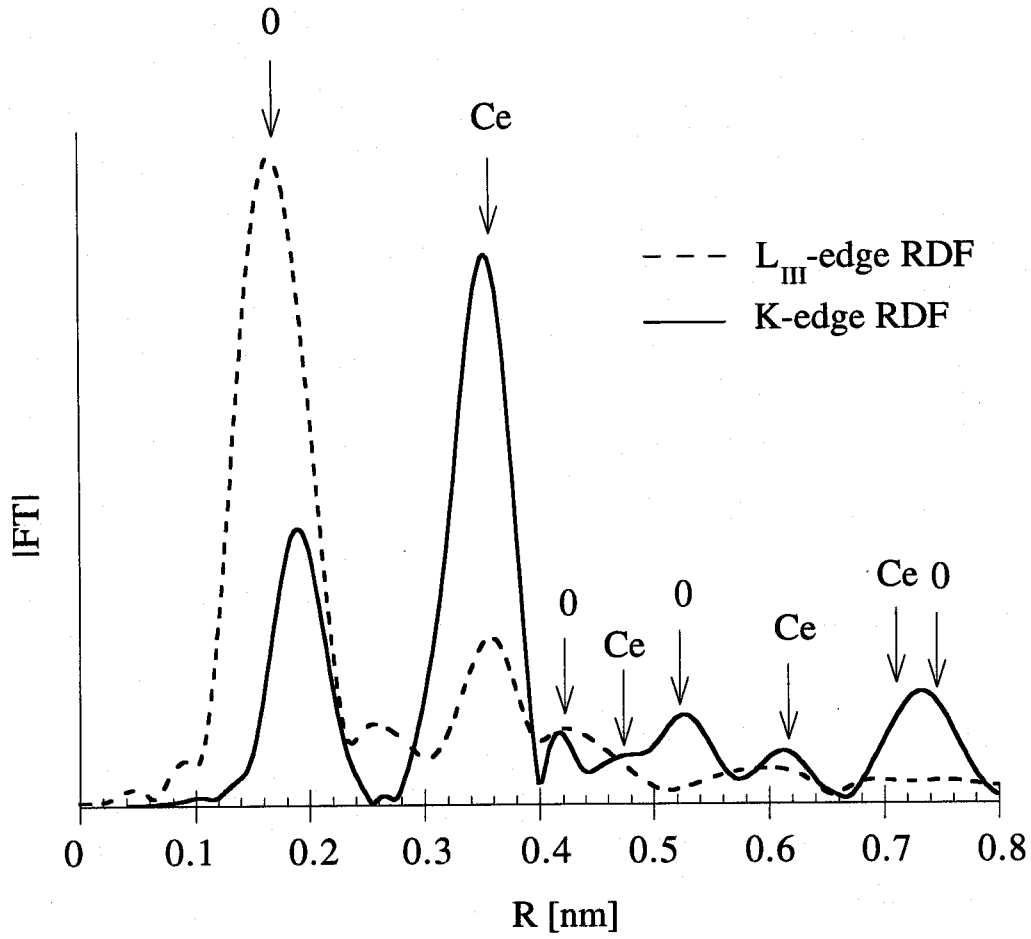

Fig. 4.4 Radial distribution fanctions of CeO_2 calculated from K-edge and L_{III}-edge EXAFS spectra

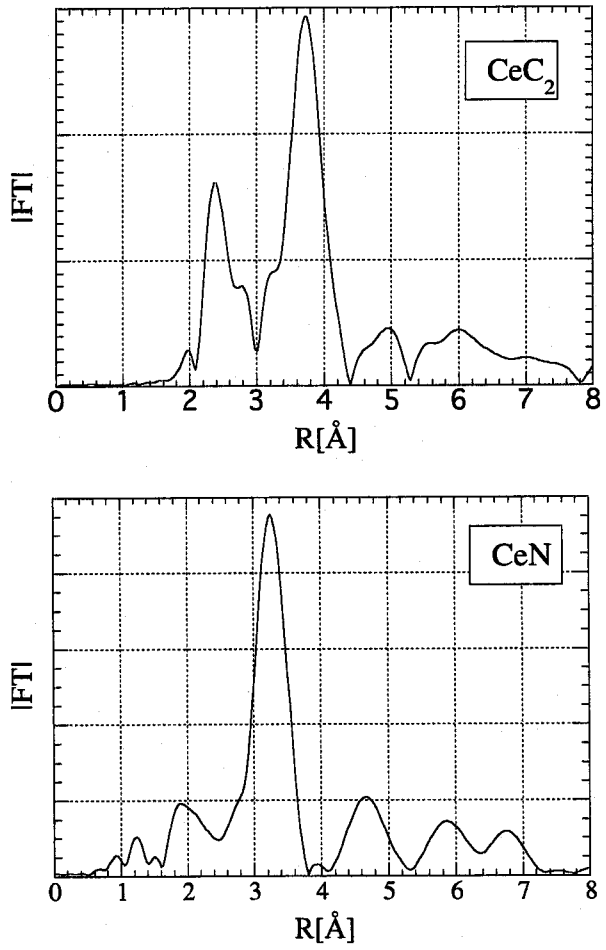

Fig. 4.5 Radial distribution functions of CeC_2 and CeN calculated from K-edge EAXFS spectra

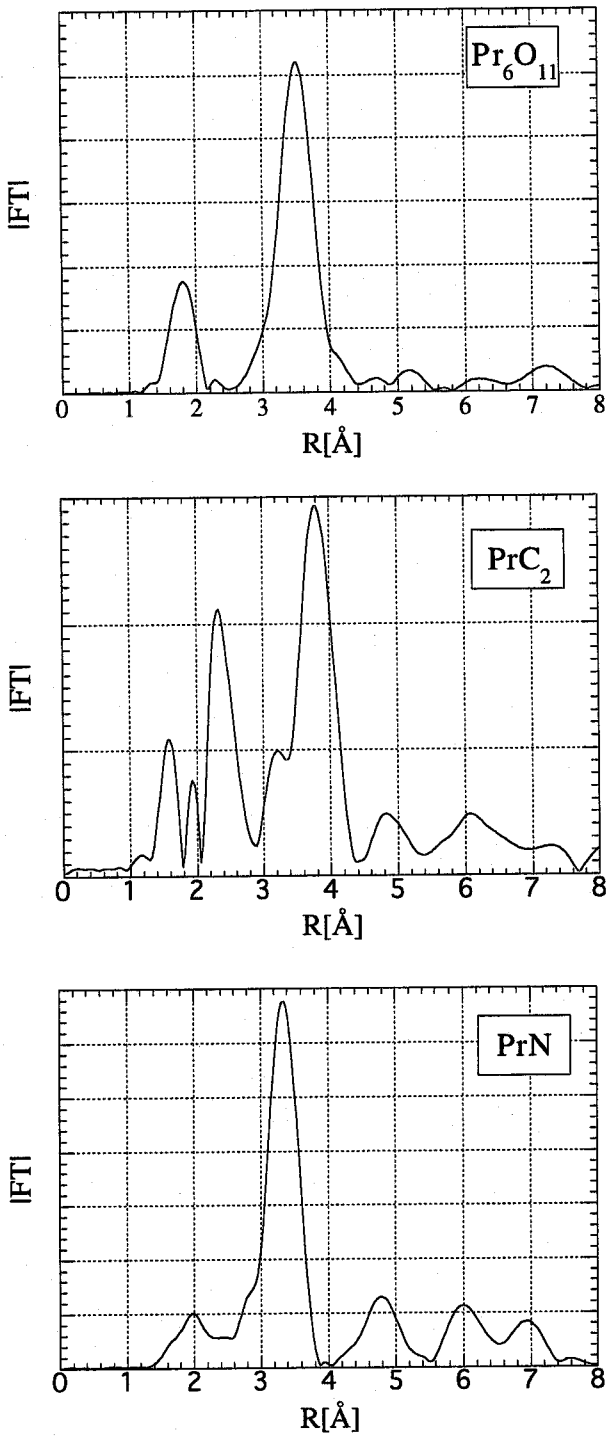

Fig. 4.6 Radial distribution functions of Pr_6O_{11}, PrC_2 and PrN calculated from K-edge EAXFS spectra

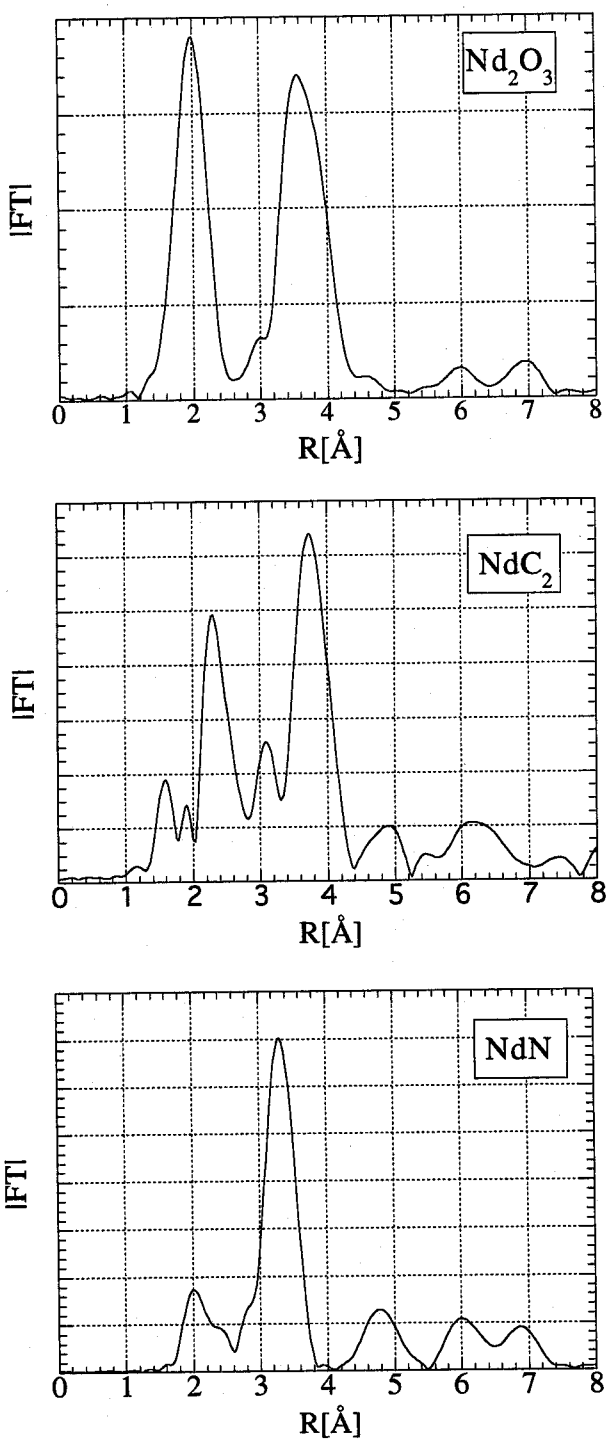

Fig. 4.7 Radial distribution functions of Nd_2O_3, NdC_2 and NdN calculated from K-edge EAXFS spectra

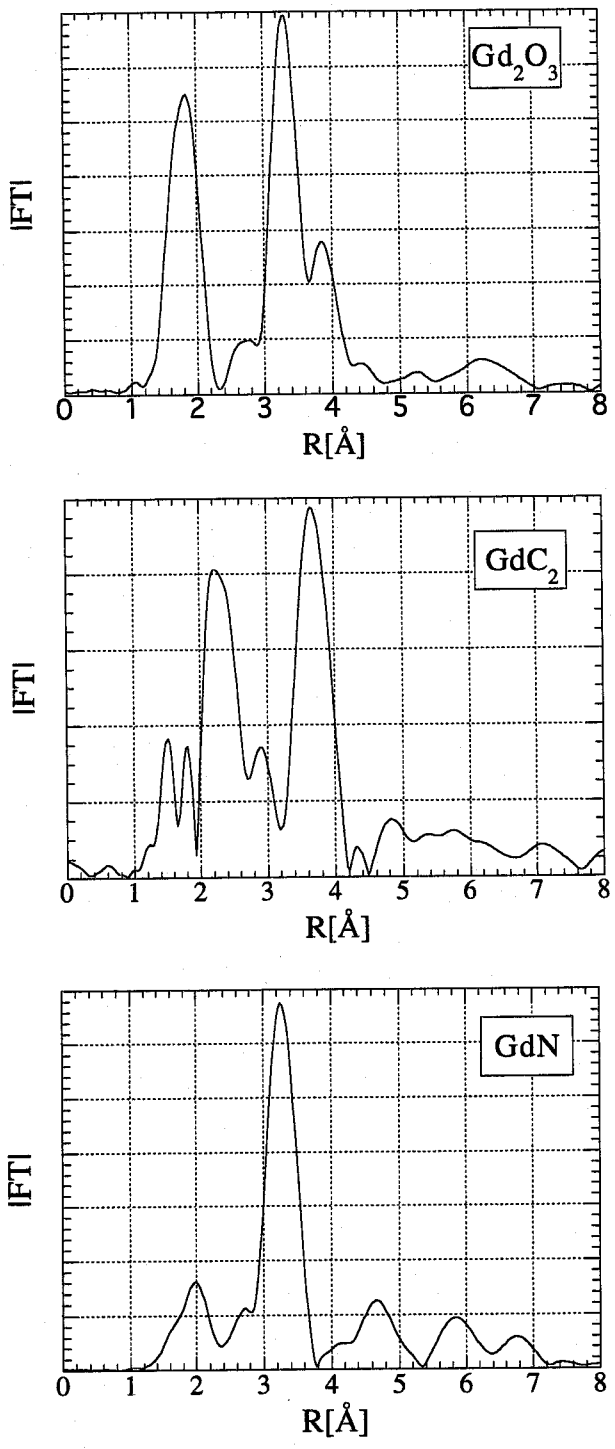

Fig. 4.8 Radial distribution functions of Gd_2O_3, GdC_2 and GdN calculated from K-edge EAXFS spectra

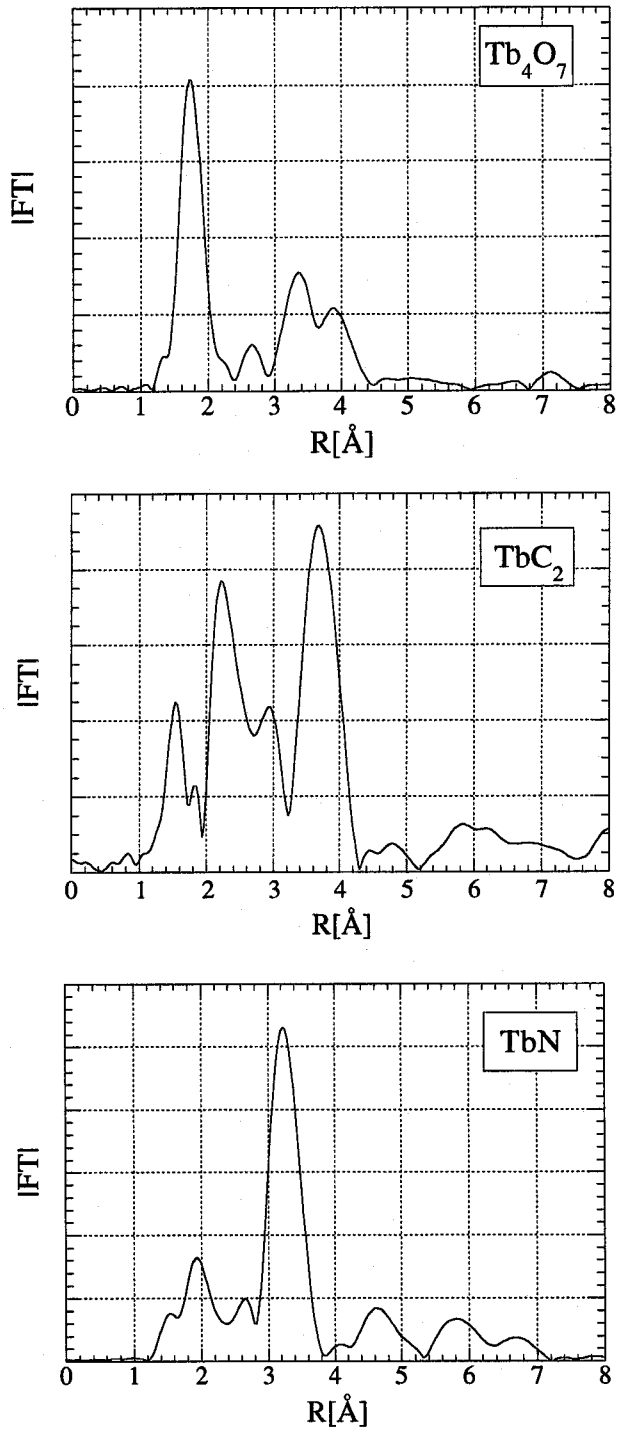

Fig. 4.9 Radial distribution functions of Tb_4O_7, TbC_2 and TbN calculated from K-edge EAXFS spectra

Chapter 5

Thermodynamic considerations of nitride formation by reactions of oxides with flowing ammonia

5.1. Introduction

In recent years, there has been increasing interest in nitride materials which possess high temperature strength, corrosion-resistance and electrical conductivities. Nitrides can be prepared in several ways. Metals, hydrides and oxides are often used as raw materials. Presently the common method for the preparation of nitrides is carbothermic reduction of metal oxides in nitrogen atmosphere [1]. However, the final product of this method will invariably contain certain amounts of carbon.

The equilibrium degrees of dissociation of ammonia are 95% at 300°C and 99.99% at 900°C, respectively. Nevertheless, at such a low temperature the dissociation rate of ammonia is so slow that the decomposition can be successfully suppressed. The choice of material and condition of the inner surface of the reaction tube would also affect the decomposition of ammonia [2]. At elevated temperatures where the decomposition reaction is accelerated, the dissociation could be effectively suppressed by flowing the reactant gas. Unstable gaseous mixture of NH_3, N_2 and H_2 as prepared by flowing NH_3 through a hot region, may act both as a nitriding agent and as a hydriding agent [3]. The mixture possesses high nitrogen and hydrogen potential, which increase with increasing instability of the mixture.

Several reports are known about the reactions of oxides with NH_3. Ta_3N_5 [4] and TiN [5, 6] can be formed at 900°C by reaction of Ta_2O_5 and TiO_2 with flowing ammonia, respectively. A little has been reported about the reactions of MoO_3 [7] and WO_3 [8] with NH_3. In these reports, it has not been, however, clarified how the reaction proceeds and no attention to the gaseous analysis during the reactions has received. The aim of this work is a thermodynamic analysis of nitride formation from oxides with flowing ammonia, with particular attention to the reduction sequence of starting

material. A modification of Ellingham diagrams which allows for rapid determination of partial equilibrium in the reduction of oxide with flowing ammonia is described

5.2. Experimental

Transition metal oxide powders used as starting material were Fe_2O_3(99.999%), Cr_2O_3(99.9%), MoO_2(99%), Ta_2O_5(99.99%), Nb_2O_5(99.9%) TiO_2(99.5%) and ZrO_2(99.99%). These oxides were supplied from RARE METALLIC Co., Ltd. Japan except for TiO_2 (Aerosil Nippon Ltd.). A quartz boat containing the specimen was placed in the center of a quartz reaction tube. The reaction tube was evacuated to the order of 10^{-4} Pa at room temperature, and the degasification of the specimen was performed at 300°C for an hour. The temperature was raised up to 900°C. Then NH_3 stream was supplied continuously at a flow rate of 200ml/min. Partial pressures of NH_3 and N_2 were measured by a gas-chromatograph (the detection limits of P_{N2} and P_{NH3} were 3.9 Pa and 5.0 Pa, respectively) and total pressure was monitored by a capacitance manometer at intervals. Partial pressure of H_2 was calculated by the relation of $P_{H2}=P_{total}-P_{NH3}-P_{N2}$. Heat treatment was continued until the steady state attained between the gas and solid phase, where the variations in the partial pressure of NH_3, N_2 and H_2 in the outlet gas were diminished. The solid product was subjected to the x-ray diffraction analysis at room temperature.

5.3. Results and discussion

The experimental results are summarized in Table 5.1. Fe_2O_3, Cr_2O_3, Ta_2O_5, Nb_2O_5, TiO_2 have been nitrided. MoO_2 has been reduced to metal. In these six reactions, formation of water was confirmed by passing outlet gas through a tube in supercooled water (-18°C). ZrO_2 has not reacted with NH_3 but phase change to the high temperature phase has occurred. The relationship between the free energy of formation of several oxides per 1 mole O_2 and temperature (Ellingham diagram) is shown in Fig. 5.1 [9]. The larger the free energy is, the more unstable the oxide becomes. Fe_2O_3 is the least stable oxide and ZrO_2 is the most stable oxide among the seven oxides treated in this work. The stable oxides are difficult to be reduced. If the

oxides are reduced to metals by flowing NH_3, the metals are nitrided feasibly because flowing NH_3 possesses high nitriding ability [10]. The reason why ZrO_2 could not be converted to nitride is that ZrO_2 could not be reduced by flowing NH_3. Therefore, the point which the author emphasizes is whether the oxides can be reduced or not by flowing NH_3.

It may be considered from these results that the nitride formation from oxide involves reduction and nitridation steps:

$$\frac{2}{x}Me_yO_x + \frac{4}{3}NH_3 = \frac{2y}{x}Me + 2H_2O + \frac{2}{3}N_2, \tag{5.1}$$

$$\frac{2w}{z}Me + 2NH_3 = \frac{2}{z}Me_wN_z + 3H_2. \tag{5.2}$$

When the equilibrium state is established according to eqn. 5.1, the following equation are obtained:

$$\frac{2}{x}\Delta G^\circ_{M_yO_x} + \frac{4}{3}\Delta G^\circ_{NH_3} + \frac{4}{3}RT\ln P_{NH_3}$$

$$= 2\Delta G^\circ_{H_2O} + 2RT\ln P_{H_2O} + \frac{2}{3}RT\ln P_{N_2} \tag{5.3}$$

where ΔG° is the standard free energy of a given substance, R is gas constant, T is temperature in Kelvin scale and P is the partial pressure in bars and 1 bar is taken as the standard state. Eqn. 5.3 is rewritten as

$$\frac{2}{x}\Delta G^\circ_{M_yO_x} = 2\Delta G^\circ_{H_2O} - \frac{4}{3}\Delta G^\circ_{NH_3} + 2RT\ln\frac{P_{H_2O}P_{N_2}^{1/3}}{P_{NH_3}^{2/3}}. \tag{5.4}$$

The right- and left-hand sides present the oxygen potential of gas and solid phases, respectively. This relation can be also obtained as follows.

When a metal is put in oxygen atmosphere, the metal may be oxidized according as oxygen potential.

$$\frac{2}{x}Me_yO_x = \frac{2y}{x}Me + O_2 \tag{5.5}$$

Thus, the free energy of formation per 1mol O_2 of an oxide, μ_{O_2}, is presented by

$$\mu_{O_2} = \frac{2}{x}\Delta G^\circ_{Me_yO_x} = RT\ln P_{O_2}. \tag{5.6}$$

On the other hand, formation of water vapor by reaction of oxygen and ammonia is written by the following chemical equation,

$$O_2 + \frac{4}{3}NH_3 = 2H_2O + \frac{2}{3}N_2. \tag{5.7}$$

At equilibrium, the following relation must hold,

$$RT\ln P_{O_2} + \frac{4}{3}\Delta G^{\circ}_{NH_3} + \frac{4}{3}RT\ln P_{NH_3}$$

$$= 2\Delta G^{\circ}_{H_2O} + 2RT\ln P_{H_2O} + \frac{2}{3}RT\ln P_{N_2}. \tag{5.8}$$

Therefore, oxygen potential of this gaseous mixture, μ_{O_2}, is

$$\mu_{O_2} = RT\ln P_{O_2} = 2\Delta G^{\circ}_{H_2O} - \frac{4}{3}\Delta G^{\circ}_{NH_3} + 2RT\ln\frac{P_{H_2O}\cdot P_{N_2}{}^{1/3}}{P_{NH_3}{}^{2/3}}. \tag{5.9}$$

Fitting free energy of formation data given in the JANAF tables [11] for H_2O and NH_3 yields the following linear relationship:

$$\Delta G^{\circ}_r = 2\Delta G^{\circ}_{H_2O} - \frac{4}{3}\Delta G^{\circ}_{NH_3} = -423430 - 43.866T \text{ (for } T \geq 500 \text{ K)}. \tag{5.10}$$

Since ΔG°_r is constant at a given temperature, oxygen potential of the gas phase depends only upon the value of $(P_{H_2O}\cdot P_{N_2}^{1/3})/P_{NH_3}^{2/3}$. A series of lines that radiate from the intercept of the line described by eqn. 5.10 is obtained as can be seen in Fig. 5.2. Oxygen potential of gas phase decreases with decreasing the value of $(P_{H_2O}\cdot P_{N_2}^{1/3})/P_{NH_3}^{2/3}$. That is to say, decrease in partial pressure of water vapor or nitrogen, or increase in partial pressure of ammonia lowers the oxygen potential of gas phase. Fig. 5.3 indicates the variation of partial pressure of NH_3, N_2 and H_2 during the reaction of TiO_2 with flowing NH_3 at 900°C. When the equilibrium is reached, 99.986% of NH_3 is decomposed into N_2 and H_2 at this temperature. However, only 60% of NH_3 are decomposed in this run as shown in Fig. 5.3. Use of flowing NH_3 leads to increase in partial pressure of ammonia and decrease in that of nitrogen because the dissociation of NH_3 is suppressed to some extent when NH_3 gas is continuously supplied into reaction region. The oxygen potentials of several oxides are also shown in Fig. 5.2. The point of intersection of oxygen potentials of an oxide and gas phase is

the equilibrium point, that is, at the equilibrium, eqn. 5.4 must hold. When the oxygen potential of the oxide is larger than that of gas phase, the oxide will be reduced to metal. For example, when Ta_2O_5 is put under a gas phase of which value of $(P_{H_2O} \cdot P_{N_2}^{1/3})/P_{NH_3}^{2/3}$ is 10^{-3}, it will be reduced to metal at the temperatures more than 1184 K.

The partial pressures of NH_3 and N_2 are expressed by the dissociation degree of NH_3, α, and partial pressure of water since $P_{NH3}+P_{N2}+P_{H2}+P_{H2O}=1$bar:

$$P_{NH_3} = \frac{1-\alpha}{1+\alpha}\left(1-P_{H_2O}\right) \tag{5.11}$$

$$P_{N_2} = \frac{\alpha}{2(1+\alpha)}\left(1-P_{H_2O}\right) \tag{5.12}$$

Substituting eqns. 5.11 and 5.12 into eqn. 5.9 results in

$$\mu_{O_2} = 2\Delta G^{\circ}_{H_2O} - \frac{4}{3}\Delta G^{\circ}_{NH_3} + 2RT\ln\left\{\frac{P_{H_2O}{}^3 \cdot \alpha(1+\alpha)}{2(1-\alpha)^2\left(1-P_{H_2O}\right)}\right\}^{1/3}. \tag{5.13}$$

Fig. 5.4 shows an Ellingham diagram for reduction of oxide with flowing NH_3, which incorporates the nomograph developed in terms of eqn. 5.13. Consider a system which partial pressure of water is known value. Further, the dissociation degree of NH_3, α, is estimated from the partial pressures of NH_3 and N_2. Then a point is fixed in the right field in Fig. 5.4. The line between this point and the intercept of eqn. 5.10 defines the oxygen potential of the gas phase as a function of temperature. Reduction proceeds when oxygen potential of an oxide is larger than that of gas phase. On the other hand, oxidation proceeds when oxygen potential of an oxide is lower than that of gas phase. In condition that partial pressure of water is 10^{-2} bar and 90% of NH_3 is dissociated, Cr_2O_3 and Nb_2O_5 cannot be reduced to metals at 900°C as shown in Fig. 5.4. However, these two oxides will be reduced to metals even under the same water pressure at 900°C, when the dissociation degree of NH_3 will be lowered to 50%.

In practice, it is difficult to measure exactly the partial pressure of water in the mixture of NH_3, N_2, H_2 and H_2O. Thus, the author takes an assumption that water vapor pressure in the reaction tube during the runs was 10^{-6} bar because nominal impurity of ammonia used in this work was $H_2O < 1$ ppm. In Fig. 5.4, the line that expresses the oxygen potential of gas phase during the reaction of TiO_2 with flowing

NH_3 is also drawn. The oxygen potential of TiO_2 at 900°C is slightly higher than that of gas phase. Therefore, TiO_2 was reduced and then nitrided by flowing NH_3. The conditions on which the respective oxides are reduced to metals at 900°C are shown in Fig. 5.5 in terms of partial pressure of water and dissociation degree of ammonia. If the water pressure is lowered below the curve, the oxide is reduced to metal. In other words, dissociation degree of ammonia is lowered even under the same water pressure, the oxide can be reduced. This figure indicates that reduction of ZrO_2 at 900°C is very difficult because dissociation of NH_3 must be suppressed to almost zero under 10^{-6} bar of the water vapor pressure. The experimental results in this work are explained by these considerations.

Finally, the author states an additional prediction for uranium nitride formation by the reaction of UO_2 with flowing NH_3. Uranium nitride, which is considered to be one of promising nuclear fuels for fast bleeder reactors or space reactors, is often fabricated by carbothermic reduction of UO_2 under mixture of N_2 and H_2 [12-16]. However, the final product of this method invariably contains certain amounts of carbon. Thus, the condition on which the direct nitridation of UO_2 by use of flowing NH_3 can be possible will be investigated. Fig. 5.1 indicates that UO_2 is a more stable oxide than ZrO_2 which could not be nitrided by flowing ammonia at 900°C. However, at higher reaction temperature, UO_2 may be reduced by flowing NH_3 as given in Fig. 5.6. The conditions on which flowing NH_3 reduce UO_2 at several temperatures are shown in Fig. 5.6 by means of dissociation degree of NH_3 and H_2O partial pressure. For example, when dissociation degree of NH_3 is lowered to 31% by use of flowing NH_3 containing 1 ppm H_2O as impurity at a sufficiently high speed, UO_2 will be reduced and nitrided at 1200°C. If UO_2 were once reduced to metal by flowing ammonia, uranium metal would be nitrided easily by ammonia.

4.4. Conclusions

The reactions of Fe_2O_3, Cr_2O_3, MoO_2, Ta_2O_5, Nb_2O_5, TiO_2, and ZrO_2 powders with flowing NH_3 900°C have been investigated. Fe_2O_3, Cr_2O_3, Ta_2O_5, Nb_2O_5, TiO_2 have been nitrided. MoO_2 has been reduced to metal. ZrO_2 has not reacted with NH_3. It is considered that oxides are once reduced followed by the nitride. ZrO_2 has not been nitrided because it could not be reduced by flowing NH_3. The oxygen potential of the

gas phase was estimated in terms of partial pressure of water, P_{H2O}, and extent of ammonia dissociation, α, in order to explore reduction ability of flowing NH_3. A modification of conventional free energy diagram is described which facilitates determination of the oxygen potential of NH_3 and H_2O mixture in equilibrium with oxides at a given temperature. At several temperatures, water partial pressure and extent of ammonia dissociation were also estimated where UO_2 would be reduced to uranium metal.

References

[1] A. W. Weimer, "carbide, nitride and boride materials synthesis and processing," A. W. Weimer, ed., Chapman & Hall, London (1997)p. 79.

[2] M. Katsura and H. Serizawa, *J. Alloys Comp.* **196**(1993)191.

[3] M. Katsura, *J. Alloys Comp.* **182**(1992)91.

[4] V. G. Brauer, J. Weidlein and J. Strähle, *Z. Anorg. Allg. Chem.* **348**(1966)298.

[5] C. H. Shin, G. Bugli and G. Djega-Mariadassou, *J. Solid State Chem.* **95**(1991)145.

[6] K. Kamiya, T. Yoko and M. Bessho, *J. Mater. Sci.* **22**(1987)937.

[7] C. H. Jaggers, J. N. Mlchaels and A. M. Stacy, *Chem. Mater.* **2**(1990)150.

[8] L. Volpe and M. Boudart, *J. Solid State Chem.* **59**(1985)332.

[9] F. D. Richardson and J. H. E. Jeffes, *J. Iron Steel Inst.* **160**(1948)261.

[10] M. Katsura, *J. Alloys Comp.* **182**(1992)91.

[11] M.W.Chase, Jr., C.A.Davies, J.R.Downey, Jr., D.J.Frurip, R.A.McDonald, and A.N.Synerud, "JANAF Thermochemical Tables, 3rd Ed.," J. Phys. Chem. Ref. Data, Vol. 14, suppl. 1, 1985, p. 1274 and p. 1293.

[12] T. Muromura and H. Tagawa, *J. Nucl. Mater.* **71**(1977)65.

[13] T. Muromura and H. Tagawa, *J. Nucl. Mater.* **80**(1979)330.

[14] R. B. Matthews, K. M. Chidester, C. W. Hoth, R. E. Mason and R. L. Petty, *J. Nucl. Mater.* **151**(1988)334.

[15] R. D. Shoup, *J. Am. Ceram. Soc.* **60**(1977)332.

[16] G. Pautasso, K. Richter and C. Sari, *J. Nucl. Mater.* **158**(1988)12.

Table 5.1 Conditions and products of reactions of transition metal oxides with flowing NH_3

Reactant	Flow rate [ml/min]	Reaction time [h]	Product
Fe_2O_3	100	13	$Fe_4N + Fe_{2\sim4}N$
MoO_2	200	20	Mo
Cr_2O_3	200	24	CrN
Nb_2O_5	200	48	NbN
Ta_2O_5	200	4.5	Ta_3N_5
TiO_2	200	5	TiN
α-ZrO_2	300	14	β–ZrO_2

Reaction temperature : 900°C

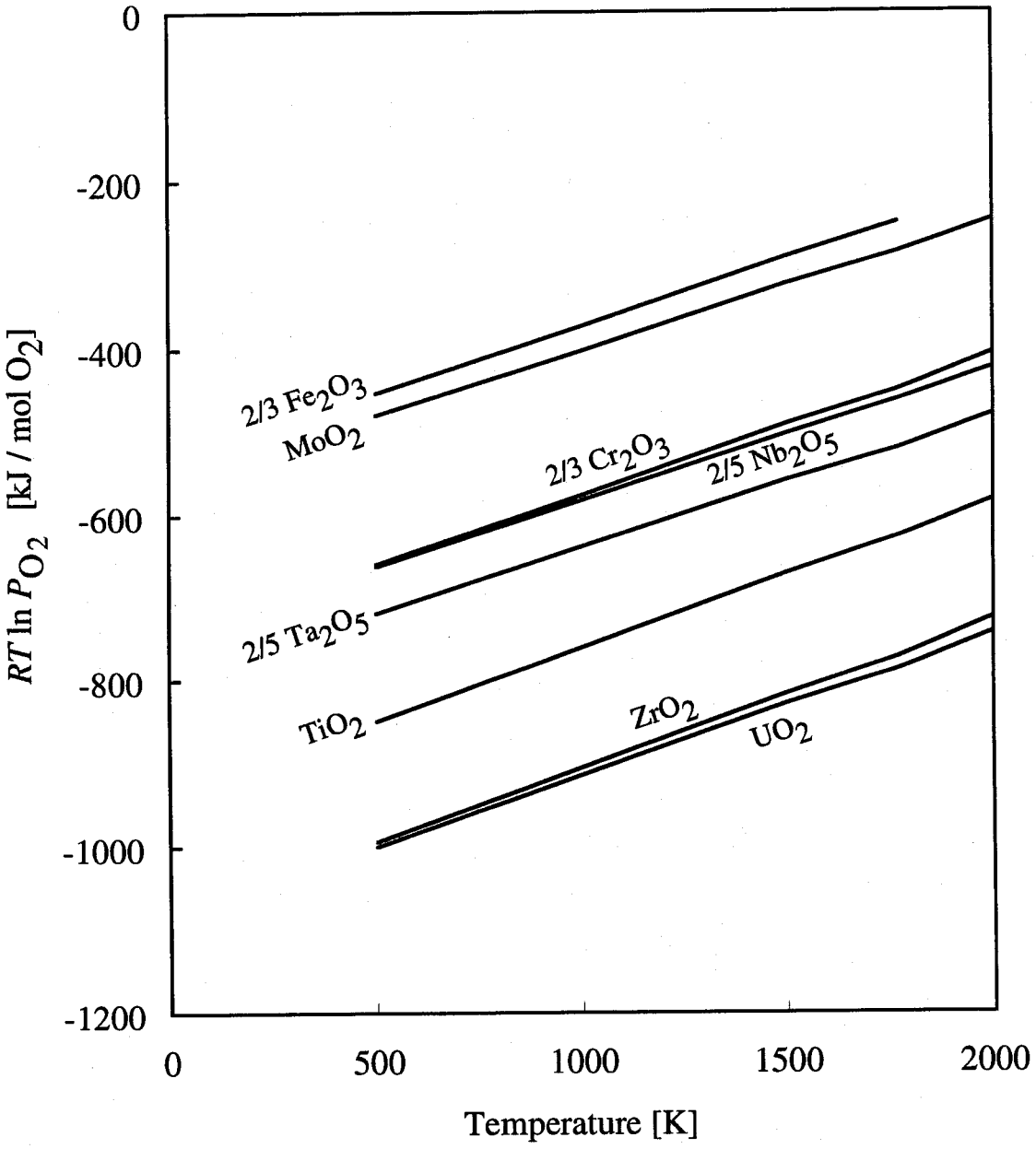

Fig. 5.1 Temperature dependence of formation free energies of several oxides.

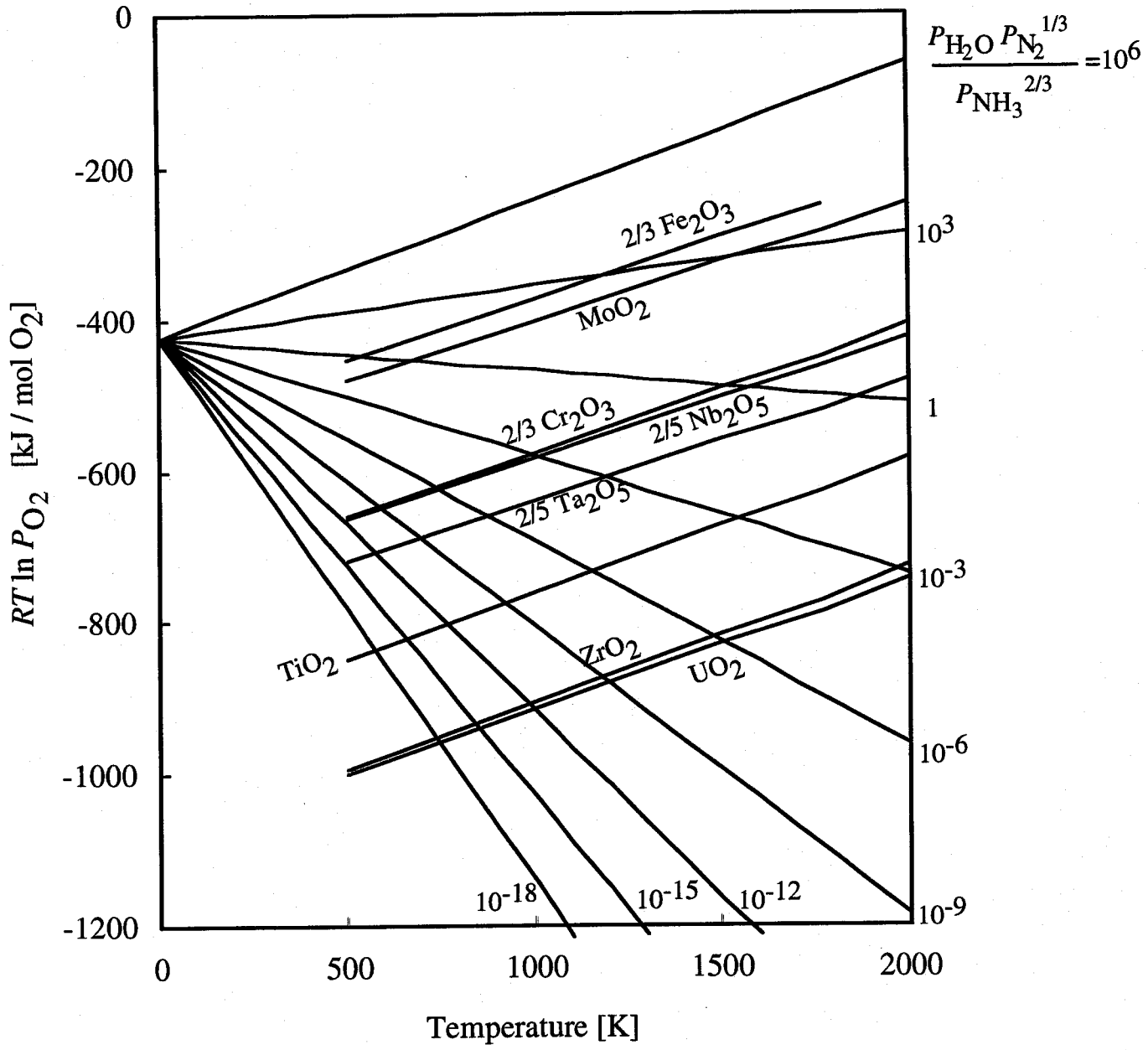

Fig. 5.2 Temperature dependence of formation free energies of several oxides

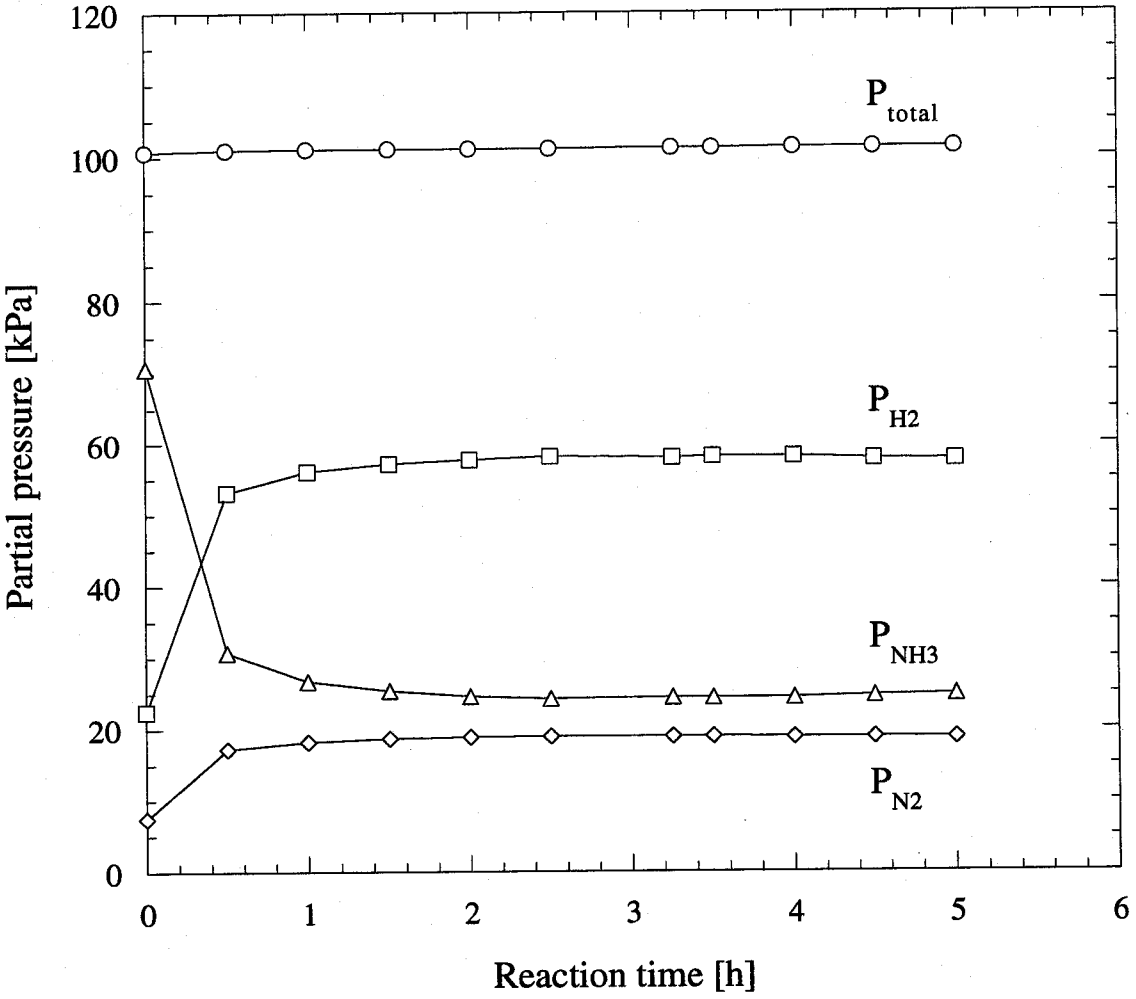

Fig. 5.3 Variation of partial pressures of NH_3, N_2 and H_2 as a function of time during the reaction of TiO_2 with flowing NH_3.

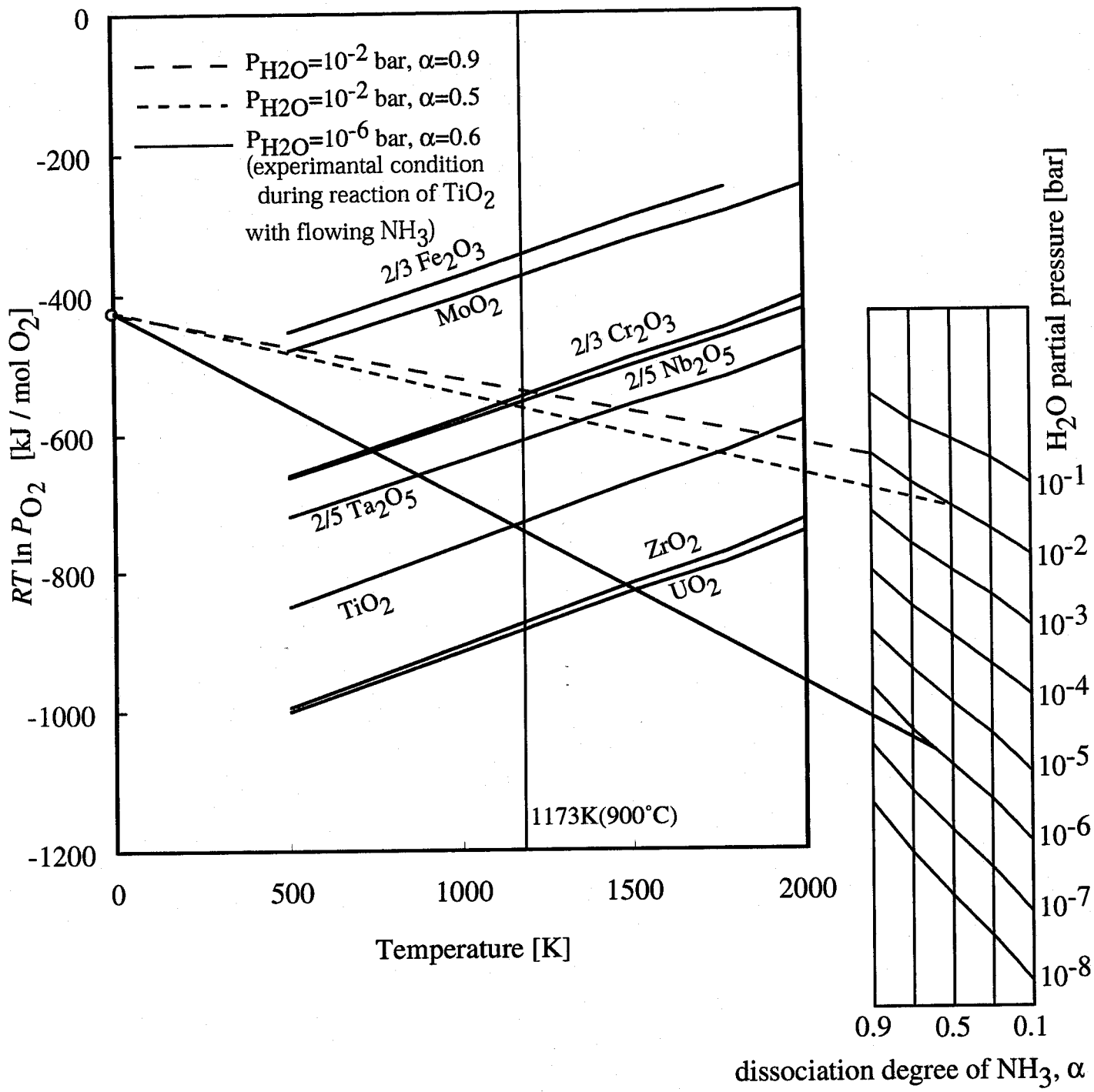

Fig. 5.4 Temperature dependence of formation free energies of several oxides in corporating the nomograph of H_2O partial pressure and dessoication degree of NH_3

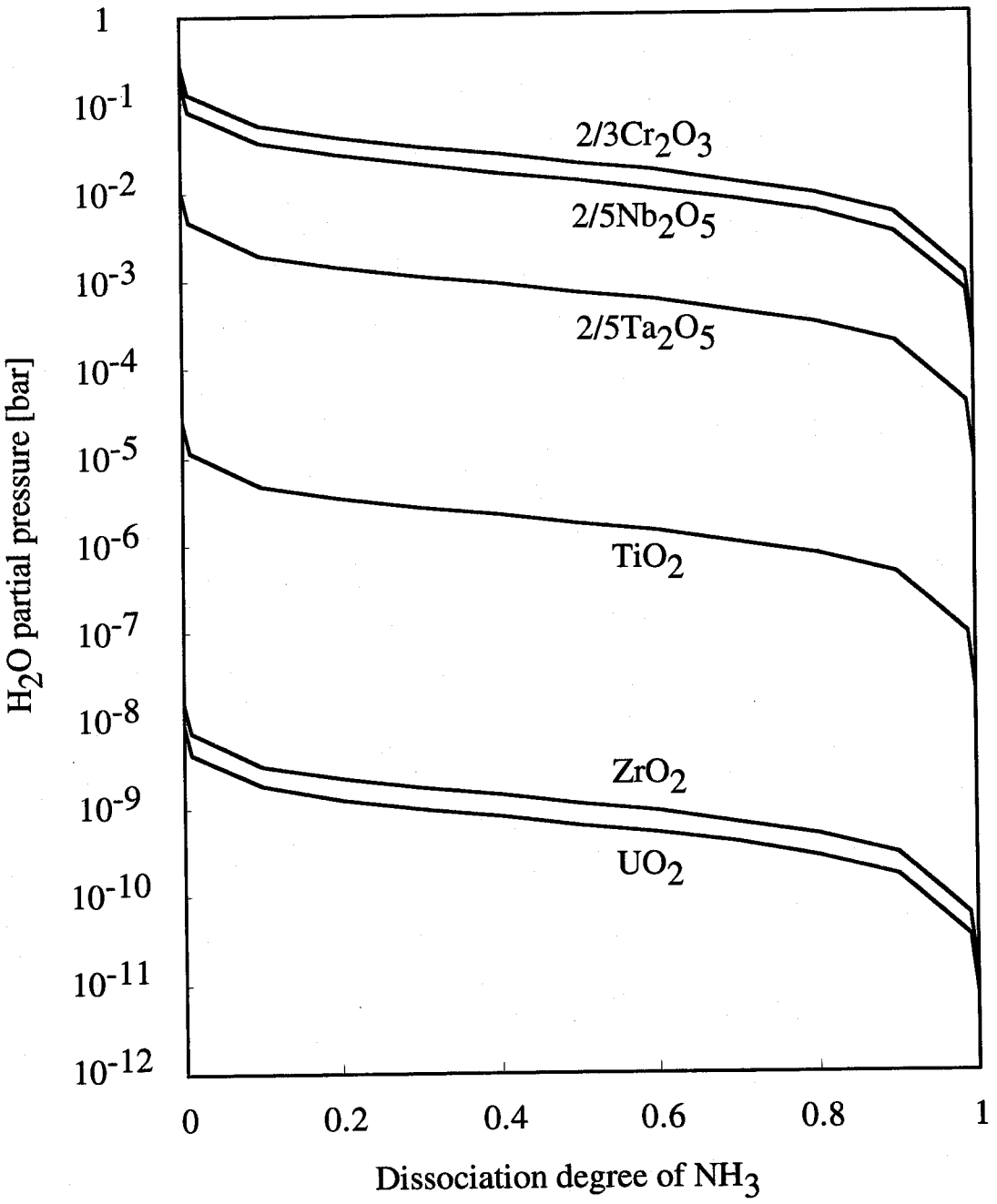

Fig. 5.5 Relationship between dissociation degree of NH_3 and H_2O partial pressure to reduce several oxides at 900°C

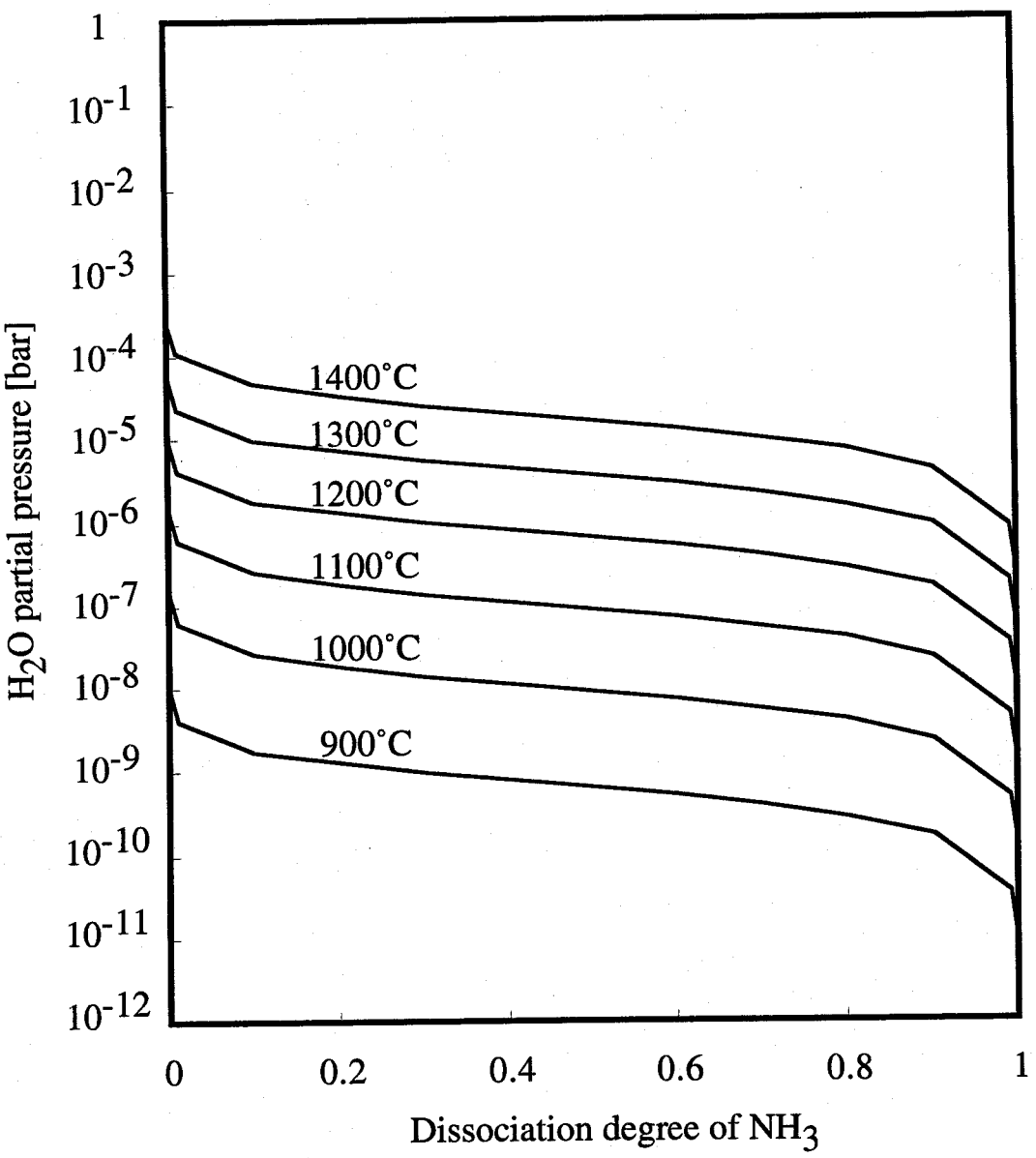

Fig. 5.6 Relationship between dissociation degree of NH_3 and H_2O partail pressure to reduce UO_2 at several temperatures

Chapter 6

Summary

In this thesis, the metal nitride formation by use of NH_3 is discussed thermodynamically based on the experimental results. In chapter 2, the experimental results of the reactions of rare earth metals with NH_3 are described. In the static ammonia method some rare earth nitrides were obtained at such low temperatures; CeN was at 200°C, LaN at 500°C and PrN at 600°C. Although neodymium was not nitrided at 700°C by static ammonia, flowing ammonia enabled us to prepare the neodymium nitride at this temperature. Other rare earth nitrides may be formed by flowing NH_3 at lower temperatures than the respective temperatures at which their nitrides were obtained in static ammonia method. No nitride formation occurred during the exposure of the rare earth metals to N_2 at the respective temperatures where rare earth nitrides were obtained by use of NH_3. These results mean that ammonia may work more effectively as nitriding agent compared to nitrogen. The experimental results of the reactions of rare earth metals with a mixture of N_2 and H_2 are also examined. The rare earth hydrides were once formed before the nitride formation. In these reactions, hydrogen seems to behave itself like, as it were, a gaseous catalyst. For example, as for praseodymium the activation energy of the hydride formation is 10.5 kJ/mol and that of the conversion of the hydride into the nitride is 50.9 kJ/mol. These nitriding methods described in this chapter may be applicable to americium nitride formation.

In chapter 3, the rare earth carbide formation by carbothermic reduction and the rare earth nitride formation by reactions of the carbides with NH_3 are described. CeC_2, PrC_2, NdC_2, GdC_2 and TbC_2 were obtained by carbothermic reduction of oxides with amorphous carbon at 1450°C. However, under the same conditions where these carbides were synthesized, SmC_2 and EuC_2 were not formed, but graphite was found in the reaction products. It is interesting and surprising that graphitization of amorphous carbon proceeded during the reactions of Sm_2O_3 and Eu_2O_3 with amorphous carbon even at a low temperature such as 1450°C. Further work is now in progress to clarify

this graphitization process. By the reactions of the dicarbides with flowing NH_3 at temperatures between 900 and 1200°C, the rare earth nitrides CeN, PrN, NdN, GdN and TbN were synthesized and free carbon was precipitated. The free carbon was removed from the reaction system as CH_4 by the reaction of amorphous carbon with NH_3. Rare earth dicarbides are nitrided by either NH_3 or N_2. The precipitated carbon, which is amorphous carbon, reacts with NH_3 at 900°C but does not react with H_2 at the same temperature. These experimental results support the idea that flowing NH_3 possesses high hydrogen activity. Solubilities between CeO_2 and Pr_6O_{11} and between CeO_2 and Tb_4O_7 were also examined. CeO_2 and Pr_6O_{11} are partly miscible but CeO_2 and Tb_4O_7 are soluble in each other only within a very narrow range. The rare earth mixed carbides, $Ce_xPr_{1-x}C_2$ and $Ce_xTb_{1-x}C_2$, were prepared by carbothermic reduction of oxide mixtures. CeC_2 and LnC_2 (Ln=Pr and Tb) are completely miscible. To form rare earth mixed nitrides, these rare earth dicarbides, $Ce_xPr_{1-x}C_2$ and $Ce_xTb_{1-x}C_2$ were reacted with NH_3. This is the first report of $Ce_xPr_{1-x}N$ and $Ce_xTb_{1-x}N$ formation. The lattice parameters of both $Ce_xPr_{1-x}N$ and $Ce_xTb_{1-x}N$ obey Vegard's law. Other rare earth mixed nitrides may be prepared in this method.

XAFS study of *K*-edges of rare earth elements in oxides, carbides and nitrides are described in chapter 4. No *K*-edge XAFS study has been reported yet for rare earth carbides and nitrides. It has been pointed out that chemical shifts could not be observed in such high energies like rare earth *K*-edge because of the much broadened transition peak forced by short lifetimes of excited core levels. However, in this work, significant and clear chemical shifts in edge energy depending on chemical states were observed. The radial distribution functions of the rare earth oxides, dicarbides and mononitrides were obtained by Fourier transform of the EXAFS functions of *K* absorption edges of these rare earth compounds. The interatomic distances between Ce and the nearest light elements calculated from Ce *K*-edge EXAFS spectra of oxide, carbide and nitride, and the values agree with those from XRD, respectively.

In chapter 5, the reactions of Fe_2O_3, Cr_2O_3, MoO_2, Ta_2O_5, Nb_2O_5, TiO_2, and ZrO_2 powders with flowing NH_3 900°C are stated. Fe_2O_3, Cr_2O_3, Ta_2O_5, Nb_2O_5, TiO_2 were converted to nitrides by flowing ammonia. MoO_2 was reduced to metal. No reaction occurred between ZrO_2 and NH_3. In most cases of the reactions of the oxides with NH_3, reduction of oxides is crucial for nitride formation. If oxides are once reduced to

metals, the metals may be easily nitrided by flowing ammonia. ZrO_2 has much large negative free energy of formation, that is, ZrO_2 is hard to be reduced to metal. In order to explore reducing ability of flowing NH_3, the oxygen potential of the gas phase was estimated in terms of partial pressure of water, P_{H2O}, and extent of ammonia dissociation, α. A modification of conventional free energy diagram is demonstrated which facilitates determination of the oxygen potentials of NH_3 and H_2O mixture in equilibrium with oxides at 500-2000 K. The conditions, water partial pressure and extent of ammonia dissociation at several temperatures, were also estimated at which UO_2 can be reduced by flowing NH_3.

Acknowledgements

The author would like to express his greatest appreciation to Professor Dr. Masahiro Katsura for his precious guidance, invaluable discussion and warm encouragement. The author also wishes to express his gratitude to Professor Dr. Shinsuke Yamanaka and Associate Professor Dr. Takao Yamamoto for their invaluable comments, suggestive discussions and careful reading the manuscript.

The author is indebted to Dr. Masanobu Miyake and Dr. Pongung Son for their encouraging advice and constructive criticism during their tenure of office.

The author greatly acknowledges to the post- and under-graduate students in Energy Materials Engineering Laboratory (Katsura Lab.), Department of Nuclear Engineering, Osaka University, especially, Dr. Masayuki Hirota, Mr. Hirotaka Matsuoka, Mr. Masaji Sawa, Mr. Katsuhiro Nishimaki, Mr. Satoru Ishii, Mr. Kenji Idehara, Mr. Yoshinori Kobayashi, Mr. Akira Nakahara, Ms. Fumi Inada, Mr. Yoshiyasu Kitauji, Mr. Koji Kanamori and Mr. Masataka Kano, for their cooperation, good-fellowship and various supports.

Finally, special thanks are offered to the author's parents, Mr. Akira Nakagawa and Ms. Yukari Nakagawa, and fiancée, Ms. Michiko Watanabe, for their supports and hearty encouragement.

Research Activities by the author

List of Publications

(1)* "Reaction of Cerium with NH_3"
M. Katsura, M. Hirota, **T. Nakagawa** and M. Miyake, *J. Alloys Comp.*, **207&208**(1994)413-415.

(2)* "Formations of Some Rare Earth Nitrides by Use of Gaseous Mixture of Nitrogen and Hydrogen"
T. Nakagawa and M. Katsura, *Tech. Rept. Osaka Univ.*, **Vol.46**(1996)297-303.

(3)* "Formation of Some Rare Earth Nitrides by Use of NH_3"
T. Nakagawa and M. Katsura, *Tech. Rept. Osaka Univ.*, **Vol.46**(1996)117-125.

(4)* "Formation of uranium and cerium nitrides by the reaction of carbides with NH_3 and H_2/H_2 stream"
T. Nakagawa, H. Matsuoka, M. Sawa, M. Hirota, M. Miyake and M. Katsura, *J. Nucl. Mater.*, **247**(1997)127-130.

(5)* "Preparation of lanthanide nitrides by carbothermic reduction using ammonia"
T. Nakagawa, H. Matsuoka, M. Sawa, K. Idehara, and M. Katsura, *J. Nucl. Mater.*, **247**(1997)147-150.

(6) "Study of the thermodynamic properties of (U, Ce)O_2"
K. Yamada, S. Yamanaka, **T. Nakagawa**, M. Uno and M. Katsura, *J. Nucl. Mater.*, **247**(1997)289-292.

---

* The present doctoral thesis includes the work described in these nine papers.

(7) "Equilibrium between Flowing NH_3 and Synthesized FeN_x at Various Positions along Flow of Reaction Gas"
K. Nishimaki, **T. Nakagawa**, T.A. Yamamoto and M. Katsura, *Tech. Rept. Osaka Univ.*, **Vol.48**(1998)153-156.

(8)* "Preparation of Ce-Pr Mixed carbide by Carbothermic Reduction"
T. Nakagawa, A. Nakahara, K. Idehara and M. Katsura, *J. Alloys Comp.*, **275-277**(1998)58-61.

(9) "The Formation of Uranium Sesquinitride by Reaction of U or UH_3 with a N_2-H_2 Mixture"
M. Katsura, K. Nishimaki, **T. Nakagawa** and K. Takahashi, *J. Alloys Comp.*, **271-273**(1998)662-665.

(10) "Thermodynamic study on α-U_2N_{3+x} using N rich startin material (x>=0.6)"
T. Nakagawa, K. Nishimaki, T. Urabe and M. Katsura, *J. Alloys Comp.*, **271-273**(1998)658-661.

(11) "Thermodynamics of nitrogen-rich uranium sesquinitride formation by reaction of uranium monocarbide"
K. Nishimaki, M. Hirota, **T. Nakagawa**, T. A. Yamamoto and M.Katsura, *J. Alloys Comp.*, **271-273** (1998)654-657.

(12)* "Thermodynamics of the Formation of CH_4 by the Reaction of Carbon Materials with a Stream of NH_3"
M. Katsura, K. Nishimaki, **T. Nakagawa**, T. A. Yamamoto, M.Hirota and M. Miyake, *J. Nucl. Mater.*, **258-263** (1998)839-842

(13)* "Preparation of some rare earth dicarbides and mononitrides from oxides"
T. Nakagawa and M. Katsura, *Tech. Rept. Osaka Univ.*, **Vol.48**(1998)325-331.

(14) "Selective Formation of Iron Nitrides by Ammonia Flow Method"
K. Nishimaki, S. Ohmae, **T. Nakagawa**, T. A. Yamamoto and M. Katsura, *Tech. Rept. Osaka Univ.*, **Vol.48**(1998)333-336.

(15)* "*K*-edge X-ray Absorption Spectra of Rare Earth Elements in Their Oxides, Carbides and Nitrides"
T. Nakagawa, T. A. Yamamoto, Y. Kitauji, Y. Kobayashi, M. Katsura and S. Emura, *Tech. Rept. Osaka Univ., in press*

(16) "*K*-Edge X-Ray Absorption Spectra of Iron Nitrides in Fe_xN/Ag Nanocomposites"
K. Nishimaki, T.A. Yamamoto, **T. Nakagawa** and M. Katsura, *Tech. Rept. Osaka Univ., in press*

(17) "Formation of Iron-Nitride/Silver Nanocomposites by Ammonia-Flow Method and Nitride Phase Identification by X-Ray Absorption Near Edge Structure"
K. Nishimaki, T.A. Yamamoto, **T. Nakagawa** and M. Katsura *J,apanese Journal of Applied Physics, received*

(18) "Magnetic Composites Composed of Iron-Nitride Nanograins Dispersed in a Silver Matrix"
T.A. Yamamoto, K.Nishimaki, T. Harabe, K. Shiomi, **T. Nakagawa** and M. Katsura, *Nanostructured Materials, in press*

Annual Reports

(19) "Fe-K XANES OF Ag/Fe_xN NANOCOMPOSITES"
T. A. Yamamoto, **T. Nakagawa**, K. Nishimaki and M. Katsura, *Photon*

Factory Activity Report, **15**(1997)174.

(20) "Measurements of Magnetization of Magnetic Nanocomposites"
T. A. Yamamoto, **T. Nakagawa**, K. Sumiyama and T. Konno, *"IMR Report of Collaborative Research with Laboratories", Institute for Materials Research, Tohoku University,* fiscal year 1996, p.76. *in Japanese.*

(21) "K-edge XAFS of rare earth elements in oxides, carbides and nitrides"
T. Nakagawa, T. A. Yamamoto, K. Nishimaki, Y. Koboyashi, A. Nakahara, Y. Kitauji, F. Inada, S. Emura, Y. Nakata and Y. Nishihata, *SPring-8 User Experiment Report,* **No.2**, 1998A, p.8.